Title

Highlighting membrane protein structure and function: A celebration of the Protein Data Bank

Authors

Li, Fei
Egea, Pascal F
Vecchio, Alex J
et al.

Publication Date

2021

DOI

10.1016/j.jbc.2021.100557

Highlighting membrane protein structure and function: A celebration of the Protein Data Bank

Received for publication, October 31, 2020, and in revised form, February 10, 2021 Published, Papers in Press, March 18, 2021,
https://doi.org/10.1016/j.jbc.2021.100557

Fei Li[1,2,‡], Pascal F. Egea[3,‡], Alex J. Vecchio[4], Ignacio Asial[5], Meghna Gupta[1], Joana Paulino[1], Ruchika Bajaj[6], Miles Sasha Dickinson[1], Shelagh Ferguson-Miller[7], Brian C. Monk[8], and Robert M. Stroud[1,*]

From the [1]Department of Biochemistry and Biophysics, [2]Department of Neurology, University of California San Francisco, San Francisco, California, USA; [3]Department of Biological Chemistry, School of Medicine, University of California Los Angeles, Los Angeles, California, USA; [4]Department of Biochemistry, University of Nebraska–Lincoln, Lincoln, Nebraska, USA; [5]DotBio Pte. Ltd, Singapore, Singapore; [6]Department of Bioengineering and Therapeutic Sciences, University of California San Francisco, San Francisco, California, USA; [7]Department of Biochemistry and Molecular Biology, Michigan State University, East Lansing, Michigan, USA; [8]Sir John Walsh Research Institute and Department of Oral Sciences, University of Otago, North Dunedin, Dunedin, New Zealand

Edited by Karen Fleming

Biological membranes define the boundaries of cells and compartmentalize the chemical and physical processes required for life. Many biological processes are carried out by proteins embedded in or associated with such membranes. Determination of membrane protein (MP) structures at atomic or near-atomic resolution plays a vital role in elucidating their structural and functional impact in biology. This endeavor has determined 1198 unique MP structures as of early 2021. The value of these structures is expanded greatly by deposition of their three-dimensional (3D) coordinates into the Protein Data Bank (PDB) after the first atomic MP structure was elucidated in 1985. Since then, free access to MP structures facilitates broader and deeper understanding of MPs, which provides crucial new insights into their biological functions. Here we highlight the structural and functional biology of representative MPs and landmarks in the evolution of new technologies, with insights into key developments influenced by the PDB in magnifying their impact.

As membranes were critical to the separation of chemistries essential to the origin of life, membrane proteins (MPs) are key players in some of the most important physiological processes in living organisms. Characterizing MPs structurally and functionally is still extremely challenging due to their frequent low abundance, and difficulties in purifying functional MPs intact from their native membrane, though it is going through an exciting revolution now due to several key factors. It took several decades to obtain the structural information that now allows pursuit of understanding MP function in health and disease, to manipulate them as drug targets, and to engineer them into new powerful tools to fuel discovery. We highlight some of the landmarks in this endeavor that drove or depended on the discovery of new technologies required specifically for structural studies of membrane, *versus* soluble proteins.

Previously, hand-written letters delivered by post requested coordinate sets that were not always readily given. The vision of Hamilton, Myer, Koetzle, and the joint venture between the Cambridge Crystallographic Data Center in the United Kingdom and the Brookhaven National Laboratories at Stony Brook University led to the Protein Data Bank (PDB). Then for the first time, one could begin to ask questions with all the relevant structures at hand. In celebrating 50 years of the PDB, we focus on some of the ingeniously crafted inventions and discoveries that led the way for entire classes of MPs, and those new approaches that now promise structures of large and complex machines from their native cellular environments, in action.

In the following *Historical perspective*, we provide a brief historical perspective of some MP insights (other than the crucial G-protein-coupled receptors (GPCRs) that are the subject of a dedicated review in this volume) and consider the value of the PDB in disseminating this information. Seemingly insurmountable difficulties were often overcome with invention of new technologies to reveal important structural features of classes of MPs that make the fabric of today's approaches.

In *How do membrane proteins accomplish key physiological functions?*, we describe how the structures of several of the major MP classes were uncovered, which often required technological developments that are now woven into the fabric of structural biology. First, how are the α-helical, tail-anchored, and all β-sheet MP broad categories correctly targeted to and inserted into membranes and allowed to fold correctly? We progress to landmark discoveries involving the roles of MPs in physiology and some of the critical barriers that had to be overcome to realize these achievements. How do water channels conduct water at diffusion limited rates without allowing leakage of protons (H^+) or hydronium ions (H_3O^+) or any other ions? How do potassium channels conduct K^+ ions, but

‡ These authors contributed equally.
* For correspondence: Robert M. Stroud, stroud@msg.ucsf.edu.
Present address for Miles Sasha Dickinson: Sauer Lab for Structural Biology (Cryo-EM), The University of Texas at Austin, USA.

Robert M. Stroud, Professor of Biochemistry and Biophysics, University of California San Francisco, has contributed fundamental insights into how signals are propagated across membranes by his work on the structures of membrane proteins and proteins associated with membrane-localized processes.

not the Na^+ ion of similar charge and smaller ionic radius? How are epithelial cells held together side by side to make a selectively permeable sealed layer of cells? The question of how substrates are transported across membranes using energy then follows. How does one superfamily of "primary" transporters, the "ABC transporters" that directly harness ATP hydrolysis on their cytoplasmic side, move materials across membranes? How does another superfamily of "secondary" transporters, the Major Facilitator Superfamily (MFS), use ion or proton electrochemical gradients to drive nutrient import, export, or efflux of xenobiotics? We progress to consider a specialized class of essential viral proteins that form channels that are essential for viral virulence.

In *Membrane protein structures instruct drug design and protein engineering*, we focus on a few examples of therapeutics and opportunities for engineering of MPs. Critical to any therapeutic drugs are the membrane-attached cytochrome P450s that are discussed in the light of their key roles in sterol metabolism, but as metabolizers of therapeutic drugs, and therefore as drug targets themselves. Structures help elucidate mechanisms of action of therapeutics to modulate MP activities. The Cystic Fibrosis Transmembrane-Conductance Regulator (CFTR) is used as an example of the impact structural studies can have on the understanding and treatment of rare diseases. Another example addresses glucose import as an anticancer target opportunity. A key example in neurology is the class of ligand-gated ion channels, represented by $GABA_A$ receptors ($GABA_AR$) and their ligands. Then the Leucine Transporter (LeuT), representing several classes of transporters with a common core of ten trans-membrane α-helices (TMs), is used to illustrate how major antidepressants work. Finally, some exciting developments in MP engineering focus on channelrhodopsins where light can trigger cellular responses and engineered dopamine sensors.

We hope that this necessarily limited perspective on the impact of selected MP structure classes may encourage opportunities in a broader context. We hope to communicate the value of MPs as guardians of the health of cells and how their structures, through the PDB, contribute important insights into many crucial aspects of physiology.

Historical perspective

A brief history of membrane protein structures and the PDB

With soluble proteins beginning with myoglobin in 1961, followed by lysozyme, hemoglobin, and digestive proteases, these were available only from large animals or from bacteria. Long before overexpression systems became available, the number of soluble macromolecular structures followed an exponential growth. This pattern was noted by Dickerson in a letter written to the PDB in 1978 (1). The first integral MP structure was not determined until 25 years later in 1985. The number of MP structures determined and deposited in the PDB since that time also increased exponentially, but with a smaller exponent reflecting the considerable challenges that pertain to MP structural biology. The amount of time for the number of unique MP structures to double was about 3 years compared with 2.4 years for soluble macromolecules (2). This doubling time for MPs slowed to ~5 years recently (Fig. 1). Most obvious challenges are functional expression in a limited lipid membrane environment *versus* expression in a soluble volume, followed by the requirement for detergents, amphiphiles, and lipids during extraction and purification of functional proteins from the membrane. There were critical breakthroughs necessary for many new classes of MPs over the last three decades. As a reflection, on January 15th, 2021, there were a total of 4569 coordinate files for MPs in the PDB, barely 2.6% of the total for all proteins, and of these 1203 represent unique structures. This is brilliantly tracked and annotated by Stephen H. White's invaluable *mpstruct* database of MPs of known structure (Fig. 1) (2) (https://blanco.biomol.uci.edu/mpstruc/), and by statistical and thermodynamic analyses from Thomas Newport, Mark Sansom, and Phillip Stansfield in their *MemProtMD* database (3). One of our aims here is to celebrate some of these developments in association with the breakthroughs by those that made them possible.

Like those in the 1960s who worked on the soluble proteins available in quantity from the tissues of large animals or bacteria, work on the first MP structures also focused on rich natural sources. The purple membrane of archaebacteria was first described in 1971 by Oesterhelt and Stoeckenius, who showed that it contained a light-driven proton pump. This validated the Mitchell hypothesis, the revolutionary concept that biological energy could be stored as a proton gradient across a membrane (4, 5). By freeze-fracture electron microscopy, they showed that "bacteriorhodopsin" formed an in-plane trigonal two-dimensional (2D) lattice. This was pursued structurally by Henderson and Unwin using electron diffraction of the arrays formed in the membrane (6), by Michel working with Oesterhelt, who attempted to crystallize the protein using detergents (7–10), and by Blaurock using X-ray scattering to demonstrate that α-helices were oriented perpendicular to the membrane plane (11, 12). Henderson and Unwin produced the first electron diffraction patterns from the trigonal latticed membranes, purified from the natural source, by sustaining its single bilayer in a glucose solution to prevent dehydration in the electron microscope (6). In a towering landmark, in 1975, they phased the patterns based on the images and reconstructed a 7 Å resolution 3D structure that beautifully demonstrated that the protein is comprised of seven TMs (6). This first discovery using electron microscopy/diffraction was at the heart of the concepts later recognized by the Nobel prize in chemistry to Henderson, Frank, and

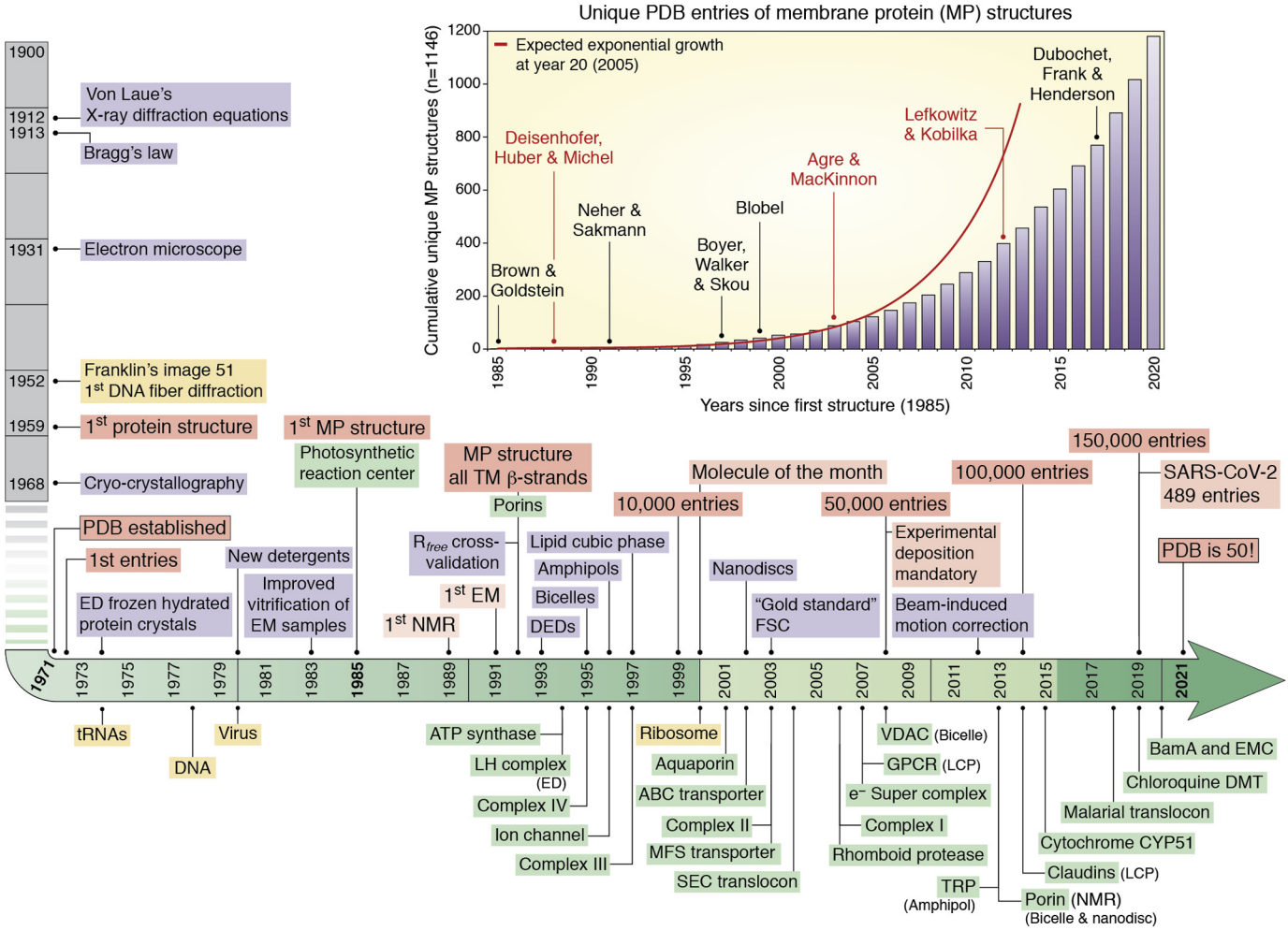

Figure 1. Timeline depicting the progress in structural biology since the PDB was established in 1971 and evolution of membrane protein structural biology since 1985. The curve showing the cumulative total of *unique* MP structures deposited in the PDB (mostly by X-ray crystallography and cryo-EM) as a function of time is adapted from the *mpstruct* website of Stephen White at the University of California, Irvine at https://blanco.biomol.uci.edu/mpstruc/. The *red curve* models the expected exponential growth at year 20 (2005). Dates corresponding to key scientific or technical discoveries that fostered breakthroughs in deciphering and understanding (membrane) protein structure and function are indicated. Some of the first protein structures reported for important classes are indicated along the timeline. Many of the first MP structures were solved in detergent but later in lipidic cubic phase bilayers LCP, bicelles, amphipols, and nanodiscs. ED: electron diffraction. DED: direct electron-counting detector. R_{free}: test set cross-validation for crystallographic refinement. FSC: Fourier shell correlation for cryo-EM single-particle reconstruction validation. LH: light harvesting complex. Chloroquine DMT: chloroquine-resistance drug/metabolite transporter. This list does not pretend to be exhaustive. The *Protein Structure Initiative* from the National Institute of Health in the United States spanned the years 2000 to 2015 (shaded in *light green*). Nobel prizes awarded for discoveries related to MP biology and structure are indicated. The central motivation behind the "Molecule of the Month" (35 MPs since its creation) is to provide a user-friendly introduction to a rich body of data, providing users with a path to get started with finding and exploring the many available structures and thus offering a resource for molecular biology educators and students around the world at http://pdb101.rcsb.org (81).

Dubochet in 2017. Soon after, in 1977 to 1979, the amino acid sequence of bacteriorhodopsin was determined by the groups of Khorana (13) and Ovchinikov (14, 15) using chemical sequencing methods. Agard and Stroud developed computational ways to extend resolution perpendicular to the membrane plane in attempts to reveal the interhelix linker regions to map sequence into the structure from electron diffraction data (16). With Glaeser, who pioneered low-temperature electron microscopy (17, 18), Hayward and Stroud developed a way of aligning microcrystalline regions to extend resolution of the reconstructions to 3.8 Å in-plane resolution (19). As a reflection of the extreme challenges for membrane *versus* soluble proteins, the bacteriorhodopsin structure reached atomic resolution by electron diffraction 20 years after the 1975 breakthrough in 1996 (20, 21) and by X-ray diffraction in 1997 (22) (Fig. 1).

The cytochrome oxidase from bovine tissues (23, 24) and the acetylcholine receptor from electric rays and eels (25–29), respectively, key to oxidative phosphorylation in mitochondria (see *Early breakthroughs in High Resolution Structures of Bioenergetic Membrane Complexes and Lipid Interactions*) and function of the neuromuscular junction, also provided highly important sources of MP complexes. Beginning in 1971, the first 3D surface shapes of the acetylcholine receptor ~300 kDa complex of five homologous subunits in a quasi-fivefold pentameric complex $\alpha\beta\alpha\gamma\delta$ were revealed using low-dose negative stain EM and small-angle X-ray scattering from stacked membranes by Stroud and Unwin (30–35). The

primary sequence, determined initially by Michael Raftery using amino acid sequencing for 50 amino acids of each of the four homologous subunits (28, 36), and in parallel by Jean-Pierre Changeux for the α-chain N-terminal sequence (27, 29), led to the cloning and sequencing of the genes (37). It became clear that like bacteriorhodopsin, it too contained TMs. The right-handed α-helix first delineated by Pauling (38) provided the necessary shielding of all polar groups, namely the carbonyls and amides of the polypeptide backbone. Hence, a sequence of ∼19 hydrophobic amino acids became a recognizable signal for TMs, while strongly amphipathic helices signal membrane surface-seeking helices (39). Remarkable insights followed from the few MP structures already determined, including the finding that their hydrophobic helices formed well-ordered 3D structures in lipid bilayer membranes and their retention even after gentle extraction in amphiphiles and detergents. Yet it took 45 years to obtain the first atomic structures for the acetylcholine receptor. This required screening of many specific genetic constructs of several members of this receptor family (40, 41).

The first atomic resolution structure of any integral MP came from the group of Michel in 1985 (42). After many years trying to crystallize bacteriorhodopsin, Michel and Oesterhelt had appreciated the value of colored proteins such as bacteriorhodopsin. Visible bands on columns aided purification, and more importantly, where the color of unique spectral features reflected the integrity of the MP (43) and signaled for monitoring structural preservation in harsh solubilizing detergents. Using photobacteria as a rich source of photosynthetic proteins, Michel and colleagues determined the first MP structure from crystals that diffracted to atomic resolution (3 Å and then at 2.3 Å). The structure of the *Rhodopseudomonas viridis* photosynthetic reaction center of 145 kDa published in 1984 (42) remains an amazing achievement. It showed that the predominantly hydrophobic α-helices are often longer than enough to span the 40 Å bilayer and can be correspondingly tilted at different angles to harbor the many chromophores that harness the light that supports life. This breakthrough discovery was recognized by the Nobel prize in chemistry in 1988 to Michel, Deisenhofer, and Huber (Fig. 1).

Ion channels in membranes were in the limelight because they accounted for the currents across membranes that are key to the nervous system, as described by Hodgkin, Huxley, and Katz in 1952 (44–46), and beautifully elaborated since then. The key was that Na^+ ions are consistently pumped out of the mammalian cell using energy from ATP hydrolysis, while potassium ions remain inside to balance the electrochemical potential across the plasma membranes according to the Nernst equation. In neurons, however, the need for fast communication relies on rapid conduction of the Na^+ ions inward that is signaled by the release of neurotransmitters at neuronal synapses that depolarize the plasma membranes of the target cell. This is then rapidly followed by release of K^+ ions though highly selective channels that do not leak the smaller Na^+ ions, but restore the transmembrane electrical potential. How is such selectivity accomplished? The alkali metal Na^+ and K^+ ions differ in ionic radius, yet why don't K^+ channels leak the smaller Na^+ ion? The answer came in MacKinnon's finding that bacterial K^+ channels existed and could be extracted for structure determination. In 1998, he reported the first K^+ channel structure (KcsA) from the bacterium *Streptomyces lividans* (47). The structure showed precisely how its selectivity was achieved. The key was in the precise arrangement of a fourfold arrangement of lines of carbonyl oxygens that surround a "selectivity filter" (SF) in the pore entry. They provide the precise counterpart for the normal water hydration shell around the K^+ ion, but were too far apart to provide similar energy balance for the Na^+ ion. MacKinnon was awarded the Nobel Prize in chemistry for this landmark discovery in 2003 (Fig. 1).

The 2003 Nobel prize in chemistry was shared with Agre, recognizing another remarkable discovery, that of water channels (48). In 1985, Benga *et al.* (49, 50) demonstrated that red blood cells had water channels that were inhibitable by mercurials, implying that a sulfhydryl containing protein was responsible. They showed that this was true across many (now all) species, and Nielsen and Agre (51) showed that water channels presented in all cells but for various physiological purposes. They showed that there were 13 different variants in human tissues and named them Aquaporins (AQPs) (52). These were more difficult to recognize than ion channels because there were no electrical properties to measure their activity. Their discovery was made while searching for the well-known rhesus (Rh) factors in red blood cells. They discovered a second major MP in these cells, and then showed that it conducted water, and at a speed up to the diffusion-limited values for a pore of the requisite size (see below). Structures of the aquaporins were determined in 2000 by electron imaging (53) and at atomic resolution by X-ray crystallography (54), showing precisely how these channels excluded passage of protons (H^+) or hydronium ions (H_3O^+), while allowing a single file of water molecules to progress, hydrogen bonded to themselves, and to eight key carbonyl oxygen atoms that act like pitons along the walls of the channel (55).

An outstanding landmark was the structure of the F_1F_o-ATPase by Walker in 1994 (56) and its dynamo-like rotation that harnessed proton gradients to drive the synthesis of ATP in mitochondria. These critical structures of a ∼500 kDa complex provided the amazing link to elucidate the subunit stoichiometry of eight different protein chain types needed to harness proton gradients to produce ATP, the major source of energy in all cells. The discoveries led to the Nobel Prizes in chemistry in 1997 to Boyer and to Walker, who reported the atomic structure of the complex in 1994 (56) (Fig. 1).

The LeuT structure determined by Gouaux's group signaled a new approach to several related transporters that are critical to mental health, responses to neurotransmitters, to therapeutic and street drugs (57–60). This first structure provided a landmark insight into the transporters that are required to repackaged and reabsorb neurotransmitters back into the neuronal cell after release into neurological synapses. Dopamine, serotonin transporters, and others from the same family are all targets of therapies for the critically important spectrum of neurological disorders (61). These transporters are also key

to the control of major mental diseases including such poorly understood disorders as schizophrenia and bipolar disease that together affect ~1/50 persons globally. The PDB now provides a critical catalyst for disciplines that need to "know what we are dealing with" in human health *versus* disease. It creates a scenario in which we can think about and design strategies for modulating therapeutic responses as well as providing an ongoing reminder of how evolution has separated chemistries in order to provide the essence of life.

With increasing impact on prospects for drug discovery, structures of membrane embedded proteases that cleave transmembrane regions to release components are critical. One of the first key examples was discovered by Brown, Goldstein, and colleagues in the critical regulation of cholesterol metabolism. In recognition of their many contributions to the broader field of cholesterol metabolism, they were awarded the Nobel prize in Physiology and Medicine in 1985. They subsequently showed that a membrane-embedded S1P serine protease cleaves the sterol regulatory element-binding protein SREBP. A second intramembrane protease S2P, a zinc metalloprotease, liberates a transcription factor from the N terminus of SREBP that then upregulates cholesterol synthesis. These proteases also coordinate fatty acid synthesis that is also required for membrane biogenesis (62–64). Rhomboid proteases constitute another superfamily of ubiquitous intramembrane proteases involved in a wide range of biological processes and were the first structures of intramembrane proteases to be determined (65). Another critical example of intramembrane proteolysis is the cleavage of the β-amyloid precursor protein (APP) by the β-site cleaving enzyme (BACE1) that converts APP to the pathogenic forms Aβ42/40. Validated by mouse gene knockouts, BACE1 and related γ-secretase (66–68) are thus targets for drugs (69, 70). In spite of extremely difficult clinical trials, these targets remain as promising modulators of Alzheimer's disease (71). Many of the intramembrane proteases destabilize the α-helical regions that characterize transmembrane proteins and often don't rely on specific amino acid side chains for specificity as do the soluble proteases.

As a portent of the impact of electron microscopy, the discovery of the TRPV1 channel structure came after several groups had purified and tried extensively to crystallize Transient Receptor Potential (TRP) channels for many years in seeking the structural basis for their roles in pain sensing (72). As cryo-EM technologies improved, driven by single electron counting "direct detectors" for cryo-EM (73), TRPV1 finally became tractable. This breakthrough by Cheng working with Julius heralded the maturation of cryo-EM applied to MPs (72, 74). It was harnessed by structural biologists particularly with integral MPs where the challenges of crystallography and pressure for discovery were already high (75–80) (Fig. 1).

As a critical library of the molecular bases for MP function, the PDB provides a historical timestamp of the progression in our understanding of these important proteins. It uniquely affords a quantitative visual imprint of the mechanisms of these proteins as the gatekeepers, importers, and exporters of the cell and of organelles within the cell, to the benefit of current and future generations.

Early breakthroughs in high-resolution structures of bioenergetic membrane complexes and lipid interactions

The story of MP structure determination and its profound impact on understanding biological systems is a fascinating illustration of the power of technology development and the value of rapid communication of detailed structural information through the PDB. The problem of transferring MPs from lipid environments to an aqueous phase is substantial and was perhaps initially underestimated due to the prevalent concept that the detergents needed to accomplish this feat were intrinsically disordered and simply required to create a not-necessarily-homogeneous hydrophobic phase to cover newly exposed membrane-embedded regions. Indeed, the importance of pure, well-defined detergents was not immediately recognized, and when it was, the chemistry for creating and purifying these amphipathic compounds was challenging. But gradually it became clear that achieving high-resolution MP crystal structures required a protein sample that had not only native activity and a high degree of purity but also was dependent on the specific structure and purity of the detergent itself for achieving these ends. In many cases, success also depended on retaining a subset of structurally important lipids (82).

Following the advent of the earliest high-resolution MP structure (42), the importance of specific lipid interactions became increasingly apparent: the lipidic detergent molecules as well as native lipids were not just satisfying the need for a disordered hydrophobic phase, but many were actually fitting into defined, conserved slots in the protein structure. The most dramatic illustrations of this fact came initially from the complexes of the electron transport chain. One of the first of these to be obtained at high resolution was the structure of mammalian cytochrome *c* oxidase, also known as Complex IV (83), in which many lipids were resolved, with up to 13 bound to each monomer of ~200 kDa molecular weight. These lipids, characterized by mass spectrometry, were found to be specific not only in their placement, occupying the same positions in each preparation, but also in head group and tail length and degree of saturation (82) (Fig. 2). Many of the same lipid-binding sites were also found to be conserved in structures of bacterial cytochrome *c* oxidase (84–87). In the bacterial enzyme structure, several of the lipid grooves were occupied by detergent (84), demonstrating that the lipid/detergent-binding sites play important and specific roles in the native protein structure. Similar results were found in crystal structures of mammalian and yeast cytochrome bc_1 (Complex III of the electron transport chain) (88–90) and the plant homolog, cytochrome b_6f (91, 92). The retention of resolved lipids in conserved positions emphasizes the importance of lipid and detergent structure in the maintenance of the native state.

As a variety of new, pure, chemically defined detergents became available (93, 94), including the successful sugar-based decyl and dodecyl maltosides (95, 96) and many more designs (94, 97), the field moved rapidly forward despite the

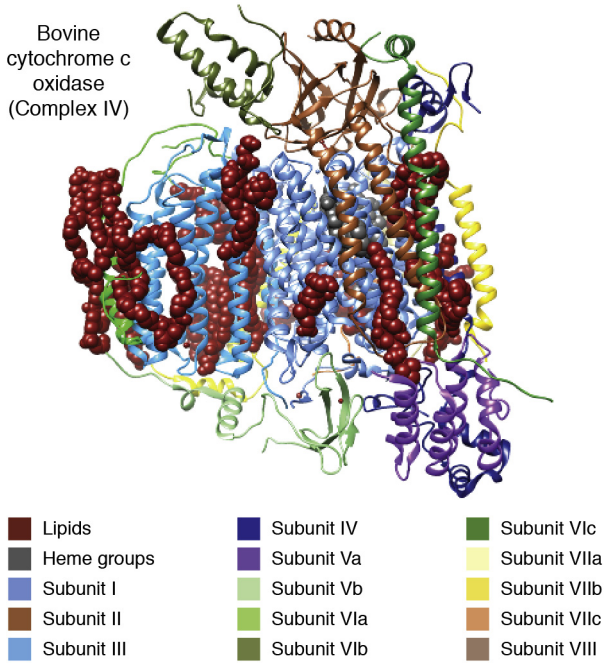

Figure 2. Bovine cytochrome *c* oxidase (Complex IV) monomer with specifically bound lipid. The 13-subunit monomer structure (PDB 2EIL chains N–Z) is shown, with associated lipids in *dark red*, buried hemes in *dark gray*, and membrane region delineated by lipid placement. Subunits: I, *cornflower blue*; II, *sienna*; III, *blue*; IV, *navy*; Va, *purple*; Vb, *light green*; VIa, *green*, VIb, *olive*, VIc, *forest green*; VIIa, *yellow*; VIIb, *gold*; VIIc, *orange*; VIII, *khaki*.

challenging fact that proteins buried in membranes often have flexible conformations required for their complex roles as receptors and transporters (98, 99). Although achieving very high-resolution structures (<2 Å) remains difficult, high resolution is essential where function involves conformational change or depends on the positioning of water. Again, the large multisubunit complexes of the mitochondrial electron transport chain have provided insightful success stories, in part due to their distinct spectral characteristics that aided purification of native forms. These membrane-embedded, spectrally unique proteins were among the first to be structurally defined at high resolution, after the groundbreaking achievement of the bacterial reaction center by Deisenhofer *et al.* (42), and helped move the field of bioenergetics into a new era of mechanistic understanding. The structures of these large complex proteins revealed the exact positioning of their many prosthetic groups, enabled the subunit composition to be confirmed, and allowed meaningful interpretation of spectral changes and fast kinetic analyses of electron transfer events. Their unique UV–visible characteristics were powerful tools for assessing the native state of the purified proteins and for analyzing the rates and ordering of electron and proton transfer events. Without structures that showed water positions and sometimes distinct hydrogen-bonded water chains (84, 100), their kinetics could not be definitively interpreted. High-resolution structures led to the clarification of the proton transfer process, by the Grotthus mechanism, first suggested in 1806 by Theodor von Grotthuss (101, 102) and brought us to our current understanding of how coupling of electron transfer, oxygen reduction, and proton transfer leads to energy conservation in most living organisms. But the supreme success story from the bioenergetics field was capturing the machinery that completes the energy transducing process, the ATP synthase (56) whose structure enabled the deciphering of how rotational motion could be driven by the proton motive force to generate ATP. Beautiful structures of this amazing machine from the Walker group and others, initially without its membrane-embedded region but still the largest asymmetric protein structure known at the time, continue to reveal new and surprising aspects of how energy is transduced (103–105).

With the understanding of the importance of specific lipid interactions came increased efforts to create more lipid-mimetic detergents (97) and to devise methods of retaining native lipids and lipid-like molecules in the purified MPs. One of the successful approaches was creating a lipidic "cubic phase" (LCP) or meso-phase (22, 106, 107) that involved mixing a specific ratio of lipid (such as monoolein) and aqueous phase to form a membranous lipid organization into which the protein could insert, maintaining a membrane-like environment. Otherwise difficult-to-crystallize proteins are able to diffuse and form well-diffracting crystals in this phase, with many success stories (107–109) including bacteriorhodopsin, the thermophilic covalent cytochrome *c*-cytochrome *c* oxidase complex (110), and many GPCRs (111) (see review by Stevens *et al.* in this issue).

Another important achievement stimulated by the need for specific lipid interactions was the design of bicelles and nanodiscs (112, 113) and surrogates to membrane lipids such as amphipols (114, 115). Nanodiscs were created by encircling a small portion of lipid and a captured MP using scaffold proteins derived from apolipoproteins (113) or with chemical polymers such as styrene-maleic acid (116). Bicelles are similar but are self-assembling small model membrane systems edged by bile salt lipids. Bicelles were initially designed to aid in aligning MPs in a magnetic field suitable for NMR analysis (112). Nanodiscs, with added stability and control of size, have been useful for many types of analysis including single-molecule studies, activity studies, and resolving aggregation state issues, as well as facilitating the use of cryo-EM. This latter major technical development has further enabled MP structure determination, with the use of single-particle cryo-EM and the nanodisc method showing great success (117).

A revolution in cryo-EM detector methodology and computational analysis has facilitated new levels of resolution of very large complexes in different conformations even in a single sample (Fig. 1). Again, the electron transfer chain has been the subject of dramatic early success stories, with the most impressive being complex I (118–120), the largest respiratory chain component with 45 subunits. These structures also show specifically bound lipids and reveal the likely proton routes through the membrane segment. Having the Complex I structure was essential, in turn, to solve the atomic resolution structures of supercomplexes up to 1.7 MDa.

The story of supercomplexes of the electron transport chain is a long and controversial one (121–124). It required the new

high-resolution cryo-EM technology to finally convincingly establish their existence. But their functional significance remains much debated (125–127). One key to successfully defining the atomic resolution structures of these unusually large assemblies has been the availability of X-ray structures of all the components, along with sophisticated computational fitting methods. A number of different assemblies have been discovered (117, 121), some with Complexes I-IIIx2-IV, others with two of complex IVs (but not associated as a dimer). A recent version of the human supercomplex denoted the megacomplex (128), which shows an assembled dimer of two supercomplexes and suggests a place into which Complex II, the only missing member of the chain, would fit. The continuing issue of the functional significance of these assemblies remains. The question of what is the true native assembled state and how dynamic it is contributes to this issue (129). A recent finding is that the cytochrome *c* oxidase (Complex IV) monomer form appears to be significantly more active than the dimer (130, 131). Since Complex IV appears as a monomer in all the supercomplexes so far established, this may be revealing an important new regulatory mechanism.

These amazing structures of the respiratory machinery have led the way in illuminating not only unique protein structures and functions, but also the fundamental role of lipid in MP integrity. Their accessibility through the PDB in the most useful formats continues to allow us to test hypotheses and to excite our imagination, stimulating new modeling efforts and new concepts in the field of bioenergetics and pushing the boundaries of our understanding of energy metabolism in health and disease. These early results provided the initial demonstration that it was possible to obtain crystal structures of MPs of even massive dimensions and expanded our understanding of lipid environments that were needed to permit this achievement.

How do membrane proteins accomplish key physiological functions?

Residing in the boundaries of cells and their organelles, MPs and their complexes underpin many important aspects of cell physiology that can be addressed through structures held in the PDB. A representative repertoire of these physiological functions includes how MPs are correctly chaperoned and inserted into their correct host membrane, how some proteins are secreted across membranes. How is osmotic balance maintained by water channels that do not leak any protons or ions, and how ions are specifically passaged by gated channels? How are cells held together in surfaces of the skin and organs with appropriate paracellular transport? The bioenergetic transformations required for ATP synthesis (respiratory electron transfer complexes, ATP synthases), maintenance of membrane potential (P-type ATPases), production and control of ion gradients (ion channels), sequestration and export of key regulators such as calcium ions (sarcoplasmic reticulum and plasma membrane calcium ATPases), transport of nutrient, toxin and xenobiotic through primary active transporters driven by ATP hydrolysis (ABC transporters) and secondary active transporters driven by proton plus electrochemical gradients. We summarize the MFS transporters and also describe viroporins (VPs), small viral MPs that form channels necessary for virulence. These structures offer routes to drug discovery that are often broader than simply inhibition, such as modulation or even enhancement of activities. While the examples we have chosen illuminate the value of the PDB in providing structure–function insight into basic biological phenomena and their possible application, our goal is to provide an instructive vision rather than a comprehensive oversight.

How are membrane proteins targeted, inserted, and folded correctly?

How do MPs come to be? How do MPs find their final destination and fold properly in a lipid bilayer? This "*chicken and the egg*" question has been partially answered over the last 50 years since the PDB was established in 1971. Like all proteins, MPs begin their journey as nascent polypeptides that emerge from the ribosome with their final destination encoded in their primary structures. Following the discovery that proteins have intrinsic signals encoded in several amino acids near the emergent N terminus, that govern their transport and localization in the cell by Sabatini and Blobel in 1971 (132), a large body of biochemical and functional studies have identified the machinery and dissected the steps involved in the sorting, targeting, and chaperoning of MPs through the cell toward their final destination. Experimental validation of the "signal hypothesis" led to powerful and widely used computational methods aimed at predicting the diverse protein-sorting signals (133) for subcellular compartments or organelles such as the endoplasmic reticulum (ER), mitochondria, lysosomes or chloroplasts, and other plastids in all living organisms.

The structural biology of MPs has not only provided remarkable insights into the architecture and mechanisms of action of channels, transporters, pumps, and receptors but also elucidated key aspects of the molecular machinery involved in their biogenesis: from the targeting and sorting as they emerge from the ribosome until their translocation across or insertion into biological membranes. The translocation/insertion step is catalyzed and assisted by translocons, a general term referring to the MP machinery facilitating this process. The Sec61/SecY *universal* translocon (Sec standing for *Secretory*) is central to the translocation of most membrane and secreted proteins while other "specialized" translocons can be highly substrate-specific.

Most proteins are thermodynamically stable in their native state. The process of translocating a polypeptide across or into a membrane is thermodynamically unfavorable. This is due to the large entropic costs associated with *i)* moving polar or charged amino acids across the inner hydrophobic part of the lipid bilayer and, conversely, *ii)* moving hydrophobic amino acids across the outer membrane surface layers consisting of the phospholipid polar head groups (134, 135). It is particularly significant for integral MPs with large soluble loops or domains and complex topological arrangements of hydrophobic TMs. In the last two decades, the PDB has been the repository of increasing numbers of structures of soluble and membrane proteins that help MPs reach their final destination and fold

properly, thus contributing to deciphering the general principles and mechanisms underlying "protein-assisted" MP biogenesis.

The signal sequence-dependent universal targeting pathway of membrane proteins

Most MPs follow the Signal Recognition Particle (SRP) dependent cotranslational targeting pathway (136). At the core of this evolutionarily conserved machinery is the catalytic and structural SRP RNA associated with the SRP54 protein. It is involved in complex assembly, signal sequence recognition, and nascent chain transfer from the ribosome to the Sec61/SecY translocon (Fig. 3*A*). The presence of an RNA component hints at its ancient origin when RNAs played more prominent roles as catalysts and structural scaffolds in primordial cells (137). Targeting relies on three crucial steps; *(i)* the interaction between the Methionine-rich (M) domain of the soluble SRP54 protein that recognizes and binds N-terminal "greasy" signal sequences as they first emerge from the ribosomal tunnel (138, 139), *(ii)* the GTP-dependent interaction between the NG (for N-terminal and *ras*-like GTPase) catalytic domains in SRP54 and the homologous domains of its membrane-associated SRP receptor (SR) (140, 141) to form a targeting complex (TC) at the ER or plasma membranes resulting in *(iii)* the delivery of the ribosome-nascent chain (RNC) from the SRP54/SR complex docked to the translocon upon structural rearrangement of the SRP54/SR core on its

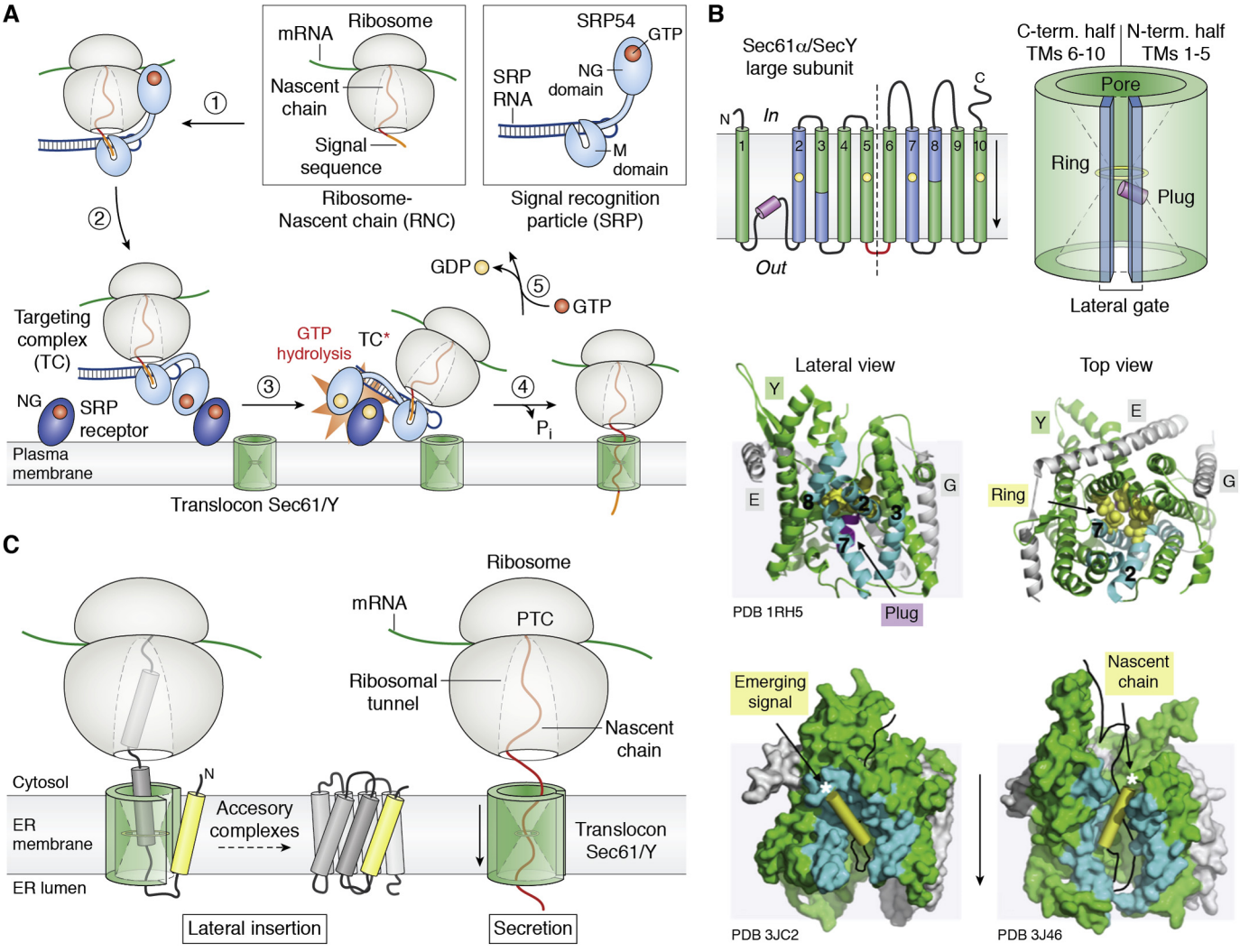

Figure 3. The machinery of the cotranslational secretion/membrane insertion pathway. *A*, the SRP-dependent protein targeting pathway (in bacteria). (1) SRP binds the signal sequence as it emerges from the RNC. (2) GTP-dependent formation of the TC between SRP and its SR receptor at the membrane delivers the RNC to the translocon (3). The translocon stimulates rearrangement and GTP hydrolysis within the TC and transfer of the RNC from the now activated TC* to the channel (4) for subsequent secretion or insertion of the translated protein. (5) GTP displaces GDP in SR and SRP to reset the targeting machinery. *B*, topology and schematic structure of the protein-conducting Sec61α/SecY large subunit. The ring, plug, and lateral gate of the channel open in order to accommodate a TM and provide an exit path into the lateral plane of the bilayer. The structure of the closed archaeal SecY (PDB 1RH5) channel shows where the lateral gate is closed and the pore occluded by the plug helix (*magenta*) and sealed by the ring of hydrophobic residues (*yellow*). Structures of mammalian Sec61 (PDB 3JC2) and bacterial SecY (PDB 3J46) translocons engaged with a nascent chain show the signal sequence (*yellow*) and nascent chain (*black*) emerging from the lateral gate. *C*, models for the lateral insertion of integral MPs in the lipid bilayer or secretion across the membrane. TMs of nascent integral MPs initiate their folding within the ribosome tunnel before moving to the Sec61/SecY translocon. In contrast, an unfolded nascent chain of a protein secreted across the membrane might not trigger opening of the lateral gate. The ring of hydrophobic residues at the constriction of the hour glass-shaped pore maintains a tight seal around the nascent chain. PTC, peptidyl-transferase center of the ribosome. Accessory complexes of Sec61/SecY are required for the insertion and chaperoning of multipass MPs.

SRP RNA scaffold and the channel-stimulated reciprocal GTP hydrolysis that dissociates SRP from its receptor (142, 143) (Fig. 3*A*).

The conserved heterotrimeric channels, Sec61$\alpha\beta\gamma$ in eukaryotes or SecYEG in prokaryotes, act as portals and gatekeepers for the insertion of most of the MPs and secreted proteins. The large subunit forms the protein-conducting pore itself and is composed of ten TMs, where the first five TMs are related to the second five TMs by a twofold quasi-symmetry in the plane of the membrane (144). This internal pseudo-symmetry divides the channel into two halves articulated around a hinge between TMs 5 and 6 (Fig. 3*B*). This channel has a unique architecture with two conducting paths oriented perpendicular to each other: An hour-glass-shaped pore for the secretion of proteins across the membrane and a lateral gate opening to chaperone TMs of integral MPs destined for insertion into the bilayer and delineated by TMs 2, 3, 7, and 8 (Fig. 3*C*). The protein-conducting pore is occluded by a short plug helix and sealed by a ring of hydrophobic residues (Leu, Ile, and Val) at its constriction point that prevent leakage of water and ions (145). Structures of free SecY channels with their lateral gates in different states (146, 147) and structures of Sec61/SecY channels engaged with different RNCs beautifully illustrate the insertion path followed by nascent TMs of integral MPs during their biogenesis (148–150). The funnel-shaped cytoplasmic vestibule of the translocon is large enough to accommodate incoming folded helices while soluble loops can extend at the interface between ribosome and channel. The α-helical signal sequence of the nascent chain emerges, opening the lateral gate as it displaces and supplants TM2. As lateral gate TMs shift, the ring and plug helix are widened and displaced/unfolded, respectively, to make room for this nascent chain that contains a folded secondary structure (Fig. 3*B*).

While the Sec61/SecY protein-conducting channel provides a clear path across or into the membrane, it is not the sole arbitrator of MP insertion topology. Proteins start to fold as soon as space allows, and the ribosome also plays an important role as the nascent chain can either fold or not, while it elongates from within the ribosomal exit tunnel into the Sec61/SecY channel (151, 152). Thus, *in vivo*, rather than start folding inside a lipid bilayer environment, MPs begin this process within the ribosome tunnel and the Sec61 translocon, where secondary structure elements can form and associate into smaller kernels of tertiary structure (153) and where, perhaps more importantly, the insertion topology is assigned as the nascent polypeptide enters into the membrane plane by lateral diffusion. Prokaryotic and eukaryotic integral MP topologies generally follow the so-called "positive inside" rule for TM orientation as established by Sipos and von Heijne (154). In this regard, the Sec complex associated with a ribosome forms an *Anfinsen* cage around the nascent chain, surrounding the nascent polypeptides with a protective "enclosure" and environment where folding occurs unhindered, thus preventing aggregation or misfolding (155). Although the folding steps occurring in Sec61 remain poorly understood, lipids do play a role through direct interactions with the nascent MP in the Sec61 channel (156) (Fig. 3*C*).

Numerous structures of Sec61/SecY complexes with other important "accessory" MP complexes such as the Sec62/63, TRAP (TRanslocon-Associated Protein), and OST (Oligo-Saccharyl Transferase) (157) in eukaryotes or SecDF (158) and YidC (159) in prokaryotes have been solved. These structures reveal that the Sec61/SecY translocon is part of a highly dynamic "MP assembly line," sometimes referred to as the *holo* translocon, with "quality control" mechanisms (160). The human genome encodes about 2500 multipass MPs (such as GPCRs, ion channels, and ABC transporters) of considerable topological complexity. Lateral insertion and folding of such polytopic MPs require the intervention of Sec61-accessory complexes such as the Endoplasmic Reticulum membrane protein complex (EMC). Although our understanding of the mechanisms governing protein secretion and insertion has progressed, the specifics of MP complex assembly into homo- or hetero-oligomers still elude us.

The targeting of tail-anchored proteins and new paradigms in membrane protein biogenesis

Most membrane-inserted proteins harbor an N-terminal signal sequence, which defines the main route for protein targeting and secretion/insertion. A significant subset of MPs uses different routes and distinct protein machineries. Tail-anchored (TA) proteins (proteins with a single C-terminal TM anchor) constitute about 5% of any given eukaryotic proteome and are targeted with exquisite specificity to the diverse organelles (*e.g.*, ER, mitochondria, lysosomes) within the eukaryotic cell. The yeast Guided-entry of tail-anchored proteins (Get) pathway, known as TRC in mammals, was discovered in 2008 (161). It represents a perfect example of a posttranslational MP targeting system in the ER. TA proteins do not follow the SRP targeting pathway because they lack an N-terminal signal sequence. Their targeting signal consists of their single C-terminal hydrophobic TM, which only emerges from the ribosomal channel once the rest of the polypeptide has been synthesized. In yeast, the Get pathway involves at least six proteins. Among these, the soluble ATPase Get3 and the two MPs Get1/Get2 are involved in the final steps of TA targeting to, and insertion into, the membrane, respectively (162, 163, 164). At the late stage of Get targeting, a Get3 dimer binds the TA of a newly translated TA protein in a hydrophobic groove rich in flexible methionine residues (165), much akin to the M domain of SRP54. The long N-terminal cytoplasmic end of Get1 captures the Get3/TA complex and targets it to the membrane where the cytoplasmic coiled-coil extension of Get2 interacts with the docked Get3/TA complex to stimulate the release of its TA cargo before insertion into the membrane (166) (Fig. 4*A*).

The exact mechanism of TM insertion by Get1 (with Get2) has yet to be elucidated. However, Get1 is a member of the YidC/Oxa1/Alb3 superfamily of proteins that insert proteins into membranes in bacteria, mitochondria, and chloroplasts, respectively (167). This superfamily not only includes the bacterial insertase YidC but also the widely conserved ER membrane complex (168–170), which is involved in the cotranslational insertion of polytopic MPs, such as GPCRs, in

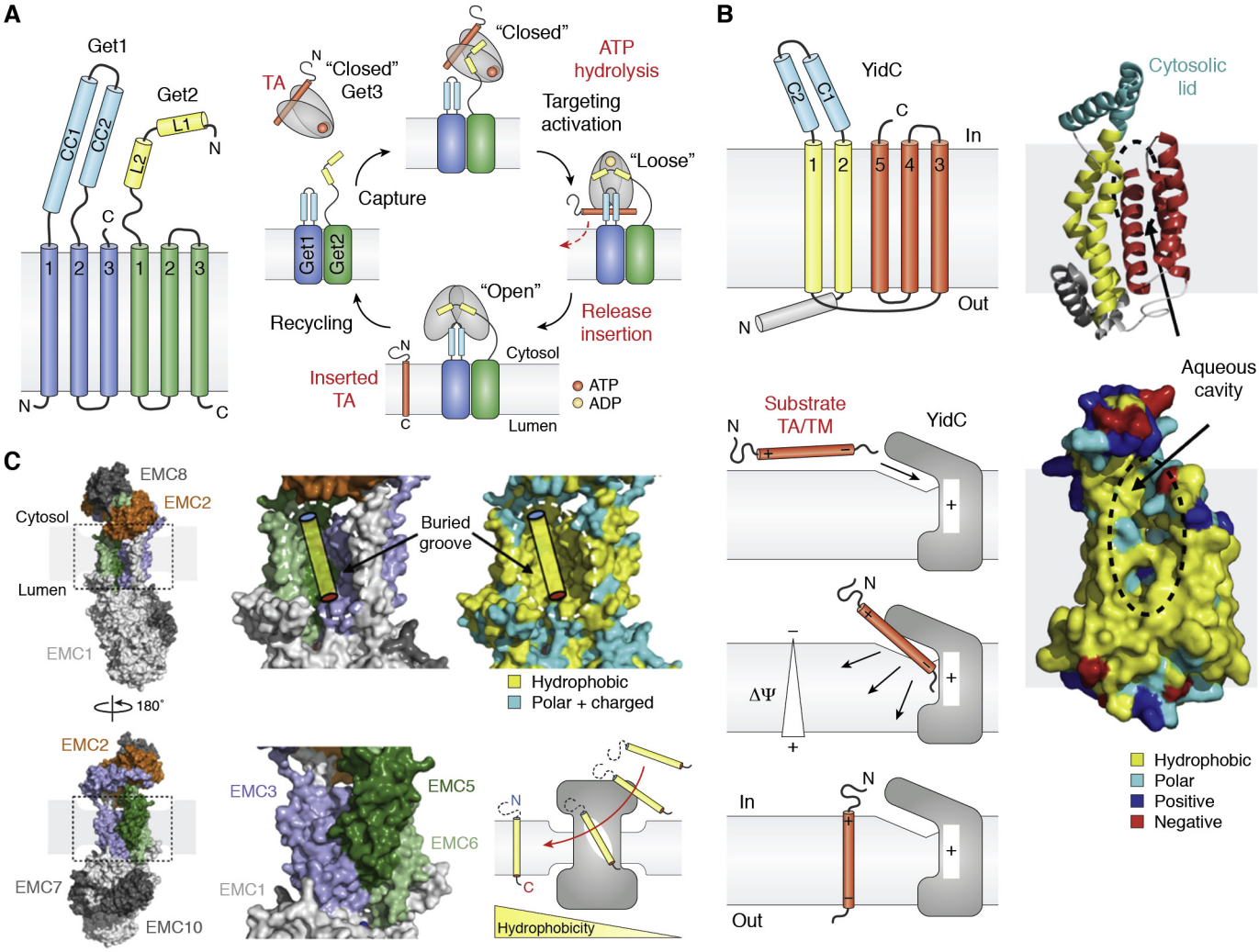

Figure 4. The Guided-entry of tail-anchored proteins pathway. *A*, simplified mechanism of the Get pathway and topology of proteins Get1 and Get2. *B*, bacterial YidC structure (PDB 6AL2) showing a lipid-exposed hydrophilic groove between TMs 1, 2, and 5 that can be cross-linked to nascent TM-containing substrates. A simplified mechanism for YidC (and possibly Get1/2)-assisted insertion of TMs and TA segments into the membrane. For bacterial YidC, membrane thinning and membrane potential facilitate and drive insertion. *C*, the EMC (PDB 6WW7, 6WB9, 6Z3W) translocates multipass MPs and some TA proteins. TMs follow a gradient of increasing hydrophobicity from the hydrophilic cytosolic vestibule into the intramembranous hydrophobic groove acting as a lateral opening for insertion into the lipid bilayer.

association with the Sec61 translocon, and also the post-translational insertion of some more hydrophilic TA proteins. In particular, EMC assists Sec61 with the insertion of MPs with complex topologies and destabilizing features in their TMs such as charged residues (171). Remarkably, the structure of another Sec61-associated complex containing five accessory factors (TMCO1-CCDC47 and Nicalin-TMEM147-NOMO), distinct of EMC but also involved in the biogenesis of hundreds of multipass MPs was recently solved (172). TMCO1 is also a member of the YidC/Oxa1/Alb3 superfamily. The structures of these machineries involved in complex MP biogenesis were determined within the last 2 years.

Unlike the posttranslational insertase Get1/2, YidC, and EMC cooperate with the SecY/Sec61 translocon for the insertion of MPs. Based on the structure of bacterial YidC (173), a model for the insertion of TMs and TAs has emerged. A "hydrophobic slide" is created between TMs 1, 2, and 5, while the hydrophilic environment generated by the groove can recruit the extracellular regions on substrates into the low-dielectric environment of the membrane, thus facilitating insertion (Fig. 4*B*). Furthermore, the protein architecture and its interactions with membrane phospholipids result in an asymmetric thinning of the membrane on the cytoplasmic side near the aqueous membrane cavity (174).

The nine-subunit structure of EMC reveals that TMs from subunits EMC3, 5 and 6, form a lumen-sealed lipid-exposed intramembranous groove large enough to accommodate a single TM, similar to YidC. Furthermore, protein translocation involves a cytosolic hydrophilic vestibule (EMC2/EMC8-9) at the interface between EMC2 and EMC3, EMC5 and EMC6, and methionine-rich loops on EMC3 to probably accommodate the bulkier and more hydrophilic ends of TA proteins and capture their hydrophobic TA, respectively. EMC uses spatially distinct yet coupled regions including lipid-accessible membrane cavities and cytosolic surfaces to function as an insertase for TA proteins and a protein holdase-chaperone for complex

polytopic MPs (175). Increasing hydrophobic interaction between the hydrophilic cytoplasmic vestibule and the buried hydrophobic membrane groove guides the translocating TAs for insertion (170). Membrane thinning around the EMC further lowers the energy barrier for translocation (Fig. 4*C*). While the Get machinery targets client proteins with highly hydrophobic TAs, the EMC seems to prefer TA proteins with lower hydrophobicity. Thus, triage of TMs and TAs into the different insertion machineries (*i.e.*, EMC *versus* Get) relies, at least in part, on their relative hydrophobicity (171, 176). These recent structures illustrate the roles of electrostatics, hydrophobicity, and protein architecture in establishing the topology of TM translocation through shaping and thinning of the surrounding membrane to facilitate insertion.

Folding it backward: The case of β-barrel transmembrane proteins

Helical MPs are ubiquitous in prokaryotes and eukaryotes. Transmembrane β-barrel proteins constitute another functionally important class of integral MPs composed mostly of membrane-spanning β-strands; they are exclusively found in the outer membranes of Gram-negative bacteria and the membranes of mitochondria, chloroplasts, and other plastids in eukaryotes. The transmembrane β-barrel scaffold is based on an antiparallel sheet of β-strands (usually an even number) arranged into a cylindrical structure delineating a central and functional pore or cavity. The first transmembrane β-barrel protein structures, PhoE and OmpF, were solved in 1991 to 1992 by the Jansonius/Rosenbusch and the Schulz groups (177, 178). Because of their cellular localization, the biogenesis of β-barrel proteins is essentially post-translational (179). What about membrane insertion of β-barrel proteins?

The bacterial β-Barrel Assembly Machine (BAM) (180), related to the mitochondrial Sorting and Assembly Machinery, accelerates folding without using exogenous energy (such as ATP or membrane potential). A recent cryo-EM structure (181) reveals a "*templating*" mechanism based on sequential β-augmentation for the folding and insertion of β-strands into membranes and the growth of the cylindrical β-barrel structure. The BAM complex is composed of the membranous subunit BamA and four lipid-binding soluble proteins (BamBCDE) (180, 182). The central component BamA is itself a β-barrel protein that forms a closed 16 β-stranded antiparallel barrel when not engaged with a substrate (Fig. 5*A*).

The structure of BamA trapped with a model β-barrel substrate (a modified version of its barrel) shows that the active BamA barrel is splayed open along its lateral gate, exposing the two N-terminal strands β1 and β2. The N-terminal β1 strand no longer hydrogen bonds with C-terminal strand β16, as seen in the resting structure of folded BamA. Instead, it forms six hydrogen bonds with the C-terminal strand β16 of its barrel substrate protein (Fig. 5*B*). However, the resulting hybrid barrel is asymmetric since the C-terminal strand β16 of BamA does not pair with the N-terminal β1 strand of the barrel substrate. By binding the N-terminal edge of BamA as an extended β-strand, the C terminus of the substrate forms a new edge that serves as a template to guide binding and folding of the subsequent β-strand by β-augmentation. As a consequence, folding is directional and proceeds from C- to N terminus (Fig. 5*B*). Interestingly, the six hydrogen bonds between strands in the membrane environment form a very stable interface between the two proteins, BAM and the nascent β-barrel substrate. Such stability enables folding but results in a high kinetic barrier for substrate release once folding is complete. Sequence features at each end of the

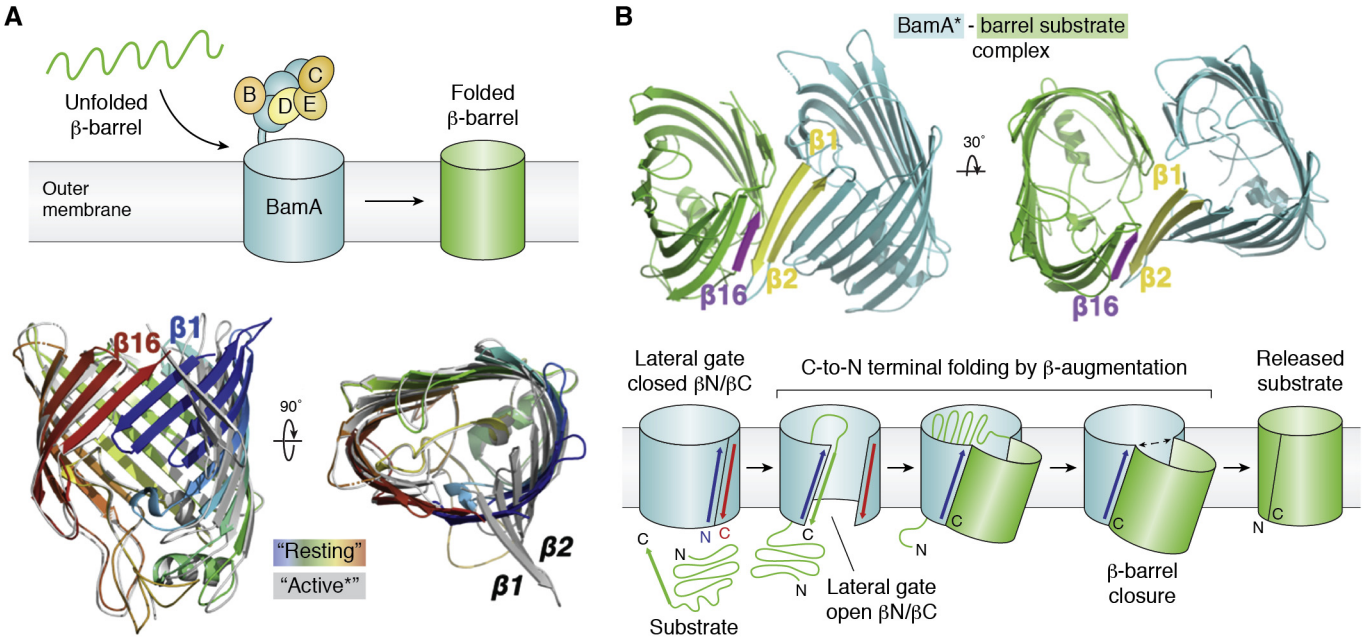

Figure 5. Bacterial β-barrel membrane proteins biogenesis by BAM. *A*, the BAM complex catalyzes posttranslational insertion of transmembrane β-barrel proteins from the periplasm into the bacterial outer membrane. Superposition of the β-barrel domain of BamA in the resting (PDB 4N75) or active (*) states (PDB 6V05) with a nascent β-barrel protein. *B*, C-to-N terminal β-barrel folding by sequential β-augmentation.

substrates overcome this barrier and favor substrate release by stepwise exchange of hydrogen bonds (181). More recently, two cryo-EM structures of the Sorting and Assembly Machinery, structurally and functionally related to BAM, also revealed an opening of the lateral gate as substrates get inserted and suggested that entire precursor proteins might fold using a β-barrel switching mechanism (183, 184).

The general dogma is that translocons must harness some form of energy to lower the energetic barrier associated with the translocation of a polypeptide and to function as translocases and/or insertases. The most common energy sources for such processes are the binding and hydrolysis energy of nucleotides (*i.e.*, ATP and GTP) and also proton gradients or membrane potential that can impart directionality. In particular, ATPases such as the SecA ATPase, which energizes the SecY-dependent posttranslational protein secretion in bacteria (185), or AAA^+ ATPases specific to secretion systems found in pathogenic bacteria or protozoa, couple ATP binding and hydrolysis energy to generate mechanical forces used to unfold and translocate their substrates. These translocons use so-called polypeptide "clamps"; they engage the polypeptide main chain nonspecifically and keep it unfolded as it is threaded through a proteinaceous pore traversing the membrane. The recent structures of the EMC and BAM machineries reveal in exquisite detail how protein-assisted translocation and insertion combine mechanisms such as *membrane thinning*, *hydrophobic sliding*, and *protein-templating* to decrease the energetic barrier associated with translocation across or insertion into the bilayer of a polypeptide without apparent expenditure of energy.

Most extreme translocation: Effector protein and virulence factor secretion in pathogens

The journey of some secreted proteins across the cell can be more arduous in the extreme cases of intracellular pathogens such as the deadly malaria parasite *Plasmodium falciparum (Pf)*. Malaria is a disease mentioned in Sumerian and Egyptian ancient texts (1550 BC). In 2018, *Plasmodium* infected some 230 million humans and claimed about 435,000 lives. Upon infection of its human host, this obligate intracellular parasite dwells within a parasitophorous vacuole derived by invagination through the membrane of infected hepatocytes or erythrocytes. *Plasmodium* is a master cell renovator; it exports hundreds of effector proteins and virulence factors across the PV membrane into the host cell in order to gather nutrients, eliminate waste, persist and thrive in its host, and evade the immune response (186, 187). Some of these exported proteins belong to a *Plasmodium* "transportome" (188)—a compendium of transporters, pumps, and channels involved in ion flux, nutrient/metabolite import, and waste/drug efflux within the parasite and the infected host cell such as the hexose transporter *Pf*HT1 and the chloroquine-resistance transporter *Pf*CRT. In 2009, de Koning-Ward *et al.* (189) discovered the complex responsible for vacuolar secretion and named it *Plasmodium* translocon of exported proteins (PTEX) (Fig. 6*A*).

PTEX is composed of three essential core subunits: The pore-forming protein EXP2, the AAA^+ protein unfoldase HSP101, and the adaptor PTEX150. Two accessory subunits, PTEX88 and TRX2, complete the assembly (190, 191). Its cryo-EM structure revealed the architecture of its ternary core (192), including the novel MP structure of EXP2 that forms the protein-conducting pore (Fig. 6*B*). Most of the effector proteins are essential to parasite survival. Thus, the vacuolar secretion pathway, with its *Plasmodium*-specific and unique vacuolar translocon, provides prime targets for the design of novel antimalarial drugs (191, 193, 194).

The 1.6 MDa PTEX complex solved by Ho and Beck was obtained from endogenous sources, expressed at its natural (low) abundance, and extracted directly from human red blood cells infected with *Plasmodium* parasites CRISPR/Cas9-edited to express HSP101 bearing an affinity purification tag at its C terminus. While purification from endogenous sources is not a novel strategy *per se*, the clever use of CRISPR/Cas9 gene editing by Beck and Goldberg (195) on an "unruly" organism such as *Plasmodium*, traditionally recalcitrant to facile genetics, opens new frontiers to tackle the structures of scarcely available complex molecular machines that could not be reconstituted using more traditional approaches based on recombinant expression. Furthermore, extraction of the endogenous PTEX structure in the presence of the slowly hydrolysable nucleotide analog ATPγS allowed the complex to be caught "in the act" under two distinct states engaged with endogenous cargo trapped in the translocation channel of the HSP101 ATPase (Fig. 6*B*). It provided valuable insights into the mechanism of effector secretion. PTEX is an example of purely posttranslational translocon and, in contrast with Sec61/SecY, it seems devoid of insertase function and exclusively provides a path for posttranslational secretion across the vacuolar membrane (191). This example illustrates the power of a "shotgun" approach combining cryo-EM (or cryo-ET) and Mass-Spectrometry-based proteomics to isolate, identify, and resolve ensembles of large macromolecular assemblies in complex mixtures such as crude cellular extracts (196).

Each of these structures brings us back to our "*chicken and the egg*" problem. During the emergence of life from primordial macromolecular systems, it is likely that primitive MPs spontaneously inserted in simple lipidic bilayers. Spontaneous insertion of very hydrophobic TMs has been observed for MPs with relatively simple topologies. The emergence of a translocon with its accessory factors and protein quality control machinery probably paralleled increasing complexification of MP folds, cellular compartmentalization, and the associated evolutionary pressure to evolve more sophisticated and dynamic proteinaceous systems to catalyze and chaperone their folding and proper biogenesis. In-depth analyses of the YidC and SecY structures and of the requirements for the biogenesis of different classes of integral MPs and secreted proteins shed light on the origins and evolution of the most ancient "translocators." Lewis and Hegde speculate that SecY originated as a YidC homolog formed of two hydrophilic grooves juxtaposed within an antiparallel homodimer (197). The proposed "molecular filiation" between the two major MP biogenesis factors offers a new perspective on a fundamental step in the evolution of macromolecular biological systems and cells.

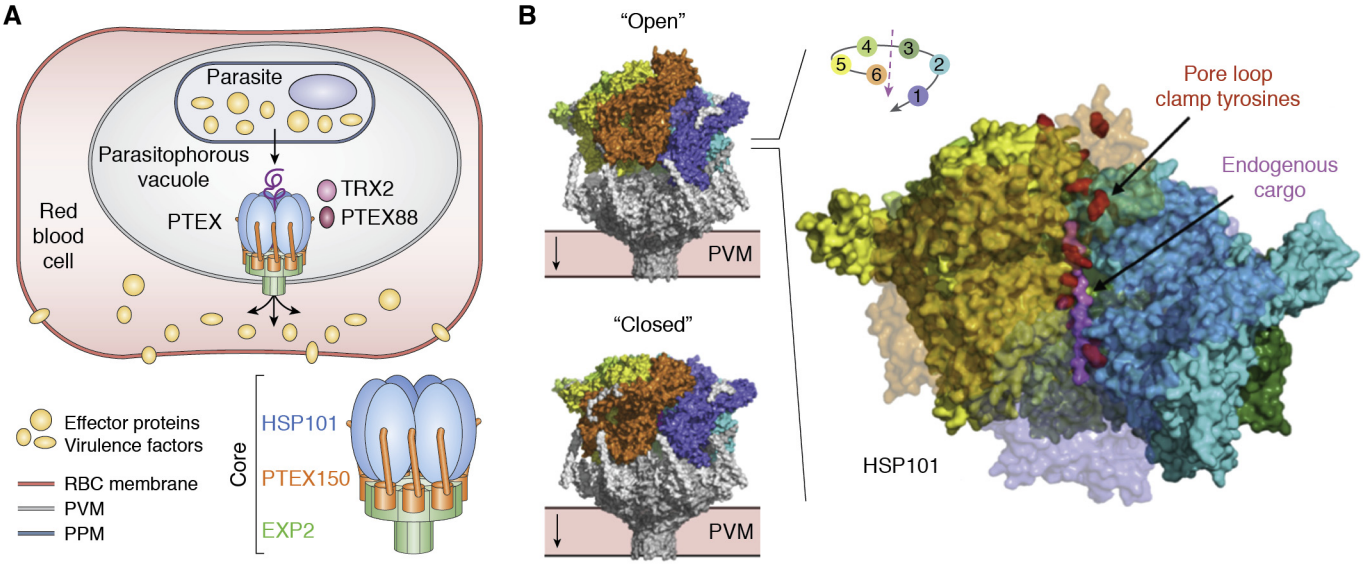

Figure 6. The *Plasmodium* translocon of exported proteins acts as the essential nexus for protein export and host cell remodeling by the malaria parasite. *A*, effector proteins and virulence factors are secreted across the encasing parasitophorous vacuole membrane (PVM) inside the host red blood cell (RBC) by the genus-specific *Plasmodium* Translocon of Exported proteins (PTEX) whose core is composed of subunits EXP2, PTEX150, and HSP101. *B*, cryo-EM structures of two distinct states (PDB 6E10, 6E11) of the ternary PTEX core complex. Both are trapped with *endogenous* cargo polypeptide engaged in the translocation path of the spiral staircase hexameric assembly of HSP101 (rainbow subunit-coloring pattern) sitting atop of the membrane inserted PTEX150/EXP2 tetradecamer (*gray*). The labile auxiliary subunits TRX2 and PTEX88 were not present in the final reconstructions. Slice-through view of the HSP101 ATPase in the open state showing endogenous cargo (*pink*) clamped by each tyrosine of the pore loops (*red*) arranged into a spiral staircase.

Water transport by aquaporins and ammonia gas transport by the Rh family

The AQPs provide a striking example of how, over two decades, the PDB coordinated structures into functional knowledge. Because life depends on water, regulation of water movement across cells without leakage of any ions or protons is an essential function. It is encoded in a family of highly regulated water channels that are expressed in the organ, tissue, and cell-specific locations (198). By the 1960s, there was evidence that water permeated membranes faster than through lipid bilayers. Red blood cells conducted water with a low activation energy barrier, while oocytes had very high resistance to conductance. Benga and colleagues showed in 1986 that this water conductance could be inhibited by *p*-chloromercuribenzoate. The reversal of this inhibition by reducing agents implied a protein channel that contained a sulfhydryl accessible to mercury ions (49, 50, 199). While radiation inactivation correctly predicted a channel of ~30 kDa in size (200), Agre (201), in a search for Rh blood group antigens in highly porous red blood cells, found two protein bands—one of 32 kDa and the other 28 kDa. Expression cloning in frog oocytes of the 28 kDa "Channel-like Integral membrane Protein of 28 kDa" (CHIP28) (202, 203) from an erythroid library showed that transfected oocytes responded to reduced osmolarity by swelling and lysing, while control oocytes barely swelled at all (48). The gene responsible was shown to be similar to others in microbes and plants (204), and Agre named the family the Aquaporins. CHIP28 became AQP1. It was shown to be a tetramer (205, 206) with a permeability estimated at a remarkable 3×10^9 water molecules per second (207, 208), which equated to the diffusion limit for a pore the size of a single file of water molecules. More AQP homologs were discovered and the family provided essential functions represented in all living species from bacteria to humans (198, 209).

In the same family, the aquaglyceroporins that conduct small organic alcohols including glycerol as well as water are interesting because of the clear need for this function (210). AQP3 is permeable to glycerol and water while AQP9 has even broader specificity. There is also an ion-conducting AQP. AQP6 conducts water poorly and is unique in conducting ions through the same water-conducting channel, supported by altered sequence in the pore, or possibly through the fourfold axis of the tetramer (54, 211).

The first atomic structure of an AQP was determined in 2000 for the Aquaglyceroporin GlpF by X-ray diffraction at 2.2 Å resolution (54). AQP1 was defined by electron crystallography of 2D crystalline arrays of AQP1 at 3.8 Å resolution (53), followed closely by the X-ray structures of AQP1 at 2.2 Å (212, 213) and bacterial AqpZ at 2.5 Å (214). The structures showed AQPs to be fourfold symmetric tetramers in which the water channels lie within each monomer and not between monomers or along the symmetry axis (Fig. 7). There are now ~60 structures reported in the PDB with some at sub Å resolution (215). AQP structures AQP0 and AQP4 were determined by X-ray crystallography (55, 216) and by electron crystallography (217, 218) of natural 2D crystalline arrays of the tetramers that are found in certain specialized environments. Natural arrays from an ordered region of the eye lens led to ~1.9 Å structure for AQP0 that showed the position of lipids that supported the crystalline array in membranes.

The structures show an uninterrupted line of permeant waters within each monomeric channel across the entire membrane. These water molecules are hydrogen bonded to

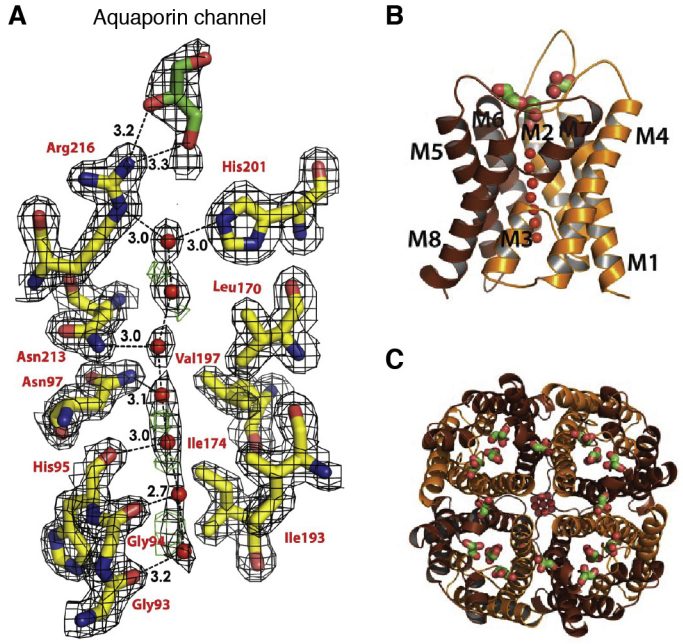

Figure 7. The aquaporin channel. *A*, line of waters in human AQP4 at 1.8 Å resolution (PDB 3GD8). *B*, single monomer of AQP4. *C*, the tetrameric arrangement in all AQPs places four channels in each tetramer. Panels derived with permission of the PNAS from Ho *et al.* (55).

each other in line and sideways as hydrogen bond donors to a line of eight carbonyl oxygens of successive amino acids—like pitons that form a line all the way to and from the polarized central pair of water molecules (219, 220). Substrates entering from the outside meet an SF formed by a highly oriented guanidinium side chain of arginine that projects hydrogen bond donors and positive charge into the pore and against a hydrophobic aromatic corner opposite the arginine. This region, termed the aromatic arginine (aR) region SF, distinguishes between water alone and water plus other small substrates. Aquaglyceroporins are specialized by two aromatic side chains that form a hydrophobic corner opposite to the aR in this region to conduct small organic neutral molecules including glycerol and urea as well as water. While compensated for by surrounding acidic side chains, the aR positive charge presents an essential electrostatic barrier to passage of all positive ions (Fig. 7*A*).

The central channel waters are oriented by two highly conserved asparagine N-H hydrogen donors within highly conserved -asparagine-proline-alanine- (-NPA-) regions that abut each other in a "fireman's grip" structure, to force the central water molecules to be hydrogen bond acceptors and orient their hydrogens always away from the center. This is augmented by the positive dipoles of the two half helices that begin with the -NPA-region and stretch diagonally outward to the two surfaces of the bilayer. This arrangement polarizes the central water molecules so that their hydrogen atoms point away from the center, then polarizing the entire line of water molecules out to the membrane surface (54, 215, 221). Early simulations over ~300 ps time scales validated these proposals, showing that "turning off" the helix dipoles reduced the tendency to bipolarize the channel waters (219). The absolute rejection of any ions, even hydronium ions or protons, through the line of waters has attracted confirmatory molecular dynamic (MD) simulations up to over 100 ns using increasingly sophisticated empirical valence bond and electrostatic approaches (222, 223).

The 13 AQPs in humans each have highly differentiated roles in physiology. This is even more so in plants with 38 AQPs in *Arabidopsis thaliana* (224)! Genetic knockouts allowed insight into the unrecognized importance of some of these aquaporins (225). AQP structures became robust models for MD simulations due to their range of conductance and specificities for small neutral organic molecules. MD simulations and electrostatic calculations allow understanding of the impact of dynamics, electrostatics, and dehydration penalties in Biology, readily accounting for water conductivity at close to the experimental levels of $\sim 10^9$ molecules per second, and specificities *e.g.*, how conversion of one histidine in the water-only aromatic arginine SF to a hydrophobic side chain allows small neutral organic compounds to pass in specific aquaglyceroporins.

How do the AQPs exclude passage of hydronium ions or protons hopping through the line of waters by the Grotthus mechanism (101, 102)? The theoretical energy profile seen by a proton or a hydronium ion passing through the channel shows that the highest barrier is an electrostatic one where the two -NPA-regions meet, along with the helical dipoles that augment the polarization of the central water (226–229). Mutations and simulations show that the SF also provides electrostatic repulsion to positive ions or protons (229). However, a hydronium (or any other) ion, on approaching the entry to the channel, needs to be partially dehydrated to enter. This requires a potentially insurmountable large energy cost that would need to be compensated for by the structure of the protein pore (230). In addition when a proton is forced through the channel, the protein requires sufficient time in the simulation to adapt to stabilizing the proton and reduce the apparent barrier at the channel center (231). The negative charge on the membrane surface may also contribute to repulsion of ions. It is argued however that the "reduced solvation" requirement is the dominant energetic term in aquaporins (232).

How is it that other channels also support a continuous line of water molecules and do readily conduct hydronium ion? The Gramicidin D (A, B, C) channels, antibacterial channels consisting of opposed helices of 15 amino acids that meet in the mid-membrane plane, kill cells by freely conduct protons or hydronium ions. So where is the key difference? The carbonyls of amino acids in Gramicidin generally point more outward than in the AQPs and therefore better accommodate the incoming hydronium ion hydration shells (233–236). While the dehydration cost for ions limits access to these channels too, it is the polarization of waters that defines aquaporin selectivity for water and prevents leakage of any charged ion or protons. Such examples exquisitely illustrate

how structural information informs critical aspects of the function that were otherwise not accessible or understandable any other way.

The phylogenetic tree shows that AQPs diverged into the water and the water plus glycerol branches among bacteria and then diverged into its many tissue-specific variants that perform essential functions. The common scaffold provides a remarkable data set of interactions that show how specificity is encoded in subtle variations in structure. The AQPs provide the most intricate insights into the character and properties of water–protein interactions and the barriers to proton transfer through hydrogen bonded lines or waters in all of biology.

Ammonia like water has a similar size and dipole moment as water and its management is crucial in physiology. How is it conducted? Ammonia/ammonium conduction is mediated by a separate ammonia transport family (AmT family in bacteria, Rh family in humans) from a genomic background completely unrelated to the AQPs. AmT/Rh proteins are all trimers of 12 TM proteins (237, 238), in which each monomer conducts neutral NH_3, although there is a controversy that they might also act partially as ammonium ion transporters. In the AQPs specificity against the ammonium ion lies in the cost of dehydrating the ionic NH_4^+ form. The more hydrophobic channel in AmT/Rh helps by destabilizing the ionic form by reducing the p*K*a of ammonium ion from ∼10 to <5 as it enters the Amt pore.

How do ions cross the membrane? Insights from structures of ion channels

The intrinsic impermeability of the membrane to ions creates two challenges for biology. First, how do ions cross the membrane? And second, how are such movements controlled? As we illustrate here, the availability of the structures of MPs (*i.e.*, ion channels) controlling such processes have played key roles in elucidating how nature's design harnesses the unique properties of membranes for biological functions.

Ever since Hodgkin and Huxley described their electrical properties in the 1950s (44, 45, 239–241), proteins that enable the axon membrane to change its permeability to Na^+ and K^+ have been under intense scrutiny. In the 1970s, Armstrong and Hille first demonstrated that Na^+ and K^+ cross the membrane through different proteins with pores that select for their respective ions, *i.e.*, the Na^+-channels and K^+-channels (242–244). With the advancements in molecular cloning methods, the genes encoding Na^+-channels and K^+-channels were cloned in the 1980s (245–249). Meanwhile, the ingenious use of natural toxins and small molecules that bind and inhibit K^+-channels and Na^+-channels also allowed the groups of MacKinnon, Miller, and Catterall to purify K^+- and Na^+-channels and define their architectures (250–255). Biochemical investigations together with sequence analysis of additional channels plus mutagenesis studies quickly led to the identification of the signature sequences for the pore, the SF, and the gate (256–262) in the late 1980s. Using knowledge acquired over 40 years by numerous investigators in the field, MacKinnon concluded in 1995 that K^+-channels must be tetrameric with their pore loops entering the central conductance pathway encircled by the four subunits (Fig. 8*A*) (263). However, how ion channels achieved both incredible selectivity and conductance at the same time remained a mystery. In particular, this model could not answer the critical question of how K^+-channels conduct K^+ ions with a Pauling radius of 1.33 Å but exclude the very similar Na^+ ion with a smaller Pauling radius of 0.95 Å. MacKinnon concluded, "the answer to this question would require knowing the atomic structure formed by the signature sequence amino acids" (264). The atomic structure of a bacterial homolog of the mammalian K^+-channels, KcsA, indeed provided the answer just 3 years later in 1998 (47, 263). The SF of KcsA perfectly replaces the bound water molecules around a K^+ ion entering the channel while the carbonyl oxygens of the SF are too far apart to correctly hydrate the Na^+ ion.

Subsequent high-resolution structures of KcsA and Na^+-channels confirmed this hypothesis and provided further molecular detail (265–268). The structures of the SF of the K^+-channels are composed of four backbone carbonyl groups from each subunit arranged into a long neck that perfectly matches the coordination configuration of a K^+ ion in water (Fig. 8*B*). Dehydrated K^+ ions in the filter are coordinated by eight oxygen atoms provided by the carbonyl groups, replacing the eight water molecules lost. This results in a minimum energy cost for a K^+ ion to lose its bound waters in the solvent and to enter the SF. On the other hand, the preference of Na^+ ion to bind to six water molecules in an octahedral configuration does not match the structure provided by the SF in the K^+-channels. The energetic cost for Na^+ to lose its bound water thus excluded it from entering the narrow pore. The long SF provides 4 K^+ binding sites. High conductance is achieved through electrostatic repulsion between the positively charged K^+ ions that pushes the ions through the filter. As a result, sites 1, 3 and 2, 4 are occupied by 2 K^+ ions in an alternating fashion. Na^+-channels on the other hand conduct Na^+ ions in their partially dehydrated form with a wider and much shorter SF filled with water (Fig. 8*C*). The highly negatively charged filter and pore in Na^+-channels would attract positively charged anions. Compared with K^+ ions, the smaller Na^+ ions would approach more closely this site of high field strength located at the extracellular mouth of the channel, with their preferred partial dehydration enabling entry into the SF and ion conductance pathway.

Activities of ion channels can be regulated in various ways (269). The nonequilibrium charge distribution due to the impermeability of the membrane itself results in an electric field across the membrane. As a result, regulation by voltage is one of the most common ways ion channels control their activities. Some channel proteins, such as the Na^+-channels represented by the voltage-gated Na^+-channel from *Arcobacter butzleri* (NavAb), can sense this electric field using charged residues embedded within the bilayer that move in response to changes in the magnitude or polarity of the field (269, 270). This conformational change can be coupled to dilation of the central pore for ions to diffuse through, as in the case of voltage-gated ion channels (VGIC). In some cases, enzymatic activity or other unexplored biological functions are used. All

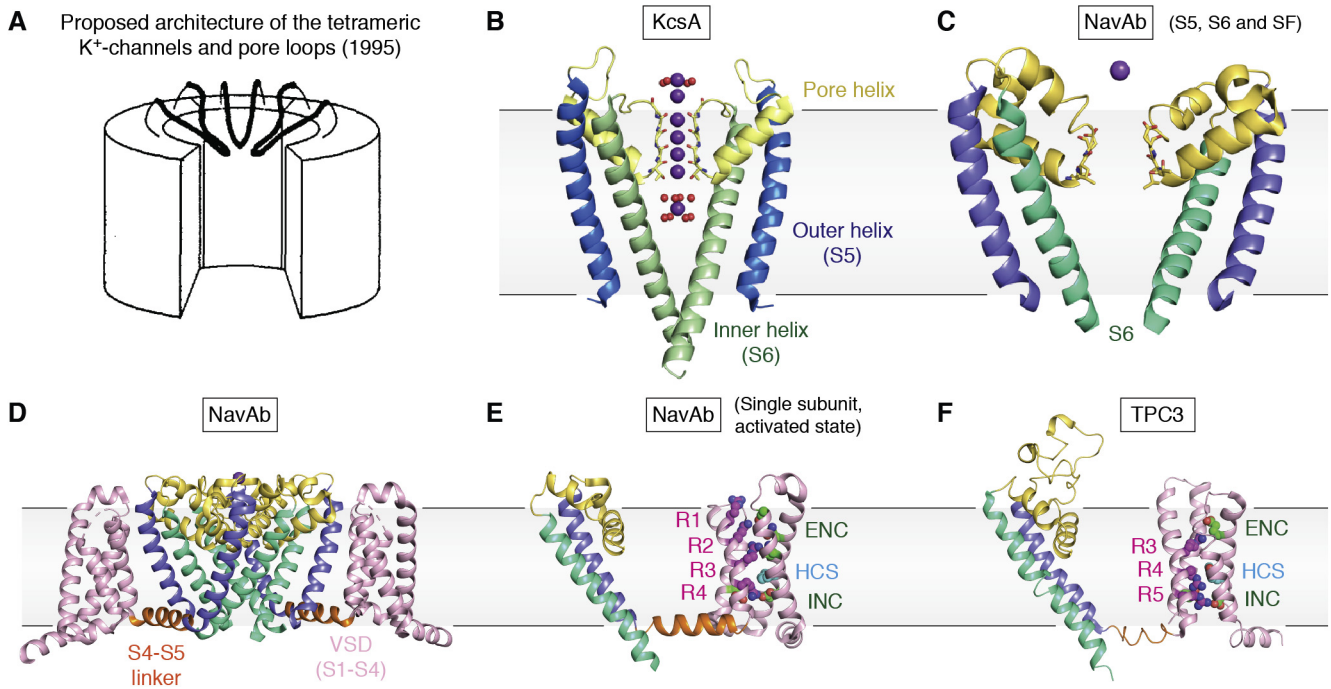

Figure 8. Architectures of ion channels revealed by structures. *A*, the proposed architecture of the tetrameric K^+-channels and their pore loops before structures were available (reproduced with permission (263)). *B*, high-resolution crystal structure of KcsA with bound K^+ ions in and around the SF (PDB 1K4C). Four dehydrated K^+ ions are coordinated by backbone carbonyls from the SF (Although only 2 K^+ ions occupy position 1, 3 or 2, 4 in the SF at any given time, all four are observed in the crystal structure as the structure represent the average between the two states). One K^+ ion coordinated by eight waters is observed right below the SF in the cavity while two more K^+ ion, one completely dehydrated and one partially dehydrated, are observed above the SF. *C–E*, crystal structure of NavAb (PDB 5VB8). Structure of S5–S6 and the SF is shown in (*C*) while the structure of NavAb is shown in (*D*). Water molecules bound to the Na^+ were not resolved in the structure. For clarity, the two subunits in the front and back are removed in (*B*) and (*C*) while the two VSDs in the front and back are removed in (*D*). The outer helix of KcsA (the equivalent of S5 of Shaker) is colored in *light blue* while the inner helix (the equivalent of S6 of Shaker) is colored in *light green* and the pore region is colored in *light yellow* in (*B*). K^+ ions are shown as *purple spheres* while waters are in *red*. In panel (*C–F*), the VSDs composed of S1–S4 are colored in *pink*; S4–S5 linker is colored in *orange*; S5 is shown in *blue* while S6 is shown in *green*; the pore region is colored in *yellow*. *E*, a single subunit of NavAb in the activated state where R1–R3 are above the HCS. *F*, the functional subunit of TPC3 (PDB 6V1Q) in the resting state where only R3 is above the HCS. The voltage-sensing residues located on S4 are shown as *magenta sticks* in panel *E* and *F* while the acidic residues they interact with at the ENC and INC are colored in *green*. The residues forming the HCS are colored in *cyan*. Membranes are indicated with the *black line*.

known so-called voltage-sensing domains (VSDs) are composed of four TMs arranged in a bundle (pink in Fig. 8, *D–F*), with at least one positively charged residue (magenta in Fig. 8, *E* and *F*) located within the bilayer. If a VSD contains multiple gating charges, these are typically arranged in an i, i+3n pattern along the helical path (Fig. 8, *E* and *F*).

In addition to gating charges that project into the four-helix bundle, VSDs often share a number of common structural and biophysical characteristics (Fig. 8, *E* and *F*). The charge-bearing gating helix (S4 in the Shaker cassette) often adopts a 3_{10} helix in order to stack the basic residues above one another. The four-helix bundle also contains a hydrophobic seal, also called the hydrophobic constriction site (HCS) or gasket (cyan in Fig. 8, *E* and *F*), which lowers the dielectric constant of the bundle and prevents leakage of ions and water through its center. Finally, negatively charged residues, denoted as the extracellular and intracellular negative clusters (ENC and INC), are often situated at either extreme of the VSD and can establish salt bridge interactions with the gating charges.

The conformational response of VSDs to changes in the trans-membrane electric field has been the subject of decades of biophysical and structural investigation. Armstrong and Bezanilla were the first to report "capacitive gating currents," whereby the current elicited by gating charges moving across the membrane was directly observed (271, 272). These currents suggested that the gating charges likely move in a direction coincident with the transmembrane electric field vector. While the voltage-dependent dynamics of VSDs can be partially inferred by fluorescence measurements or chemical modification experiments (273, 274), direct visualization of these conformational transitions has not been possible simply because it is not possible to impose electrical gradients across the VGIC in either a lattice state suitable for X-ray diffraction or as a dispersion of single particles for cryo-EM. Therefore, the only states of the voltage-dependent specimen accessible to structural techniques are those that exist at 0 mV potential.

Early structures of voltage-gated K^+-channels (K_V channels) at 0 mV potential suggested that the vertical motion of S4 couples directly to the S5 pore helix *via* a S4-S5 linker helix, which is situated in the plane of the membrane (275). As S4 moves upward, it tugs on the S4-S5 linker and in turn S5, causing the pore to dilate in a process known as electromechanical coupling (Fig. 8, *E* and *F*). Later structures of prokaryotic voltage-gated Na^+-channels (Na_V channels) allowed for structural comparison of VSDs (266, 276, 277). While the

overall structure of the VSDs was remarkably conserved, the observed orientations of the VSD with respect to the pore domain differed between channels. This was confirmed in the structures of two-pore channels where the VSD can move as a rigid body with respect to the pore domain, in addition to undergoing canonical charge transfer (79, 278). Unlike most VGICs that are activated at 0 mV, the two-pore channel 3 (TPC3) is only activated at extremely high voltage ($V_{50} \sim +75$ mV). The recently determined cryo-EM structure of TPC3 thus provides a unique opportunity to "see" a VGIC at resting state at 0 mV where the cryo-EM structure is captured (278). Consistent with the earlier hypothesis, S4 adapts a down position where only one out of the three arginine residues is above the HCS (Fig. 8*F*). In comparison, three out of the four arginine residues on S4 of NavAb are above the HCS, representing an activated state (Fig. 8*E*). Both structures confirm that S1–S3 also play critical roles in voltage sensing by providing residues in the ENC and INC that would stabilize the S4 in either the activated or resting state through salt bridge formation involving the arginines.

The ability to see the inner working of an ion channels by determining their atomic structures was critical for understanding how these amazing machines elegantly perform their functions that underly various essential biological processes. With more than 852 structures of ion channels in the PDB, we now understand how different ions selectively cross the membrane through specific ion channels and how their activities are regulated. As many ion channels have been implicated in various diseases, molecular understanding of their mechanisms and ready accessibility of their structures in the PDB are playing critical roles in the hope of treatments that target ion channels.

How do vertebrate tissues prevent the passage of molecules through the spaces between neighboring cells? Claudins are molecular gatekeepers between cells.

In epithelium and endothelium, spaces exist between cells but molecules are restricted from unfettered transport. The restrictions imposed on these molecules force them to enter cells *via* transcellular transport mechanisms instead of passing between them. Vertebrate epithelium and endothelium regulate molecular movements between adjacent cells, paracellular transport, at narrow strands beneath the apical surface at specialized cellular contacts called tight junctions (TJs). As compartments within tissues require molecular exchange to maintain homeostasis, TJs assist here by forming membrane-associated multiprotein complexes to govern paracellular transport. The assembly of several families of MPs at TJs, specifically, creates either barriers or charge- and size-selective pores to small molecules and ions. The molecular properties of a given tissue or cell type, therefore, are determined by the MPs that assemble their TJs. As some molecules are only transported by paracellular means, regulation of this transport mechanism by TJs is critical to certain biological processes. Molecular transport through the paracellular space may have evolved in animal tissues as an energy conservation strategy, as a result of aerobic respiration. Impairing paracellular transport in mouse kidney results in normal ion absorption but increased oxygen consumption and hypoxia, demonstrating that the transcellular transport pathway alone is less energy efficient and that paracellular transport enhances kidney efficiency (279).

TJs were identified in 1963 by EM analyses of mammalian epithelial cells (280), but it was not until 1993 (281) and 1998 (282) when Tsukita and coworkers established the essential roles of integral MPs in TJ structure and function. Only one group of integral MPs, claudins (CLDNs), were capable of reconstituting TJ strands in TJ-less fibroblasts (283), distinguishing them as the structural backbone of TJs. Soon after, these were shown to be cell/cell adhesion molecules (284), which hinted at an ability to interact across paracellular space. The discovery of CLDNs led to newfound insights into the diverse functions of TJs and how these functions were enabled by CLDNs. These functions range from maintaining salt/water balance in fish gills (285), forming barriers in human skin to prevent dehydration (286), to sealing the blood–brain barrier —highly selective interfaces that provide a defense for the brain against pathogens and toxins in the blood (287). The plethora of TJ-linked diseases further demonstrates the diversity of TJ functions and how errors in TJ protein assembly contribute to these disorders, which include cancer (288–290), Alzheimer's (291, 292), Parkinson's (293) and Huntington's (294) disease, amyotrophic lateral sclerosis (295), stroke (296), food poisoning (297) and irritable bowel disease (298, 299), hepatitis (300, 301), and diseases of the skin (302–305), kidney (306–308), eyes (308–310), and ears (311–313).

Identification of the first two CLDNs led to subsequent classification of a CLDN family and the prediction of four TMs by cloning and sequence hydrophilicity analyses (314). In vertebrates, mammals have at least 24 subtypes, humans possess 27 (315), while pufferfish of the genus *Takifugu* have 56 claudins (316). Human CLDNs range in size from 23 to 34 kDa and are classified by a conserved WGLWCC motif. In addition to four TMs, most CLDNs contain a short N terminus and variable length C terminus and one intracellular and two extracellular segments (ECS). The two ECSs vary in length between subtypes, but ECS1 is larger and contains a conserved C54–C64 disulfide bridge. CLDN topology facilitates TJ assembly through: *i)* lateral CLDN/CLDN interactions within the same membrane (*cis*), *ii)* paracellular interactions with CLDNs on adjacent membranes (*trans*), and *iii)* cytoskeletal anchoring by soluble scaffolding proteins (317). *Trans* interactions between the ECS of adjacent CLDNs form paracellular barriers or pores to small molecules and ions. Because CLDN subtypes have specific permeability characteristics and tissue expression patterns, it is thought that the combinations and ratios of CLDN subtypes in given tissues' TJs determine tissue barrier or pore properties. CLDNs are indeed classified by their barrier or pore-forming nature (318) and can be further delineated by levels of homology outside of the WGLWCC motif (319).

In April 2013, Suzuki *et al.* (320) uncovered the first ~7 Å structure of a CLDN-like protein from the single-cell flagellate *Euglena* by electron crystallography. This protein, IP39, was

predicted to have four TMs and a WGLWCC motif. Although the resolution of the IP39 structure obtained from 2D crystals was insufficient to determine the fold, the 3D EM density map revealed unique arrangements of IP39 in the lattice. IP39 molecules were packed in strands of antiparallel double rows, with trimeric units longitudinally polymerized, and one molecule of the trimer rotated 180° from the other two. These interactions were hypothesized to be important for linear polymerization of IP39 on *Euglena* membranes and potentially for TJ strand formation based on IP39's sequence and topology similarity to CLDNs.

One year later, Suzuki *et al.* (321) determined the first structure of a CLDN by X-ray diffraction at 2.4 Å resolution. Mouse CLDN-15 (mCLDN-15) is a cation-selective pore-forming CLDN (322, 323). To obtain 3D crystals of mCLDN-15, they employed a newer MP crystallization strategy, LCP (324), using a construct truncated of 33 amino acids at its C terminus and lacking four palmitoylation sites. The structure revealed the CLDN fold, which is composed of four TMs arranged in a left-handed bundle, one unstructured intracellular segment connecting TM 2 to 3, and two ECS linked together by a 5-stranded anti-parallel β-sheet (Fig. 9*A*). Unresolved in the structure was the loop connecting strand β1 to β2 and the N terminus, while two monooleins were resolved and located near F11 and W49. The crystal structure suggested a potential pathway for paracellular transport by revealing that a negatively charged electrostatic surface exists in the C-terminal half of ECS1, specifically the area between β3 and β4. As mutations to residues in this area were known to reverse ion charge selectivity (325), the structure explained how CLDNs may govern ion selectivity in TJs. In addition, like IP39, the mCLDN-15 packing within the lipid-filled crystal lattice suggested how CLDNs may polymerize. It was hypothesized that lateral *cis* assembly of CLDN-based TJ strands *in vivo* resembles the linear arrangements found *in crystallo* between certain symmetry mates. These packing arrangements would be used as a basis for modeling of larger TJ polymer strands and paracellular pores.

Throughout animal evolution, CLDNs and the paracellular barrier have likely been subjected to many attempts at disruption by pathogenic organisms seeking entry into epithelial tissues. The spore-forming Gram-positive bacterium *Clostridium perfringens*, for example, secretes a 35 kDa enterotoxin (CpE) within the gastrointestinal tracts of humans and domesticated animals that binds select CLDN subtypes through recognition by its C-terminal domain (cCpE) (326). The CLDN ECS2 alone was thought to be used for this recognition (327, 328). However, structure determination of CLDNs in complex with cCpE has revealed that cCpE binding encompasses both ECSs (Fig. 9*B*). The cCpE has proven to be an important tool for structural determination of CLDNs because the toxin fragment adds a ~15 kDa hydrophilic mass to hydrophobic CLDN/detergent complexes, which allows for formation of 3D crystals *via* traditional vapor diffusion methods. The cCpE has enabled structural determination of mCLDN-19 (329), human CLDN-4 (hCLDN-4) (330), mCLDN-3 (331), and hCLDN-9 (332). To date, 89% of CLDN structures in the PDB are CLDN/cCpE complexes, highlighting cCpE's value to CLDN structural biology.

In addition to enabling structural determination of several CLDNs that were recalcitrant to crystallization alone, cCpE-bound CLDN structures facilitated our understanding of both fundamental and clinical aspects of TJ biology. CpE binding to CLDNs is thought to disable both lateral and paracellular CLDN/CLDN interactions, inhibiting paracellular pore and cell adhesion functions (329–332). Crystal structures of CLDN/cCpE complexes explain how cCpE may disable both types of CLDN/CLDN interactions (Fig. 9*B*). By encompassing both ECS, cCpE can prevent CLDN/CLDN *trans* interactions through steric shielding. The cCpE can also disable lateral CLDN/CLDN interactions through cCpE-induced structural perturbations of two extracellular helices shown to be involved in *cis* assembly (329–332). In drug development and in the clinic, the intermolecular interactions between cCpE and CLDNs revealed by these structures are empowering efforts to engineer cCpE for targeted destruction of CLDN-expressing cancer cells (333–3335) and for improving drug delivery through the blood–brain barrier (336, 337).

Structures of CLDNs have allowed for the modeling of the other subtypes and their functional pore-forming assemblies using *in silico* methods. The linear polymers of mCLDN-15 observed in LCP-grown crystals, packed in crystallographic symmetry arrangements, form potential *cis* interactions using adjacent ECS domains (321) (Fig. 9*C*). Building complexity from this experimentally determined organization, a more complex model was proposed where a row of linear polymers could interact with a second row of linear polymers to arrange in antiparallel double rows, with the ECS of neighboring protomers creating β-barrel-like channels in paracellular space (338) (Fig. 9*D*). Since, researchers have computationally modeled an array of possibilities for how mCLDN-15 (339–341) and other CLDNs (342–344) may assemble into large complexes essential for paracellular barrier and pore function. These predictions have provided testable models of CLDN self-organization, pore structure and selectivity, and the *cis* and/or *trans* interfaces that enable these assemblies and functions. Although some models or portions of them have been verified *in vitro* and/or *in vivo* using cross-linking, mutagenesis, freeze-fracture EM, fluorescence confocal microscopy, and FRET (338, 341, 342), an experimentally derived structural basis for CLDN interactions and assemblies has yet to be elucidated.

Recent progress in determining structures of CLDNs has rapidly advanced our understanding of the interconnected structural and functional biology's of CLDNs and TJs and the mechanisms by which a bacterial enterotoxin gains access to the mammalian gut. These advances are somewhat limited by a lack of structural information for the multimolecular CLDN assemblies required to form TJ barriers and pores and CLDN complexes with other TJ-constructing proteins. The dynamic associations between soluble proteins and MPs that properly assemble TJs under various physiological stimuli, which are thought to contain >40 proteins (345), make for a potentially arduous yet exciting future for

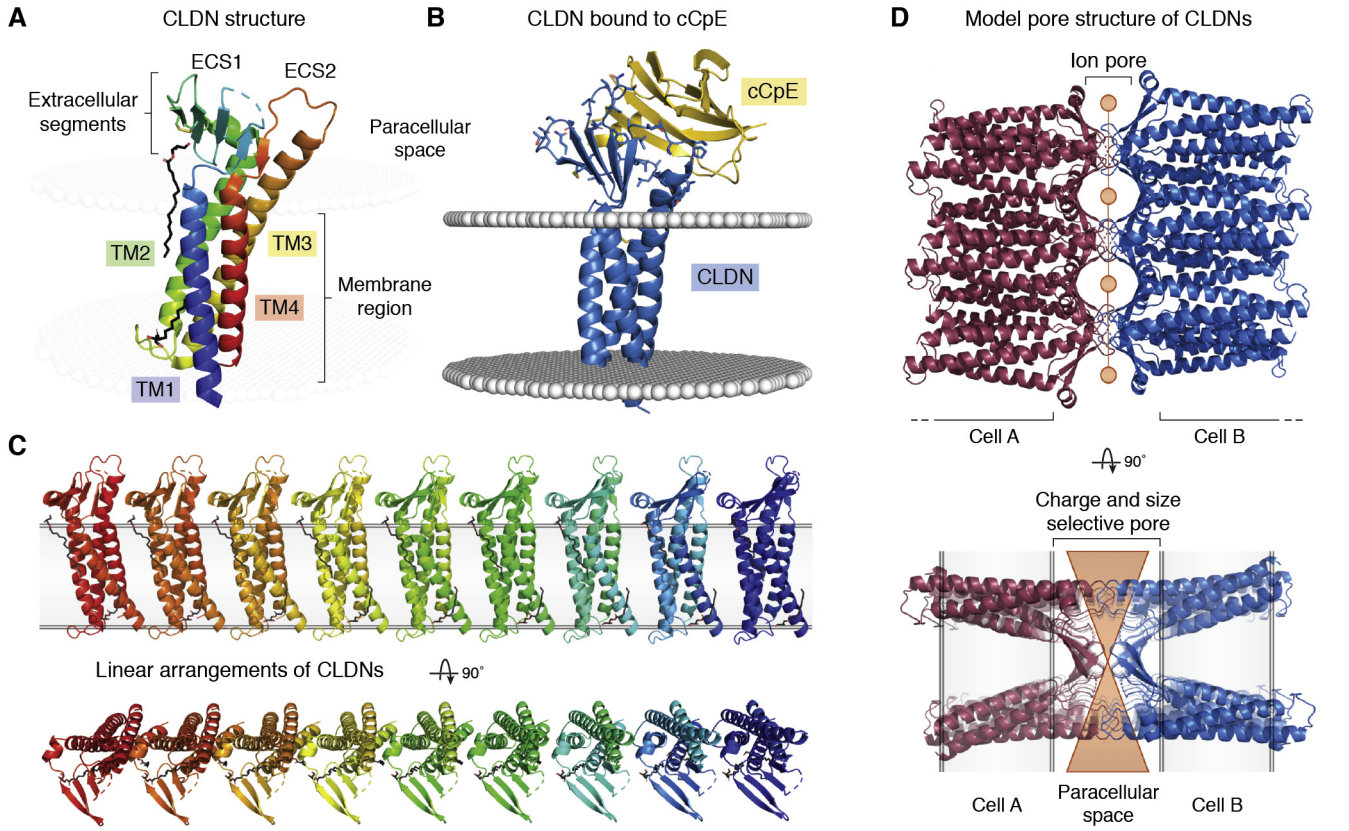

Figure 9. Claudin structures and models for assembly at tight junctions. *A*, 3D structure of mCLDN-15 (PDB 4P79). *B*, 3D structure of hCLDN-9 in complex with cCpE (PDB 6OV2). *C*, the proposed linear arrangements of CLDNs as observed from the LCP crystal structure of mCLDN-15. *D*, structural model of CLDN-based paracellular ion pores.

the field. It is expected that structural biology will make critical contributions to deconvolute and demystify how TJs form and function at the subnanometer levels. Such discoveries will provide a rich source of information for making new inroads in the design and development of therapies to treat the plethora of TJ-linked diseases—like cCpE-based therapeutics targeting cancer and neurological disorders—effective, possibly, at the level of specific tissues, cell clusters, or even individual TJs.

How do solutes cross the membrane?

One of the important categories of MPs are transporters for solutes to cross the lipid membrane (346). These solutes either become part of a metabolic cycle (*e.g.*, glucose transporters) and generate energy for the cell, or these solutes can act as signaling molecules (*e.g.*, Ca^{2+} ATPase that transfers Ca^{2+} ions) to activate various biological processes (347). Active transporters, which utilize energy to transport substrates, are classified into primary and secondary active transporters based on the energy source (348). Primary active transporters such as P-type ATPases (*e.g.*, Na^+/K^+-ATPases, Ca^{2+}-ATPase, gastric H^+/K^+-ATPase, fungal and plant H^+-ATPases), V-type (vacuolar-ATPase), and ABC transporters depend on ATP hydrolysis to fuel the transport of solute across the hydrophobic lipid membrane (349). Secondary transporters transport solutes against their gradients by using the potential energy from downhill electrochemical gradient of another solute (350). We describe the impact of the PDB in the field of one of the primary transporter classes, the ABC transporters (351). For secondary active transporters, we focus on the major facilitator superfamily (352).

ATP-binding cassette transporters

ABC transporters are one of the largest superfamilies of MPs, ubiquitously present in all prokaryotes and eukaryotes (353). They are involved in major physiological functions by transporting diverse types of solutes including sugars, ions, drugs, lipids, bile salts, amino acids, peptides, nucleotides across membranes (354). Mutations are associated with a number of diseases including cystic fibrosis, Tangier's disease, Dubin–Johnson syndrome, and also account for multidrug resistance in human cancers (355). ABC transporters are classified as importers or exporters based on the direction of substrate transport relative to the cytosol (356). According to the new classification, based on different structural folds, ABC transporters are divided into type I to VII classes (357). These transporters consist of two transmembrane domains (TMDs) and two nucleotide-binding domains (NBDs). NBDs bind and hydrolyze ATP to power the translocation of substrate across the membrane through the transmembrane domains (358, 359). Some ABC importers also use accessory proteins to bind the substrate with high affinity and then transport it across the

membrane (360). Structure entries since the 1990s demonstrate how the PDB remarkably impacted the field of ABC transporters (361).

Structures of ABC transporters not only provided insights into the architecture of ABC transporters, but also contributed toward understanding the alternating access mechanism in the family. The *Escherichia coli* maltose transporter or $MalFGK_2$, a well-characterized model system of the ABC transporter superfamily (362, 363), imports maltose or maltodextrins with lengths of up to 7 to 8 linked glucose units in coordination with cell metabolism (364). Crystallographic snapshots of the maltose transporter in different states demonstrate how it utilizes an alternating access mechanism to transport maltose from the periplasmic side to the cytosol using a periplasmic maltose-binding protein (MBP, also named MalE) to feed the transporter from the periplasm and ATP hydrolysis on the cytoplasmic NBD domains (365). These studies revealed that in the absence of MBP and nucleotide, the NBDs of maltose transporter are well separated and do not hydrolyze ATP; a state known as inward-open resting state (366). Binding of maltose-binding protein charged with maltose and ATP binding to the NBDs induces a conformational change that brings the transporter into a pretranslocation semiopen state in which the NBDs are not fully closed (Fig. 10*A*) (367). In the next step, it undergoes a concerted motion in which substrate is released into the intracellular cavity and NBDs dimerize or close completely to initiate ATP hydrolysis; a state known as the outward-open transition state (Fig. 10*B*) (368). ATP hydrolysis returns the maltose transporter to the resting state through an intermediate posthydrolysis semiopen state and releases the substrate to the intracellular side (Fig. 10, *C* and *D*) (365).

In addition to elucidating the catalytic cycle of the maltose transporter, structural biology of this transporter also explained the biphasic behavior of its MBP-independent mutants such as MalG511 (366) and informed about substrate specificity toward malto-oligosaccharides (369). MBP- independent mutants had high basal activity and showed an interesting biphasic behavior in maltose transport assays, as well as in ATPase assays in response to increasing equimolar concentrations of MBP and maltose (370–372). Equimolar concentrations of MBP and maltose had an activating effect at low concentrations, but inhibitory effects at higher concentrations on these mutants (371, 372). These MBP-independent mutants were hypothesized to resemble the transition state of the maltose transporter, with lowered activation energy and increased affinity toward MBP (372, 373). The mutated residues in these mutants are located at regions near a periplasmic gate involved in transition from the inward-open to the outward-open state (366, 368, 374). Mutations in these regions destabilize the maltose transporter in the resting state and shift the equilibrium toward a transition state, which explains the high basal activity of these mutants in the absence of MBP (366, 372). Higher affinity of MBP for the transition state *versus* the resting state explained the biphasic behavior of these mutants (372).

Along similar lines, TmrAB, a thermophilic bacterial homolog of the mammalian antigen-presenting ABC transporter TAP1/TAP2 (375), was one of the first ABC transporters with pseudo-twofold symmetry, whose subnanometer resolution structure was determined by Fab-assisted single particle cryo-EM (376). In a remarkable tour de force, crystallographic studies combined with cryo-EM studies determined the conformational landscape of TmrAB in lipidic environment during turnover conditions (375, 377). These studies demonstrated the inward-open and outward-open states as a part of general alternate access mechanism and showed induced conformational changes upon ATP binding and hydrolysis, coupled with substrate movement across the membrane (Fig. 10) (377). Advances in cryo-EM technology have enabled deciphering the alternating access mechanism in individual ABC transporters including the chloride transporter CFTR (378–382), MRP1 (383–385), P-glycoprotein (386–388), and BCRP (389–392).

The PDB facilitated further understanding of the catalytic cycle of ABC transporters. As an example, the crystal structures (PDB 2R6G) of the maltose transporter (368) enabled detailed dynamics studies using EPR (393, 394). The dynamics of the maltose transporter determined by EPR complemented the crystallographic structures representing the catalytic cycle (395–397). Other ABC transporters including MsbA, LmrA, $ModBC_2$, BtuCD, P-glycoprotein, and TmrAB were also probed by EPR spectroscopy to understand similarities in catalytic cycles and the differences that define unique features of each ABC transporter (398).

Major facilitator superfamily (MFS) transporters

The MFS transporters are the largest family of secondary transporters in which individual members translocate one of a diverse range of particular substrates. The substrates include sugars, ions, amino acids, and diverse metabolites (399, 400). This superfamily is ubiquitous, found in all kingdoms of life, and in all cells, and in humans many members are of direct medical and pharmaceutical significance.

The key aspect is that they alternately bind or release substrate on one side of the membrane and bind or release that one molecule on the other side, termed alternate access. If the cycle in Figure 11 is described as if a clock face, this is schematized in the 9 to 12 to 3 o'clock parts of Figure 11 (and vice versa). This process can be proved using radioactive substrate on one side of the membrane that appears on the other side of the membrane, even against a concentration gradient of total substrate in the opposite direction. It occurs between opposite sides of a membrane-enclosed volume without any ion gradient across the membrane. So-called "uniporters" do this without coupling to any other ion or proton gradient and so simply allow equilibration of substrate from one side to the other to achieve equilibrium where both sides eventually reach equal concentration. The glucose transporter GLUT1 falls into this category. In biology the metabolism of glucose inside the cell reduces cytoplasmic glucose inside and thus ensures that GLUT1 actually leads to net import of glucose.

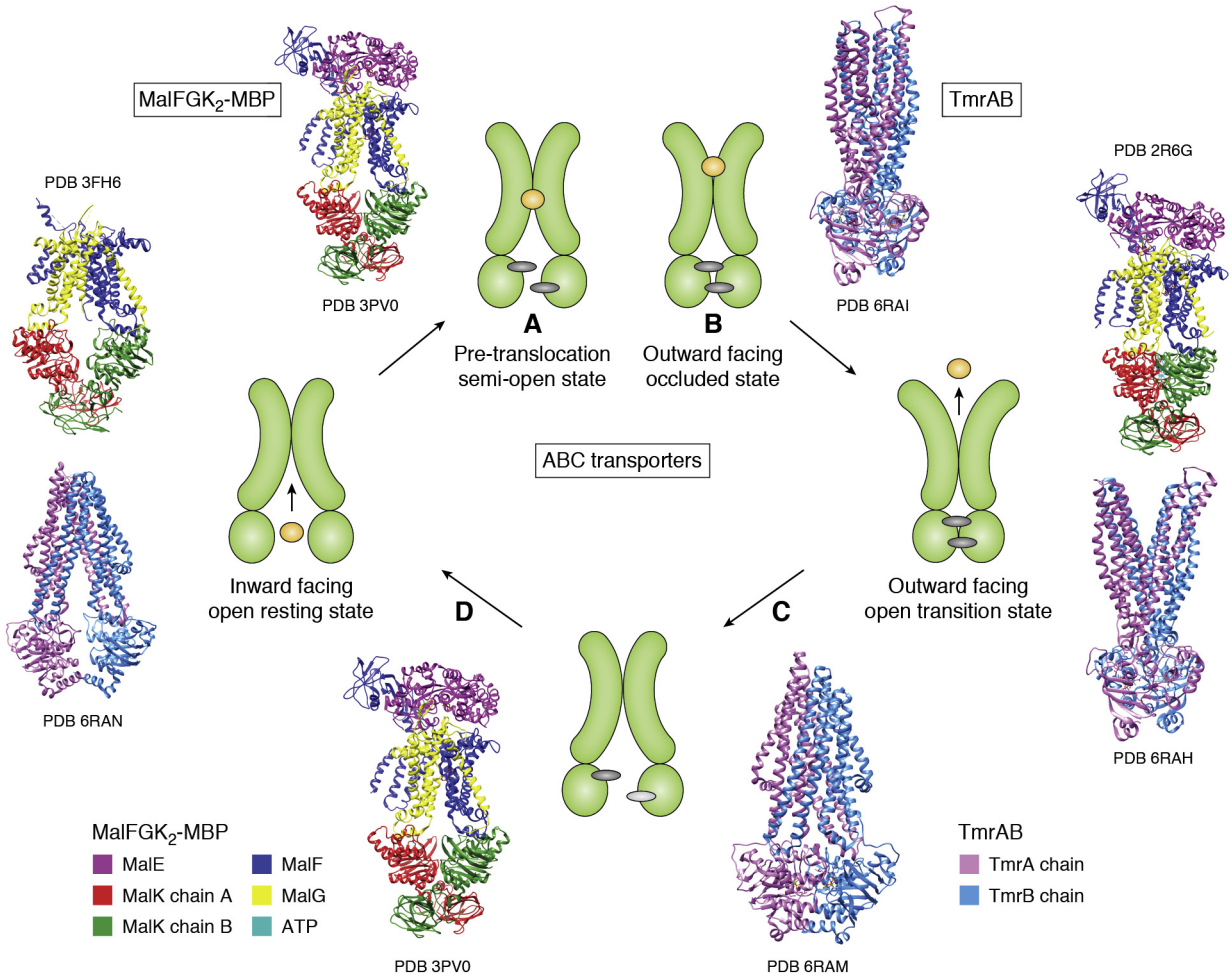

Figure 10. The alternating access mechanism in ABC transporters deciphered by structural tools. For simplicity, the cycle direction describes an exporter. Importers function in the opposite direction of the *arrows*. An ABC transporter in its inward-facing open resting state (PDB 3FH6 for $MalFGK_2$, PDB 6RAN for TmrAB) binds to ATP in the presence (in the case of maltose transporter) or absence of substrate [A] to adopt an intermediate state (semiopen pretranslocation state (PDB 3PV0) in the case of the maltose transporter, or an outward open occluded state in case of TmrAB (PDB 6RAI)). NBDs dimerize for ATP hydrolysis in an outward-open transition state (PDB 2R6G for the maltose transporter, PDB 6RAH for TmrAB) [B]. ATP hydrolysis separates NBD domains, and the ABC transporter adopts an inward open post hydrolysis state (semiopen state for maltose transporter (PDB 3PV0), inward-facing unlocked state for TmrAB (PDB 6RAM)) [C], which resets the resting state [D]. To simplify the figure, the binding and release of substrate are shown only for the case of exporters. Substrate is effluxed outside at step [B] in the case of the exporters. In importers, the substrate is released inside at step [C and D]. Color coding: MBP (MalE) = *magenta*, MalK chain A = *red*, MalK chain B = *green*, MalF = *blue*, MalG = *yellow*, ATP = *cyan*, maltose = *brown*. TmrA chain = *pink*, TmrB chain = *sky blue*.

In the vast majority of MFS transporters, transport is obligately coupled to an electrochemical proton or Na^+ gradient. The gradient drives the transport of substrate against their substrate concentration gradient, using the downhill free energy change of one process (*i.e.,* the electrochemical ion gradient) to drive the uphill process of the other (*i.e.,* substrates). In transporters the movement of ion and substrate may be in the same direction, termed symporters, or in the opposite direction of the substrate transport, termed antiporters, and the processes are reversible, determined by the relative concentration gradients of the driving ion and of the substrate. In a closed system, they would reach a two-substrate equilibrium. In cell biology though, the gradients of the driving ions are continuously being generated by ATP-driven pumps that then determine the direction of transporters that use those gradients (352, 401). The PDB harbors ~150 structure entries of full-length or truncated MFS transporters bound to substrates and small molecules determined by various methods, most by X-ray crystallography with a few by cryo-EM. These structures each outline different states around a transport cycle (Fig. 11) that shows how small are the energy barriers between different states around the Figure 11 clockface.

Mutations and misregulation of human MFS transporters contribute to human diseases. GLUTs (glucose uniporter family) are linked to various genetic and metabolic diseases. Essential for maintaining glucose homeostasis their loss of function or regulation can underlie type-2-diabetes (402). GLUT1 is also overexpressed in many cancer types due to the increased demand for glucose that plays a key role in tumor growth (403–405). The substrates of GLUTs are not restricted to glucose as some of the homologs transport urate or other sugars broadening their contribution to human physiology. As an example, GLUT9 transports urate and is implicated in

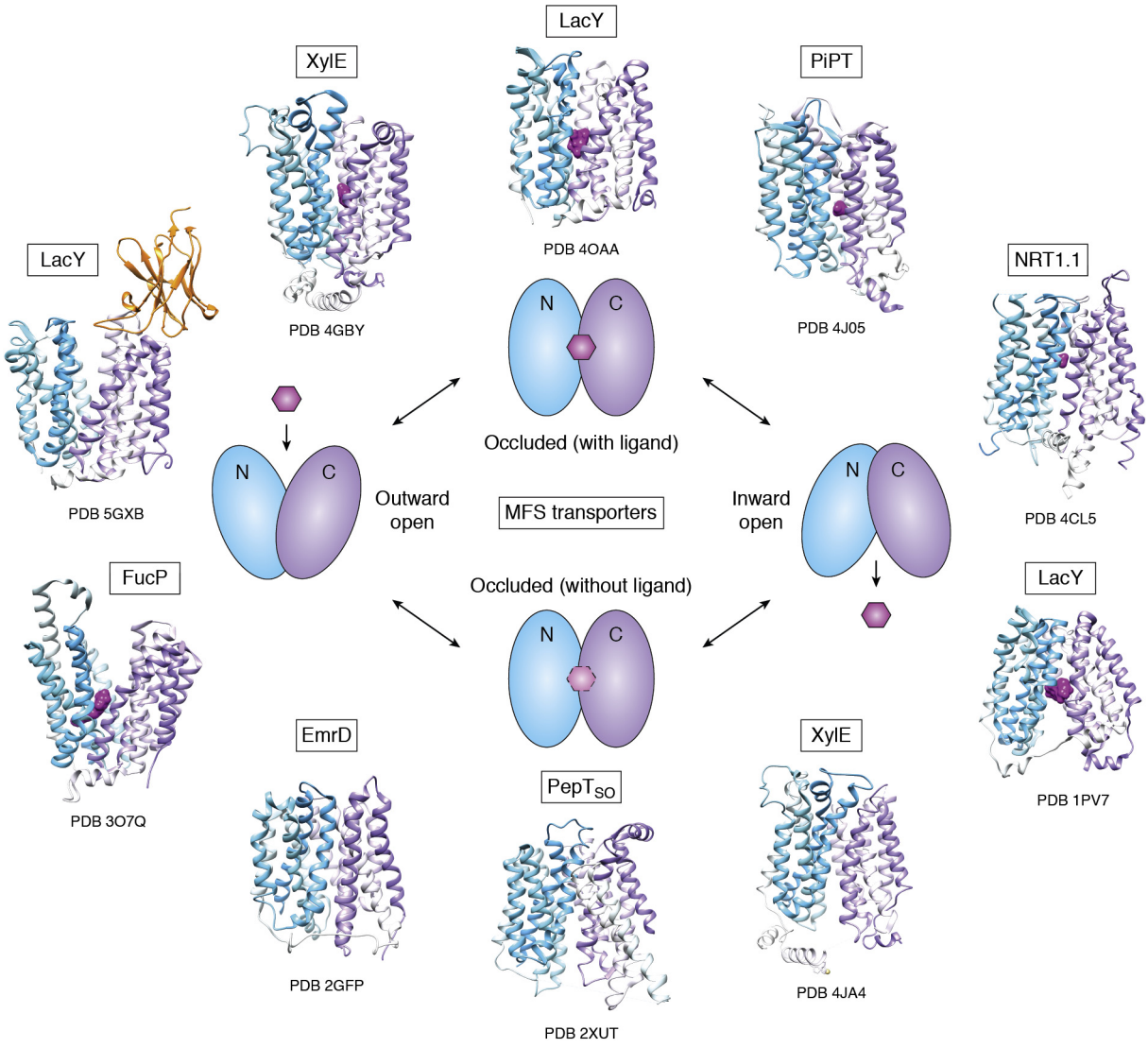

Figure 11. Distinct conformations of major facilitator superfamily transporters. Representative structures for the distinct conformations in the substrate transport cycle are shown. The cytoplasmic side of the membrane is "down" and the outside of the cell upward in this figure. In the text the cycle is described as if on a clock face. The structures of several MFS transporters are shown in their relative positions around the "clock." A key point is that there is no leakage in these transporters. The 9 to 12 to 3 and in reverse (clockface numbers) indicate exchange 1:1 of substrate. The 3 to 6 to 9 and back to 6 to 3 indicate the substrate-free transfer, which in the case of LacY is the critical part that then delivers the proton.

hyperuricemia and gout (406, 407). Other human MFS transporters implicated in disease include human PEPT1 and PHT1. They are involved in transport of small peptides, and their misregulation can cause inflammatory bowel disease (IBD) (408). Organic anion and cation transporters transport large hydrophobic ions including neurotransmitters, hormones, various drugs and are associated with coronary heart disease, IBD, prostate cancer, rheumatoid arthritis, and other conditions (80, 409–411). Given the role of MFS transporters in human health and disease, their structures are an important driver for drug design.

The structures of MFS transporters shed light on their fundamental mechanism (352, 400, 412). They have a single central substrate-binding site and operate *via* an alternating-access mechanism that involves a rocker-switch type movement of the two halves of the protein (Fig. 11). The 12 TMs are arranged into two six-helix bundle domains (TM1-6 and TM7-12) and the motion of the N- and C-terminal domains results in alternating access, with the substrate-binding site as a pivot point. Structures guide the notion of a shared MFS fold, irrespective of their particular function as symporter, uniporter, or antiporter, or substrate (Fig. 11). Salt-bridge formation and breakage are involved in the conformational changes of the protein during transport (352, 401). The structures of MFS transporters suggest that there is more to the mechanism of substrate translocation than just rigid-body movement of the two transmembrane halves. A more compact arrangement of helices around the bound substrate is found in some structures (413–415). Homology modeling, MD simulations, and double electron–electron resonance measurements suggest a similarly compact structure for the substrate-bound lactose permease (LacY) (416–418). A comprehensive analysis of MFS transporter structures by Quistgaard *et al.* (401) revealed a possible gating mechanism

for substrate transport. Therefore, the atomic resolution structures of these transporters describe the unique aspects of their functions and provide an overarching view of an underlying mechanism (Fig. 11).

Structural information helps classify MFS proteins into subfamilies (352, 400) as some proteins with no detectable sequence similarity may exhibit almost identical structural arrangements. Mutants designed using biochemical and biophysical analysis of MFS transporters help stabilize otherwise unachievable conformations within the transport cycle (419, 420).

The lactose permease LacY of *E. coli* is one of the best understood MFS transporters (421). It couples the proton electrochemical gradient from outside to inside across the plasma membrane of a bacterial cell to cotranslocation of a galactopyranoside against its concentration gradient, into the cell (422). The stability-conferring C154G mutant (in TM5) binds substrate in the same manner as the WT LacY but with negligible transport (423). This conformationally restricted mutant led to the first X-ray crystal structures of LacY, perhaps because it was locked into position by the mutation (424, 425). Later structures showed how LacY binds substrates without this mutation (426) and related the difference in binding of substrate *versus* water in the binding site to changes in the environment of a nearby arrangement of titratable side chains including E325, H322, K319, Y236, D240 that serve to capture and release protons (412). Surprisingly the binding (or unbinding) of substrate (the 9 through 12–3 position in Fig. 11) did not change the protonation state of the protein as measured by any release of protons upon binding substrate. And the *Kd* for binding substrate remains unchanged up to pH 10.5 (427). So where does the coupled movement of the driving H^+ ion, that is, protonation and deprotonation, occur to drive the process? Proton delivery occurs only if the protein goes through alternate access *without* the substrate bound (6 o'clock in Fig. 11). The H^+ ions get "squeezed out" from the side that closes (3–6 or 9–6) to reach the occluded state (6 in Fig. 11), but only when water rather than substrate fills the substrate site (6 in Fig. 11). Effectively the active substrate-binding site loses protons as water retunes the substrate site. Once on the "other side" of the membrane, the site rebinds protons from that "other side" (6–9, or 6–3 in Fig. 11) as the *pK*a again quickly rises from around p*K*a of ∼5 in the water-occluded state (6 in Fig. 11), to 10.5 when it opens to the other side (Fig. 11). The process is driven by a sharp drop in the *pK*a of the titratable substrate proximal region associated with glutamate E325 when water is in the site, *versus* when there is substrate in the site, *i.e.*, the loss of a proton from that conjugate site (428, 429). As the transporter closes, for example, from the cytoplasmic side, if no substrate is bound, the *pK*a of E325 system is lowered to release protons to the closing side, and those protons are rapidly moved away *via* water molecules.

In an effort to visualize the alternate access mechanism, two conserved Gly-Gly pairs (G46/G370 and G159/G262) in LacY were mutated to tryptophans to pry the alternate sides open. The mutants modified the structure and were investigated using transport and stopped-flow binding measurements (430, 431). The double Trp mutant G46W/G262W locked the LacY conformation into the outward (periplasmic)-open conformation and led to structures that defined interactions in the outward-facing state. A camelid-nanobody against the G46W/G262W double mutant was screened against WT LacY and selected for the locked conformation similar to the double mutant (430, 432) beautifully validating these structures as reflecting on pathway states of the "rocker switch" (419, 420) (Fig. 11).

The sugar-transporting MFS transporter XylE (433), a bacterial hGLUT1 ortholog, was one of the first MFS transporters for which the structures of multiple conformations were deciphered. XylE structures in complex with *D*-xylose and *D*-glucose led to the structural understanding of its specificity and provided the basis for subsequent mechanistic understanding of hGLUT1 specificity (see *How does understanding of a glucose transporter selectivity and conformational changes inform the development of GLUT1-specific inhibitors?*) (403, 434). A mixture of detergents and substrate during crystallization led to an inward-open conformation of XylE (435). Inspired by the double Trp mutant of LacY, a similar mutant designed for XylE (G58W/L315W) gave an outward-facing conformation (433).

Several general conclusions from MFS transporter structures ensue. Substrate binding, *versus* absence of substrate binding, changes the environment of the titratable/ion-binding sites nearby the substrate so that the affinities for proton/ion are altered. In LacY, the "active site" p*Ka* drops (releases a proton(s)) only when LacY returns to the other side empty of substrate. This mechanism beautifully explains how an intrinsically reversible transport function couples substrate delivery to one side (opening on that side), to "squeezing out" the proton(s) on that same side, when recycling empty of substrate to be available for another substrate to be bound on the other side. There is no exact stoichiometry of proton/ion to substrate, as determined by the p*K*a values and may involve several H^+ in this case, or Na^+ ions in eukaryotes. Thus the driving proton(s)/ion(s) and substrate transport are coupled but differently in space and in time (412).

Other superfamilies also work by alternate access. As an example, several other Na^+-driven transporters from different gene families share a common fold with LeuT (see *How do drugs control our minds? Molecular insights for psychiatric drugs*) for the central core of ten TMs and seem to share a common mechanism for coupling to Na^+ even though they are not conserved in sequence with LeuT itself. These include the clinically important Na^+-driven glucose transporters of the SGLT family (436–440). Together these structures show how their structures, rather than their sequences, identify common mechanisms of transport.

How small viral transmembrane proteins could be a linchpin of viral infection?

Now more than ever there is an increased interest in the study of viral proteins. The focus has been rightfully placed on

replicases, polymerases, and receptors that enable viruses to pursue their dichotomic life cycle transitioning from a "lifeless" state as a viral particle to a prolific replicator when hijacking the host-cell machinery. In the particular case of membrane-enveloped viruses, the viral proteins essential to the ingress of the virus into the host cells are MPs that are important drug targets, as demonstrated with the spike protein from Severe Acute Respiratory Syndrome Coronavirus 2 (SARS-Cov2) (441–443). However, there is a class of membrane-embedded proteins termed VPs that are essential for virulence and infectivity (444–446) and have proven to be a valuable but yet elusive targets for therapies. VPs are small transmembrane proteins (60–120 amino acids) that oligomerize into ion channels capable of permeabilizing cell membranes (447). They are classified into class I for single pass TMs and class II for helix-turn-helix hairpin motifs (445, 447). Among the most studied VPs are the M2 proteins from Influenza A (IA) (448–455) and Influenza B (456, 457), VpU from HIV (458–467), the Envelope protein from Coronaviridae (468–471), and the p7 protein from Hepatitis C virus (472–476) (Fig. 12). Although all of the above have structures of either the full-length protein or of the TM monomer deposited into the PDB, the oligomerization state and ion conductance mechanism of some of these ion channels remain elusive given that the channel pore lumen is often lined by hydrophobic amino acids (*e.g.*, VpU and Envelope protein SARS-Cov1 (467, 471)). Moreover, VPs play diverse roles during the viral life cycle, modulating different host cell functions by directly interacting with host proteins (445, 458) or, as in the case of Influenza A VP M2, effecting the membrane curvature associated with the maturation and release of viral particles (451).

The M2 proton channel of IA is a canonical VP with more than 30 structures determined over the years informing many biochemistry studies. This tetrameric ion channel is essential for the IA infection. Upon acidification of the endosome by the cell machinery, M2 is activated to shuttle protons inside the viral particle, triggering disassembly of the viral core protein M1 and subsequent release of the ribonuclear protein complex (477). The proton shuttling process from the virus exterior to its interior by VP M2 is dependent on the protonation of residue H37 (448, 450, 478–480). Another major player involved in the proton conduction is W41, which, unlike other MPs where the aromatic residues are located with polar moieties oriented out from the membrane surface to act as anchor, faces the interior of the pore lumen to function as the channel's primary gate (481).The S31N mutation in M2 (Fig. 12*C*), first identified in 2006 and now prevalent in all strains of the virus, has rendered M2 IA resistant to amantadine and rimantadine, antivirals widely used for the treatment of flu (482). The functional core of this channel is comprised of a tetrameric helix bundle spanning the membrane and a juxtamembrane amphipathic helix that anchors the channel to the membrane and is essential for the process of nascent viral particle release from the host cell membrane (451) by inducing negative curvature around the nascent virion budding neck (483). The available structures of M2 IA have shown that the mechanism by which amantadine and rimantadine block ion conductance is by physically plugging the ion channel pore with their cage-like bulky adamantane chemical moiety. The S31N mutation seems to prevent such inhibition by placing a bulky Asn side chain in the pore entrance while the V27A mutant accomplishes this by removing the bulky Val side chain from the pore lumen that secures the inhibitor in place (Fig. 12, *B* and *C*). Many structures of the S31N mutant have been determined with the goal of understanding the mechanism by which this mutation blocks the entrance of a bulky ligand such as amantadine without affecting ion conduction (454, 484, 485). Recent studies, built on previous work by screening adamantane-derived compounds as well as non-adamantane compounds (485–492) against the S31N mutant, have identified inhibitors blocking the channel *via* the same mechanism used by amantadine and rimantadine *i.e.*, obstructing the channel pore (Fig. 12*E*).

Membrane protein structures instruct drug design and protein engineering

More than 50% of approved drugs target GPCRs and ion channels. Many drugs are metabolized by membrane-associated cytochrome P450s and/or exported by members of the solute carrier family (SLC) or ABC transporters involved in absorption, distribution, metabolism, and excretion of drugs (493–496). The democratization of protein structures since the establishment of the PDB has significantly contributed to the development of new therapies and the understanding of their mode of actions. The availability of MP atomic coordinates that can be accessed free of charge, viewed and manipulated on any researcher's computer opens endless possibilities such as *i)* designing mutagenesis studies to understand the roles of different residues in protein structure, function, and disease, *ii)* guiding rational protein engineering and design efforts aimed at improving the biophysical properties of protein targets to facilitate drug discovery and *iii)* modeling of putative binding sites. Structure-based drug development is one major area where PDB continues to foster and benefit the drug development process and ultimately leads to the more effective treatments for patients.

Protein engineering allows use of proteins for new applications including many advances in structural biology. Without the various purification tags/fusions we now use commonly, the PDB would still be limited to proteins from natural sources (497). Protein engineering also had significant contributions to the structural determination of many MPs themselves. The flourishing field of GPCR structural biology would not have been possible without the use of fusion proteins (such as modified T4 lysozyme) as crystallization chaperones (498). With increased knowledge of MPs, they can be used as powerful tools in many biochemical and biophysical applications. However, they need to be modified and optimized for applications under experimental conditions. The availability of structures of MPs is critical for optimizing properties of interest.

In this section, these contributions of the PDB to understanding MPs in the context of therapy and the new ways of understanding biological processes enabled by structure-based

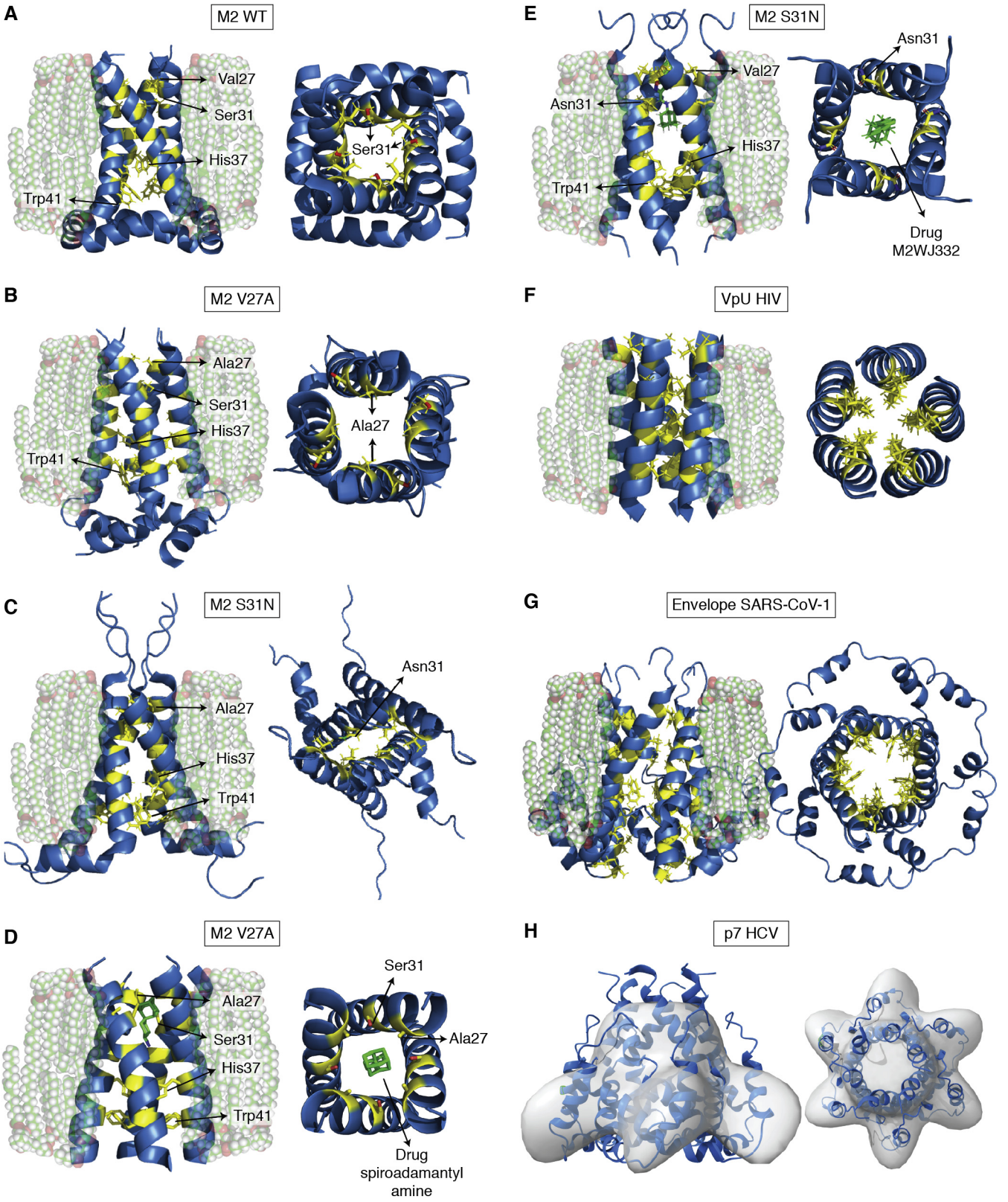

Figure 12. Viroporin structures. *A*, M2 PDB 2L0J (wild-type). Pore residues V27, S31, H37, and W41 highlighted in *yellow*. *B*, M2 PDB 2KWX (V27A mutation). Pore residues A27, S31, H37, and W41 highlighted in *yellow*. *C*, M2 PDB 2N70 (S31N mutation). Pore residues V27, N31, H37, and W41 highlighted. *D*, M2 V27A mutant (PDB 6NV1) in the presence of the spiroadamantyl amine inhibitor. Drug in *green* and pore residues A27, S31, H37, and W41 in *yellow*. *E*, M2 S31N mutant (PDB 2LY0) in the presence of the drug M2WJ332. Drug in *green* and pore residues V27, N31, H37, and W41 in *yellow*. The mutants V27A and S31N are both resistant to amantadine, the S31N mutant is the most common and now present in most Influenza A infections. The structures in panels *C* and *E* differ by the length of the construct, the absence and presence of drug, and the environment in which the structures were solved. While the M2 S31N structure in panel *C* was solved in liquid crystalline lipids environment, the structure in panel *E* was solved in a micellar environment. *F*, VpU TM pentameric structure (PDB pi7) *side* and *top view* showing in *yellow* the residues V9, V13, I17, and V21 lining the channel pore. *G*, structure of SARS-Cov1 Envelope protein TM and C-terminal domain (PDB 5X29) with pore lining residues N15, L18, A22, F26, V29, and I33 highlighted in *yellow*. *H*, Hepatitis C Virus p7 protein structures PDB 2M6X (pentamer) and PDB 2MTS (monomer) fitted to the cryo-EM density map (emd_1661) using *ChimeraX*.

protein engineering of MPs will be explored through a few illustrative examples.

How do structures of the membrane-bound cytochrome P450 enzymes inform the functional basis of monooxygenase activities, contribute to understanding of drug–drug interactions, and aid drug discovery?

Cytochrome P450 enzymes are monooxygenases with a highly conserved and unique fold (499). They have evolved to carry out specific metabolic reactions that help produce and modify metabolites including sterols, some lipids, and vitamins, or they can act as more broadly specific activators or detoxifiers of drugs. Despite this diversity of function and substrate clientele, all cytochrome P450s have the ability to generate, in a buried substrate specificity-conferring active site, an Fe(IV)-oxo-porphyrin cation radical (compound 1) that cleaves aliphatic carbon–hydrogen bonds by introducing an oxygen and producing water (500). When the PDB Molecule of the Month provided a succinct summary of current knowledge of the structure, function, and mechanisms of cytochrome P450s in 2006 (https://pdb101.rscb.org/motm/82), there were about 13,000 DNA sequences for cytochrome P450s described in databases and the PDB was dominated by crystal structures of microbial cytochrome P450s. The cytochrome P450s of higher eukaryotes had just begun to assume prominence in the PDB with the lodging of crystal structures of the catalytic domain of some membrane-bound drug metabolizing liver enzymes, such as cytochrome 3A4 in complex with various ligands (501). Now there are at least 600,000 cytochrome P450 DNA sequences and about 7000 NMR and crystal structures in the PDB for these molecules, primarily due to genome sequencing, the use of heterologous expression systems, and the exploration of substrate and ligand binding by academia and industry. This is enabling efforts to design more specific ligands for pharmaceutical and agricultural purposes (502–504), the use of mutagenesis and metal substitution to engineer new activities (505), and experiments that increase understanding of mechanistic features of cytochrome P450s.

Membrane-bound cytochrome P450s, which locate to the endoplasmic reticulum or mitochondria of eukaryotic cells, have catalytic domains with a comparable fold but were classified as significantly structurally different from the soluble P450s that occur in bacteria (506). This finding was based primarily on the interaction of the heme ring C propionate with the helices A–B loop in the case of the membrane-bound enzymes and with helix C for the soluble enzymes. The membrane-bound CYP51 enzymes provide an illustrative exception to this generalization. Both soluble and membrane-bound enzymes in this phylogenetically ancient cytochrome P450 family have their heme C propionate in an ionic interaction with a basic residue in helix C. A second factor used to discriminate between soluble and membrane-bound cytochrome P450s was the increased length and more complex disposition of the F–G helix region in the membrane-bound cytochrome P450s.

The short region linking the F–G helices together with the $\beta1/\beta2$ loop has considerable importance in membrane-bound CYP450s as they interact with the lipid bilayer surface and contribute to the mouth of a substrate entry channel through which hydrophobic substrates migrate from the membrane to the active site. While structures of recombinant N-terminal truncated eukaryotic cytochrome P450s, which present the enzyme's catalytic domain, are consistent with this relationship, it can be more directly inferred from biochemical labelling studies, computer simulations, and most importantly, the crystal structures obtained for the full-length fungal CYP51 from *Saccharomyces cerevisiae* (Fig. 13, *A* and *B*) and the more recent crystal structures of *Candida glabrata* and *Candida albicans* CYP51s (507, 508). These molecules include an N-terminal membrane associated α-helix and a TM that also interfaces *via* hydrophobic and hydrogen-bonding interactions with a portion of the surface of the catalytic domain. This feature not only provides a membrane anchor but it also orients the catalytic domain so substrates and inhibitors can enter the substrate entry channel from the lipid bilayer. The substrate entry channel and active site have been mapped in numerous structures of *S. cerevisiae* CYP51 complexed with ligands including a range of antifungal azole inhibitors including posaconazole, itraconazole, fluconazole, voriconazole, and VT-1161 plus several azole fungicides used in agriculture (508–511). These structures identify interactions between these ligands and the heme, specificity-conferring amino acid residues lining the interior cavity of the protein, and with key water molecules. Also visualized were interactions affected by species-specific substitutions that confer inherent resistance to some classes of azole drugs (512) or mutations that confer acquired resistance to some or all classes of azole drugs (513, 514). The structural and phenotypic impacts of these substitutions and mutations are important drivers of efforts to identify novel antifungals that will circumvent these target-based azole-resistant phenotypes (503).

A feature invoked for rational antifungal design is the similarity across phyla of CYP51 structures and the absence of major structural rearrangements in complexes with various inhibitory ligands or structural analogs (503, 515). However, structures obtained for full-length and truncated CYP51s in complex with the short-tailed tetrazole inhibitor VT-1161 and the long-tailed triazole inhibitor posaconazole suggest that the disposition of the mouth of the substrate entry channel required for broad spectrum antifungal activity may be compromised in truncated structures liganded with the short-tailed azole due to structure distorting intersubunit crystal lattice interactions (509). Furthermore, poor substrate binding for both truncated and full-length CYP51 molecules led to conflicting proposals for substrate orientation. The likely orientation of sterol substrates was recently clarified using an I105 F mutant of *Trypanosoma cruzi* CYP51 (516). The mutation converted a fungi-like eburicol-specific CYP51 to a plant-like obtusifoliol-specific enzyme but with substrate occupancy increased to ~85%. This allowed reliable visualization of this substrate in the binding cavity formed by the B–C loop, helix C, and helix I, with the obtusifoliol hydroxyl group oriented into the substrate access channel. Comparable

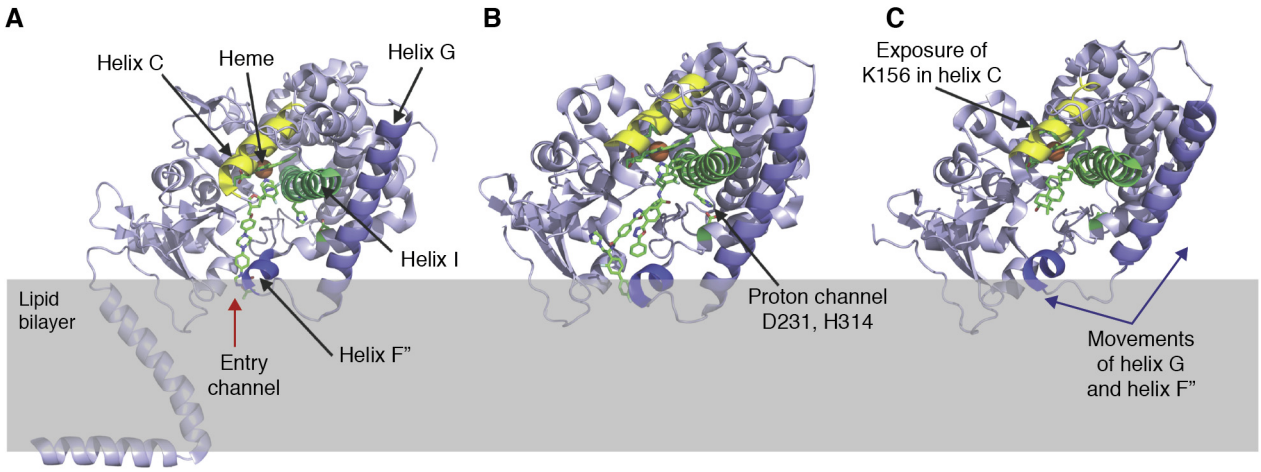

Figure 13. Comparison of the full-length *Saccharomyces cerevisiae* CYP51 structure with structures of the human CYP51 catalytic domain. Helix B and the B–C loop have been removed to visualize the interior of these molecules and their ligands. The catalytic domain of the full-length yeast CYP51 enzyme (*A*) in complex with posaconazole and the human catalytic domain in complex with two molecules of the inhibitor VFV (*B*) have essentially identical folds, with their helix C K151 and K156 sidechains, respectively, making ionic interactions with the heme propionate. Ablation of the proton transfer pathway in the human CYP51 D231/H314 mutant catalytic domain (*C*) gives substrate occupancy sufficient to visualize lanosterol bound in an inactive but catalytically competent state that demonstrates significant conformational change in comparison with *B*. K156 no longer binds to the heme propionate—its side chain projects above the enzyme's proximal surface and the C-helix rotates slightly, uncoiling its center section, and facilitating binding of the cognate NADPH-cytochrome P450 reductase in the vicinity of helix C. A slight reorientation of helix I caused by interaction with the hydrophobic tail of lanosterol contributes to a significant repositioning of the F-G helices. It changes in the ionic and hydrogen bond interaction between D298 and 299D, at the N-terminal end of helix I, with basic residues (H257, K261, R272) and Y265 on helix G. This modifies the position of helix G so that the F″ helix almost completely closes the entry to the substrate channel at the membrane surface. A positional change in the M487 side chain adjacent to helix F″ is also involved in substrate entry channel closure. This includes the formation of a water-mediated hydrogen bond network involving M378 and I379, located in a substrate entry channel-lining internal loop, and the hydroxyl group of the bound lanosterol.

visualization of the substrate lanosterol was achieved with the human CYP51 D231A H314A mutant (Fig. 13, *B* and *C*) that has the salt bridge involved in proton delivery ablated (517). Furthermore, with productive substrate binding by both the protozoan and human enzyme, a significant reorientation of helix C occurred; the heme propionate-helix C ionic linkage was lost and the freed basic side chain projected outward from the enzyme surface.

Membrane-bound cytochrome P450s operate in a more complex environment than the soluble enzymes and may perform as molecular machines. They interact with a cognate NADPH-cytochrome P450 reductase (CPR) that supplies pairs of electrons, in some instances with cytochrome b_5 and, when taking part in metabolic pathways, with multiple downstream enzymes that use the product of the cytochrome P450. For example, an additional channel in the fungal CYP51 enzymes bifurcates from the substrate entry channel (508). This channel has been proposed to mediate product egress and interaction with enzymes immediately downstream in the ergosterol biosynthesis pathway, such as the Erg24 reductase and the demethylating complex of Erg25, Erg26, and Erg27 that are mounted on the Erg28 scaffold protein. Some of these enzyme–enzyme interactions have been mapped in yeast systems using the split-ubiquitin system (518).

A recent study using docking techniques and molecular dynamics has modeled possible interactions between membrane-bound mammalian CPR and membrane-bound CYP1A1 (449). The mimicking of complementary ionic, van der Waals, and hydrophobic interactions between the CPR FMN domain and the residues on the B, C, and L-helices, the J-K loop and the loop structure in the proximal surface near the CYP1A1 heme, plus the inclusion of a hydrogen bond between the FMN phosphate group and the Q139 sidechain in helix C, appeared to enable efficient electron transfer to the heme. Crystallographic and NMR analysis of the bacterial cytochrome P450s, the camphor binding CYP101A, and mycinamicin biosynthetic enzyme MycG, indicate the movement of particular secondary structure elements during substrate binding (450, 451). This finding has been validated by site-directed mutagenesis experiments and used to suggest a generally conserved mechanism for substrate binding and recognition in the P450 superfamily. In CYP51s, accommodation of the substrate in a catalytically competent position is now expected to drive reorientation of helix C and CPR binding, close the substrate entrance channel, and activation of the proton relay machinery *via* F-F″-G arm repositioning and the His-acid salt-bridge opening required for the O–O bond heterolysis (Fig. 13, *B* and *C*). This process has been suggested to prepare the CYP51 catalytic machinery for the three consecutive reaction cycles using compound 1 characteristic of this class of cytochrome P450. It occurs without the substrate release after its first and second monooxygenation reactions, distinguishing it from most other cytochrome P450s (447).

A major challenge in the P450 field is understanding how the membrane-spanning domains impact on the mechanistic basis of eukaryotic cytochrome P450 function. For members of the membrane-bound CYP51 family this will include determining how the protein subunits of this complex molecular machine interact in an ordered fashion and how its sterol

substrate is extracted from the membrane and reoriented in order to present appropriately to a series of active sites. This is now feasible through the incorporation of full-length eukaryotic cytochrome P450s, along with their cognate MP partners, into membrane-mimicking environments such as nanodiscs, together with the application of NMR and cryo-EM (452, 453). Using structural knowledge of cytochrome P450 conformational states to generate new classes of antifungal agents not susceptible to side effects caused by drug–drug interactions with drug metabolizing cytochrome P450s in humans is an exciting and much needed endeavor.

Can structural data provide a mechanistic understanding of the loss-of-function mutations in the cystic fibrosis transmembrane-conductance regulator and guide the development of compensatory therapies?

CF is a well-known genetic disease affecting approximately 70,000 people worldwide (519). It is caused by diverse mutations in the gene coding for the ABC transporter CFTR, which leads to defective biosynthesis or misfolded or dysfunctional CFTR protein. Lack of functional CFTR in epithelial tissues disrupts salt homeostasis, leading to progressive lung disease, exocrine pancreatic insufficiency, and intestinal abnormalities, among many other symptoms. In the lung, CF is characterized by excessive mucus accumulation contributing to obstructive pulmonary disease, which is the main cause of morbidity and mortality. Although still an incurable disease, life expectancy for CF patients has steadily improved to around 40 years thanks to better disease management and treatments that resulted in part from a better understanding of CFTR (520–522).

Since the discovery of the linkage between CF and mutations in the CFTR gene in 1989 (523–525), significant progress has been made in mechanistic understanding and therapy design. CFTR is an ABC transporter that shares the two TMDs and two NBDs that hydrolyze ATP characteristics of this superfamily (see *How do drugs control our minds? Molecular insights for psychiatric drugs*), but includes an additional regulatory (R) domain and an N-terminal lasso motif (526). It is the only known member of the ATP-gated ion channel family, transporting chloride in an ATP-dependent and R domain phosphorylation-dependent manner (361, 527, 528). More than 350 CF-causing CFTR variants have been identified (http://cftr2.org/). Two classes of CFTR-modulator therapies have been designed to compensate for the malfunctioning protein generated by these mutations. These include correctors such as lumacaftor, tezacaftor, and elexacaftor that assist in CFTR protein folding and trafficking to the cell surface, while potentiators such as ivacaftor improve CFTR's activity (529, 530). Without structural information available, the main discovery and optimization approaches involved intensive high-throughput screening and structure–activity relationship (SAR) campaigns (531, 532).

Recent structural efforts by Chen and colleagues are changing that scenario, by solving CFTR structures in the dephosphorylated ATP-free form (379, 381), phosphorylated ATP-bound form (380, 533), and phosphorylated ATP-bound form in complex with potentiators (534). Many CF-causing mutations could be mapped into these structures, and their negative effect rationalized as affecting the pore construction, protein folding, the ATPase site, or the NBD/TMD interface. The cryo-EM structure of the phosphorylated ATP-bound human CFTR (hCFTR) E1371Q mutant in complex with potentiators ivacaftor (an FDA-approved drug developed by Vertex Pharmaceuticals) and GLPG1837 (an investigational drug developed by Galapagos) shed light on how these molecules improve hCFTR activity in CF patients (Fig. 14*A*) (534). Ivacaftor-bound E1371Q, phosphorylated and ATP-bound, exhibits the same conformation as the ivacaftor-free structure. Interestingly, ivacaftor binds CFTR at the protein–lipid interface in a clef formed by TM helices 4, 5 and 8. As shown in previous structures, TM8 rotates upon phosphorylation and ATP binding, and ivacaftor appears to stabilize this rotation. Ivacaftor might thus function by favoring the open conformation of the pore. Residues L233, F236. Y304, F305, S308, F312, F931, and R933 are identified as key in the CFTR–ivacaftor interaction (Fig. 14*B*) and correlate with previously published SAR studies that led to ivacaftor's development (531). The elucidation of GLPG1837-bound E1371Q, phosphorylated and ATP-bound structure (Fig. 14*C*) showed that although chemically dissimilar to ivacaftor, its interaction with CFTR largely overlaps ivacaftor's binding site. Both ivacaftor and GLPG1837 were discovered by extensive high-throughput screening, followed by further optimizations through SAR (531, 532). The availability of these potentiator-bound structures, and future corrector-bound structures, could represent a new avenue for the development of more efficient CF treatments.

Other structures of ABC transporters have contributed to therapy. It is noteworthy that the breast cancer resistance protein (BCRP or ABCG2) and P-glycoprotein efflux a number of drugs, affecting their pharmacokinetics and bioavailability and mediate multidrug resistance. Their structures were elucidated in different conformations, in the presence and absence of drugs, paving the way for the development of a newer generation of drugs that can inhibit or evade multidrug resistance associated with these transporters (386–392).

How does understanding of a glucose transporter selectivity and conformational changes inform the development of GLUT1-specific inhibitors?

Glucose is an essential source of energy used by tumor cells to produce ATP, maintain the reduction–oxidation balance, and generate biomass (535). Glucose transporter GLUT1 is overexpressed in many types of cancers, including the brain, colon, kidney, lung, ovary, and prostate, and represents a promising target for therapy (536). However, there are 14 GLUT transporters in humans, and due to their high sequence homology, many GLUT inhibitors lack isoform specificity (537–541). The development of GLUT1-specific inhibitors would thus benefit from the understanding of its atomic structure and the identification of key residues that could be targeted for selective inhibition.

Initial structural and mechanistic understanding of glucose transport by GLUTs was provided by studies focusing on

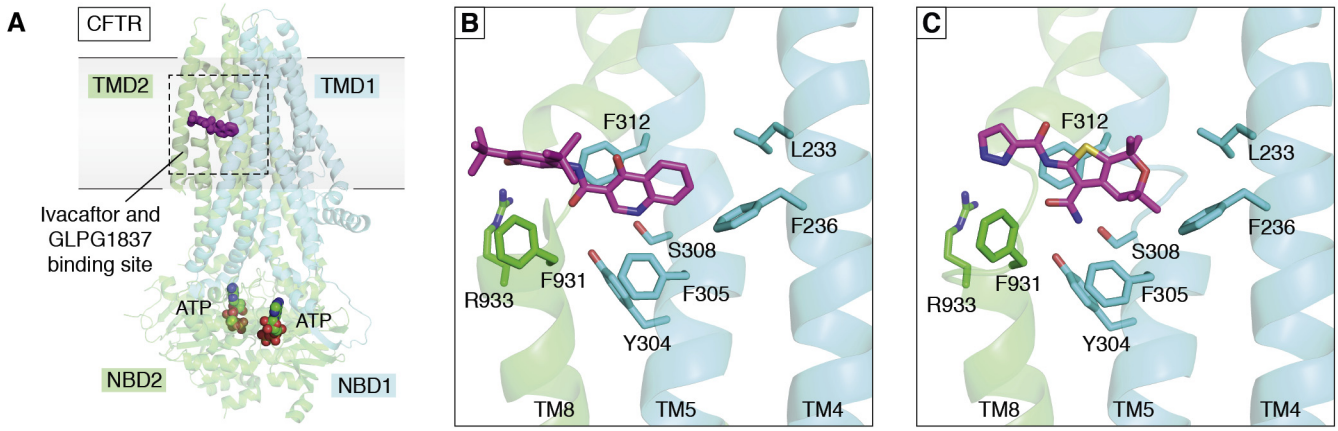

Figure 14. Structural understanding of CFTR function and therapeutic targeting. *A*, structure of the phosphorylated, ATP-bound hCFTR in complex with ivacaftor (PDB 6O2P). *Ribbon* representation, with TMD1 and NBD1 colored in *cyan*, TMD2 and NBD2 in *green*. The approximate location of the lipid bilayer is shown in *gray*. Ivacaftor is shown in *magenta*, in *stick* representation. ATP-Mg^{2+} molecules are shown in *sphere* representation (carbon in *green*, nitrogen in *blue*, oxygen in *red*, Mg^{2+} in *yellow*). *B*, close-up image of main interactions between hCFTR and Ivacaftor (PDB 6O2P). A selected number of interacting residues are shown in *stick* representation, carbons are colored in *cyan* (TMD1) or *green* (TMD2), nitrogen is *blue*, oxygen is *red*. *C*, close-up image of main interactions between hCFTR and GLPG1837 (PDB 6O1V). Main interacting residues are shown in *stick* representation, carbons are colored in *cyan* (TMD1) or *green* (TMD2), nitrogen is *blue*, oxygen is *red*, sulfur is *yellow*.

bacterial homologs (see *How do drugs control our minds? Molecular insights for psychiatric drugs*). The first human GLUT1 (hGLUT1) structure was determined by Deng *et al.* (403). It contained mutations N45T, which removed a glycosylation site, and E329Q, which blocked the transporter in an inward-facing conformation. Interestingly, a molecule of β-nonyl glucoside, the detergent used during purification, was present in the inward-open cavity, with the D-glucopyranoside headgroup bound to the C-terminal domain near the center of the membrane, overlapping with the glucose-binding site observed in the bacterial homolog XylE structure in complex with glucose (434). The structure provided a molecular basis for interpreting mutations linked to disease. These inactivating variants could be clustered within the substrate-binding site, at the interface between the TMDs and the intracellular helix (ICH) domain, and throughout the lining of the transport path.

Kapoor *et al.* (405) reported three structures of wild-type hGLUT1 cocrystallized with drug leads, the cell-permeable mycotoxin cytochalasin B, and two new inhibitors identified by high-throughput screening, GLUT-i1 and GLUT-i2. Despite different chemical structures, the three inhibitors bind to the proposed glucose-binding site in the central cavity, with hGLUT1 residues S80, T137, Q282, W388, N411, and W412 interacting with all three ligands (Fig. 15). The IC_{50} values of cytochalasin B, GLUT-i1, and GLUT-i2 bound to GLUT2-4 highlighted differences in specificity. When combining the crystal structure of GLUT1 bound to these compounds with the corresponding structure-derived molecular models for hGLUT2-4 bound to them, comparison of interacting residues and potential differences could inform the development of future, more-specific compounds.

The structural information generated represents a practical basis for the development of more specific GLUT1 inhibitors. While the previous development of GLUT inhibitors was based on high-throughput screening and SAR-based optimizations (536), activity-based and *in silico* screening campaigns to identify specific GLUT inhibitors relying on structural information are starting to bear fruit (542–544). The structure of the main sugar transporter *Pf*HT1 from the malaria parasite was determined recently by two groups (545, 546). In one of the studies, the high-resolution structure was used to allow rational design of more potent and selective inhibitors of *Pf*HT1 that could be used to treat malaria. With an increasing number of GLUT structures being determined, one can expect a new generation of potent and specific GLUT inhibitors developed with similar structural-based strategies to treat diverse diseases. Public access of structures through PDB is no doubt a pillar for such endeavors.

How do drugs control our minds? Molecular insights for psychiatric drugs

The majority of signal transduction events in our brain are mediated by small molecules known as neurotransmitters. Neurotransmitters in the cytosol must be packaged into synaptic vesicles by vesicular neurotransmitter transporters before they can be released from the presynaptic axon by exocytosis upon action potential stimulation (547–549). The released neurotransmitter then elicits their effects by binding to two kinds of membrane receptors on the postsynaptic dendrite: ionotropic ligand-gated ion channels (LGICs) for fast response or metabotropic GPCRs for slow effects (550, 551). To ensure proper synaptic transmission, it is equally important to terminate the signal promptly by rapid removal of neurotransmitters from the synapses after their release. This is often achieved by high-affinity neurotransmitter transporters located on the plasma membrane of presynaptic termini and in the surrounding glial cells (552, 553) or by diffusion and hydrolysis of the neurotransmitter (554).

Use of chemical substances to change mood and behavior dates back several thousands of years with well-known examples including coca (cocaine), coffee (caffeine), alcohol, and

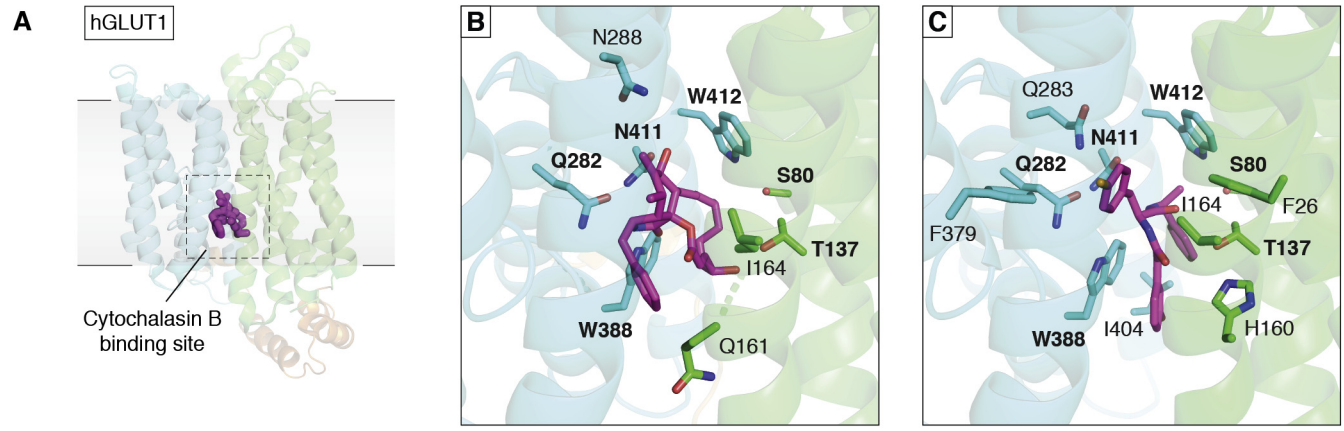

Figure 15. Structural understanding of the function and transport inhibition of human GLUTs. *A*, structure of hGLUT1 bound to cytochalasin B (PDB 5EQI). hGLUT1 is in *cartoon* representation, with its N-terminal domain colored *green*, ICH *orange*, and the C-terminal domain *cyan*. Cytochalasin B is shown in *stick* representation, colored in *magenta*. The approximate location of the lipid bilayer is shown in *gray*. *B*, close-up image of main interactions between hGLUT1 and cytochalasin B (PDB 5EQI). Main hGLUT1 interacting residues and ligand are shown in *stick* representation, carbons are colored in *green* (N-terminal domain), *cyan* (C-terminal), or *magenta* (ligand), nitrogen is *blue*, oxygen is *red*. Residue labels in *bold* highlight common interacting residues with cytochalasin B, GLUT1-i1, and GLUT-i2. *C*, close-up image of main interactions between hGLUT1 and GLUT1-i1 (PDB 5EQG). Same labeling and coloring scheme as in (*B*), with the addition of fluorine (*orange*).

marijuana (cannabis). Modern research on these compounds as psychiatric drugs began after World War II with advances in chemical synthesis and animal testing. In parallel, critical advancements in neuroscience and molecular biology allowed the identification of the target proteins for these drugs and understanding of their effects. It is not a surprise that most of these compounds target MPs located at the synapse. In fact, almost all MPs that bind neurotransmitters are intensively studied as drug targets. Particularly, LGICs and neurotransmitter sodium symporters (NSSs) are amongst the top ten families of all FDA-approved drugs, accounting for 7.9% and 2.7% respectively (555). On the other hand, the recent epidemic of drug abuse spotlights a lack of advancement in this area. In fact, most currently used psychiatric drugs were developed in the mid-to-late 20th century. Their use/misuse is associated with side effects, and they are criticized for contributing to addiction. This highlights the need to develop more specific drugs with less side effects and that are less likely to be addictive. The availability of structures of these MPs in complex with their endogenous ligands and/or drugs in the PDB is the basis for such efforts. Research on psychiatric drugs over the past 50 years is a good example of how structures of MPs have helped to elucidate the mechanisms of action of drugs.

LGICs located on the postsynaptic cells are the major effectors of neurotransmitters. They underlie the rapid phasic synaptic transmission. The receptor for the major inhibitory neurotransmitter GABA is a Cl^- channel that hyperpolarizes the postsynaptic cell and reduces the firing probability of the receptor neuron when activated (550). As a result, ligands of $GABA_AR$ are highly sought-after as psychiatric drugs. $GABA_AR$ belongs to the Cys-loop receptor family together with the receptors for glycine and acetylcholine, all of which have had their structure and pharmacology intensively investigated (41, 75, 550, 556–569). The structure of the Cys-loop receptors forms a pentameric ion channel made of five similar but nonidentical subunits (Fig. 16, *A* and *B*). Each heteropentameric channel is typically assembled with 2 α, 2 β and 1 γ (or δ) subunits. There are 19 genes encoding for the α, β, and γ subunits of the $GABA_AR$ in humans that are differentially expressed in different regions of the brain. The assembly of different subunits of $GABA_AR$ results in complex heterogeneity in their structures and is the major determinant of their differing functions in distinct regions of the brain and their complex pharmacological profile (570, 571). Several recent structures of $GABA_AR$ in complex with various ligands have provided unprecedented insight into the molecular mechanism of some commonly used psychiatric drugs (556, 564, 566–568). For instance, both Valium (benzodiazepine) and Xanax (alprazolam) bind to $GABA_AR$ at the benzodiazepine site between subunit α and γ on the extracellular ligand-binding domain (Fig. 16*C*) while the endogenous ligand GABA as well as bicuculline binds at the interface between the α and β subunits (Fig. 16*D*). Structures of $GABA_AR$ revealed that Benzodiazepines potentiate the effect of GABA by improving the connectivity between subunits allosterically while bicuculline competes with GABA at the same binding site to prevent the channel from opening. On the other hand, Flumazenil, which is used clinically to treat benzodiazepine overdose, competes with benzodiazepines at the same binding site (Fig. 16*C*). The neurotoxin picrotoxin, which is used as stimulant and convulsant, directly blocks the ion-conducting pore (Fig. 16*H*). The structures also revealed a previously unknown second binding site for the benzodiazepine at the transmembrane region (Fig. 16*E*) as well as several binding sites for anesthesia agents in the transmembrane region (Fig. 16, *F* and *G*). This information highlights new possibilities for drug interaction. The structures of $GABA_AR$ bound with substrate and drug ligands are major step forward toward better psychiatric drugs.

Another way of modulating synaptic transmission is by regulating the concentration of neurotransmitters at the

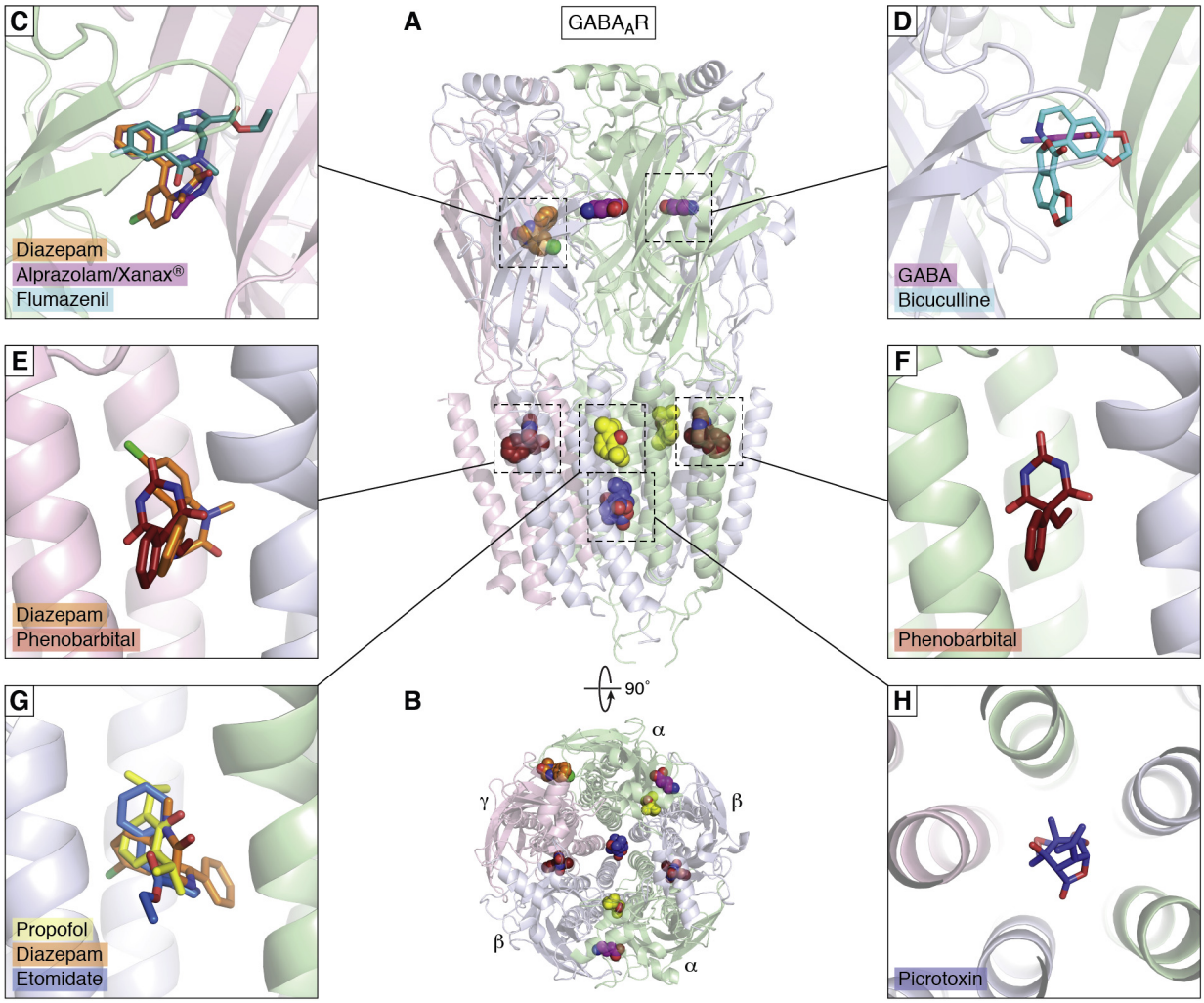

Figure 16. Structural basis of psychiatric drugs targeting GABA$_A$R. *A* and *B*, overall structure of GABA$_A$R with one representative ligand at each distinctive binding site shown in *sphere* representation. *C–H*, composite structure of GABA$_A$R with ligands binding at different sites (PDB 6HUO, 6HUP, 6HUK, 6HUJ, 6HUG, 6I53, 6D6U, 6X3X, 6X3U, 6X3Z, 6X40, 6X3S, 6X3W, 6X3V, 6X3T).

synaptic cleft. In fact, the most popular marketed antidepressants, such as Prozac (Fluoxetine), Zoloft (Sertraline), Celexa (Citalopram), all use this strategy. The selective serotonin reuptake inhibitors (SSRIs) are a group of drugs targeting serotonin transporters on the plasma membrane of the presynaptic neurons (572). As deficiency of serotonin and dopamine (DA) is implicated in depressive disorders, increasing their availability at the synapse through blocking their reuptake is commonly used to treat depression. The dopamine pathway has been targeted for the treatment of depression since the early 1950s with the use of monoamine oxidase inhibitors (MAOIs) and tricyclic antidepressants (TCAs) (572). However, they have undesirable adverse effects and a high potential for toxicity. With the identification and cloning of the transporters for serotonin (SERT), dopamine (DAT), and noradrenaline (NET), SSRIs are designed to specifically inhibit SERT but with minimal inhibition of NET, which was the source of side effect of antihistamine used earlier. Major chemical synthesis efforts together with *in vitro/in vivo* screening and testing from major pharmaceutical companies successfully identified several SSRIs that were much more selective and with less adverse effects compared with TCAs. Since 1987, an increasing number of SSRIs have been marketed and used to treat depression till the current day and hailed as a great success for rational drug design. However, the secret of success remains somewhat mysterious, as no one really understood how these drugs were able to interact selectively with SERT, but not the very similar DAT and NET, at the molecular level. The availability of structures of these transporters in complex with substrates and drug ligands is starting to provide the answer.

SERT, DAT, NET all belongs to the SLC6 family of NSSs. They are high-affinity transporters for biogenic amines (dopamine, serotonin, and noradrenaline) driven by the sodium gradient across the plasma membrane. Following intense efforts, the structure of a bacterial homolog of SLC6 family transporters, a leucine transporter from *Aquifex aeolicus*, LeuT, was first determined in 2005 (60). LeuT revealed the "5 + 5" inverted repeat structural fold for the first time (Fig. 17*A*), which is highly conserved throughout evolution. The structure of LeuT also identified two highly conserved

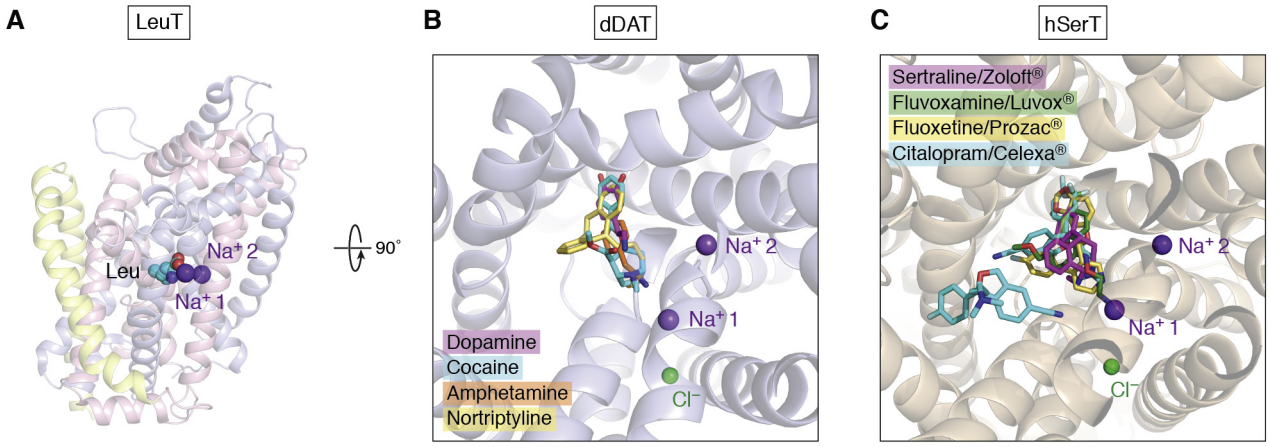

Figure 17. Structural basis of antidepressants targeting SLC6 family NSSs. *A*, structure of LeuT (PDB 2A65) defines the common structure of the SLC6 family transporters. LeuT is composed of 12 TMs. TM1-10 forms the signature "5 + 5" inverted repeat with TM1-5 (*light blue*) and TM6-10 (*pink*) forming the core domain repeating each other with a pseudo twofold symmetry along the substrate binding site. TM11 and TM 12 (*yellow*) are located at the peripheral of the core domain. The substrate leucine is shown as *cyan sphere* while the two sodiums are shown in *purple*. *B*, ligand-binding site structure of dDAT in complex with substrate dopamine as well as other psychostimulants (PDB 4M48, 4XP6, 4XP9, 4XP1, 4XP4, 4XP5). *C*, ligand-binding site structure of hSERT in complex with common antidepressants (PDB 6AWO, 5I73, 5I6X, 6AWP). Na^+ is shown in *purple* while Cl^- is shown in *green*.

Na^+-binding sites and elucidated the substrate transport mechanism. More importantly, the structure of LeuT provided a blueprint for understanding the substrate specificity of SLC6 transporters, which are central for the selectivity and efficacy of the SSRI antidepressants. In one approach, the substrate-binding site of LeuT, which binds to leucine naturally, was engineered to harbor residues that would bind to the biogenic amines. Structures of the chimeric transporter LeuBAT in complex with four classes of antidepressants (SSRIs, serotonin norepinephrine reuptake inhibitor, TCA, and Mazindol) were determined, and this provided the first glimpses of how these drugs interact with NSS transporters (573). The structures of *Drosophila* DAT in complex with endogenous substrate dopamine, as well as cocaine, amphetamines, and TCA antidepressants were subsequently determined in 2013 and 2015 (574, 575) (Fig. 17*B*). Finally, the structure of the human SERT was determined recently in complex with several TCAs and SSRIs by both X-ray crystallography and cryo-EM (576–579) (Fig. 17*C*). These structures clearly illustrate that the majority of antidepressants targeting NSSs function through competing with the endogenous substrates at the central binding site. However, a second allosteric binding site at the entrance to the central binding site was observed in several structures, suggesting additional factors that may influence the selectivity. These structures also further elucidated the transport mechanism of eukaryotic NSSs, which are also regulated by Cl^-, K^+, and membrane lipids. These structures provide a much better understanding of how antidepressants act upon NSSs. Their availability in the PDB provides an invaluable resource for structure-based drug discovery and development that will surely lead to better antidepressants.

How can membrane proteins be engineered to advance biological discovery?

Neuroscientists have dreamed for decades of controlling specific groups of neurons in free-living animals to interrogate functions of neuronal circuits. Optogenetics enables exactly that, with the help of a family of light-sensitive algal membrane channels called Channelrhodopsins (ChRs). Protein engineering is enabling fine-tuning of the properties of ChRs to allow an ever-growing range of applications (https://web.stanford.edu/group/dlab/optogenetics/index.html). This topic has been reviewed previously by the founders of the field, Deisseroth and Hegemann (580, 581). Here we briefly illustrate the contribution of PDB in the exciting endeavor to understand the human brain and behavior.

Although naturally existing ChRs have been used in pioneering optogenetic studies since 2005 (582), it was really structure-based protein engineering that fueled the tremendous developments that allowed it to become a powerful and versatile tool for neuroscience. ChRs are seven TM integral MPs that use retinal as chromophore and function as cation channels. Fortunately, the structure of their remote cousin, bacteriorhodopsin, was among the first MPs to be determined. Bacteriorhodopsin and ChRs share the same 7-TM structure fold with a similar binding site for the chromophore retinal (Fig. 18, *A* and *B*). With hundreds of structures already determined and detailed biophysical characterization available, bacteriorhodopsin allowed models of ChRs to be built. These helped in optimizing the optical properties and resulted in several useful modified ChRs. For instance, the ChETA variant was obtained by mutating E123 of ChR2 and allows fast-firing at 200 Hz or more (583). Modification of TM3-TM4 interaction at the CD pair (C128-D156 in ChR2) resulted in the step-function opsins, SFOs, which enable bistable excitation photon-spike logic (584–586). A diverse family of red-shifted C1V1 ChRs were created by modification of the ChR from alga *Volvox carteri* (587–590). The crystal structure of a chimera between ChR1 and ChR2, C1C2, determined in 2012 (591, 592) (Fig. 18*B*) further clarified the location and structure of the light-activated pore and made even more designer ChRs possible. In particular, the structure revealed that the internal

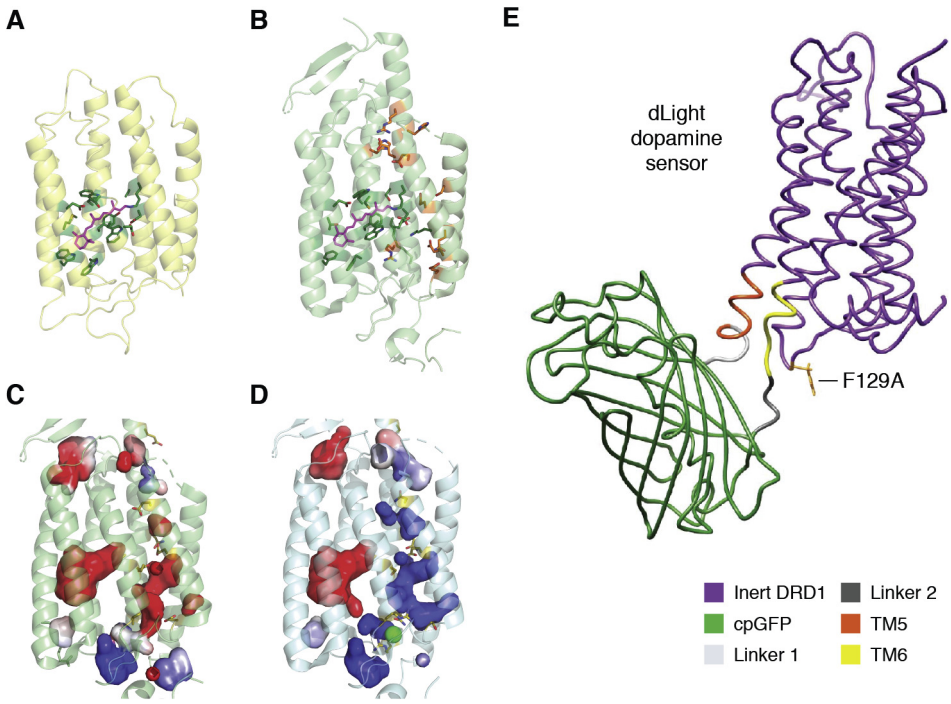

Figure 18. Protein engineering applications based on membrane proteins. *A*, structure of the bacteriorhodopsin (PDB 1AP9). *B*, structure of the C1C2 ChR (PDB 3UG9). In both (*A*) and (*B*), the retinal is shown as *magenta sticks* while residues forming the retinal binding site are shown as *dark green sticks*. Residues along the ion-conducting pathway of ChRs are shown as *orange sticks* on the C1C2 structure in (*B*). Refer to Ref. (580) for more details. *C*, electrostatics of the vestibule of C1C2 ChR. *D*, electrostatics of the vestibule of the designed anion channel iC^{++} (PDB 6CSN). *E*, design of the dLight dopamine sensor (used with permission (602)).

vestibules of the cation conducting ChRs are lined with negatively charged residues (Fig. 18*C*). Guided by the structure, mutagenesis of residues lining the vestibule reversed the charge. This resulted in a highly Cl^- selective ChRs (iC^{++}) (Fig. 18*D*) (593, 594) now widely used to elicit inhibitory stimulation. Optogenetic is a fast-growing field with applications requiring ChRs with a wide range of properties. As illustrated here, the availability of the structures of the natural and designed ChRs will continue to be a major driving force for further advancements.

Genetically encoded sensors are widely used in biophysical and cell biological investigations. It is not an overstatement that fluorescent proteins, such as the green fluorescent proteins (GFP), enabled modern cell biology. Structure-guided protein engineering that combines a fluorescent protein with another functional group has allowed various physiological processes to be monitored and investigated by fluorescent methods in cell cultures and in animals. For instance, the calcium sensor GCaMP was created by fusing of the GFP with the calcium-binding protein calmodulin and an M13 peptide from myosin light chain kinase (595). Similarly, the glutamate sensor iGluSnFR (intensity-based glutamate-sensing fluorescent reporter) was obtained by fusion of a circularly permutated enhanced green fluorescent protein (cpEGFP) with a bacterial glutamate-binding protein (596, 597). Both GCaMP and iGluSnFR, as well as their variants, are now widely used to study calcium signaling and glutamate neurotransmission. Due to the difficulties with MPs, applications of genetically encoded MPs lagged behind those of soluble proteins by a few decades. In recent years, however, with the exponential growth in the available structures of MPs, applications of MPs as genetically encoded sensors are gradually emerging.

Dopamine is an important neuromodulator of complicated behaviors such as motivation, rewards, learning, and motor control. There is thus a large demand for monitoring its concentration in cells and in animals. However, unlike other neurotransmitters, such as glutamate and GABA, dopamine exclusively activates the metabotropic GPCRs. Without eliciting any direct electrical response, it is hard to monitor dopamine by using electrophysiological techniques. Fortunately, the structures of three out of the four dopamine receptors (all members of the GPCR family) were determined recently (598–600). The structures allowed two groups to independently design fluorescence sensors for dopamine based on the dopamine receptors. Tan's group designed several dopamine fluorescent sensors (dLight) by replacing the third intracellular loop of human dopamine receptor D1, D2, and D4 with the cpGFP module from the GCaMP6 (Fig. 18*E*). The first generation of dLight sensors have already been successfully used in cell cultures, slice preparations, and free-moving mice. Similarly, Li's group obtained the GPCR-activation-based dopamine sensors, $GRAB_{DA}$, by inserting the cpEGFP into the intracellular loop 3 of the D2 dopamine receptor. This construct enabled successful measurement of dopamine concentration in mice, fishes, and flies (601).

With an increasing number of MP structures determined in recent years, there is no doubt that more applications in addition to those illustrated here will emerge. The free availability of structures to all protein engineers is critical knowledge that will allow this field to thrive.

Future perspective

The Coronavirus Disease 2019 (COVID-19) pandemic dominated world attention in 2020 (603, 604). The main routes to eliminate this infectious disease currently focus on two MPs: the viral spike protein (605, 606), and the membrane-bound form of the Angiotensin Converting Enzyme 2 (ACE2) on the lung epithelial cell (607). Vaccines target the viral spike protein to activate an immune response. Peptides attempt to target the ACE2 site without altering its essential human function (608). The primary preventative focus now includes mRNA-based and virus-based vaccines that encode the Spike protein and other membrane proteins that then excite the immune response ahead of encounter with the virus. Vaccines encoding the Spike protein mRNA use lipid-based micelles or viral vectors for entry into human cells. The lessons learned in 2020 provide a template to combat pandemics. Can we now develop general strategies for COVID-19, and for inevitable future infectious agents, by preventing the early-stage interactions required for pathogenesis? Prevention of the spike protein–ACE2 interaction, a feature that was swiftly determined at the structural level, has the potential to provide stop-gap therapy until a much-needed cure can be discovered and implemented. For example, monoclonal antibodies or VH domains could block critical entry interactions. Structural science has produced several exciting templates for this important direction.

The newest exciting tool in this endeavor is a protein folding program, *AlphaFold 2*, created by Google's DeepMind group and showing revolutionary accuracy in predicting protein structure directly from sequence in a blinded competition (the 14th Critical Assessment of Structural Prediction competition, CASP14) (609). The program, utilizing "*Artificial Intelligence*" trained on the high-quality structures available in the PDB, follows closely on the heels of the cryo-EM revolution and heralds a future with rapid access to more precise MP structures, potentially solving the bottleneck in structure-based drug design. The structures of MPs are, so far, less accurately predicted, but the Tidow group reports that after 2 years of unsuccessful work on solving the crystal structure of the MP FoxB, they succeeded using DeepMind's prediction in a few hours by molecular replacement (610). Undoubtedly the program will become even more precise and valuable for MPs as new structures are solved by the powerful technological advances discussed above.

Traditionally, many long-standing and emerging diseases have been accorded low priority by the pharmaceutical industry due to the limited commercial value of potential therapies. We might imagine that MP-based strategies that target key first steps in the pathogenesis of such diseases could become a focus of the World Health Organization. Given the experience of 2020, there should be good reason to hope that scientific funding organizations will have the insight and preparedness to accelerate funding for approaches that investigate the key membrane-associated mechanisms defining the pathogenicity of each newly found infectious agent, be it viral or microbial, as soon as its danger is recognized. There are some critical limitations in readily obtaining the structures of MPs. These include "pulling out" the full complement of molecular machines from their wild-type living organism in action, expressing functional MP at the levels required for structural studies, addressing the underrepresentation of the full-length structures of low-membrane pass proteins, and the ongoing challenge of obtaining relevant structures that reveal the key conformational changes during reaction or transport cycles. Advances in X-ray laser-based structure determination for small crystals and cryo-EM already provide valuable technological additions to the current armamentarium of biologists interested in MP structure and function (611, 612).

Few proteins work alone! Proteomic mapping has expanded the prospects for understanding MP function in greater detail, particularly in contexts in which complexes of proteins come together to regulate and coordinate multiple regulated functions. Mass spectrometry is key to identifying the proteins that associate with each other over time and circumstance (603, 604). One very exciting approach is to ask such questions in a normal cell without the overexpression of proteins. This can be achieved by genetically adding an affinity tag then "pulling it down" with the proteins actively associated with it (613). Cryo-EM is well suited to determining structures of larger complexes of proteins, including those at low endogenous levels (*Most extreme translocation: Effector protein and virulence factor secretion in pathogens*). This process will dramatically expand horizons over coming years, with affinity purification of large complexes of proteins revealing the mechanisms of such assemblies. Furthermore, cryo-EM can visualize multiple structural states at different stages in their reaction cycles and even model multiple and anharmonically coupled states. In principle the distribution of these states provides snapshots of the system in action and can be used to estimate the free energy difference between states of similar probability. Such approaches promise numerous new structures and insights that will close the gap between the functions of proteins acting as individuals and their roles within the complexes in which they function, in different states across time within a normal cellular environment.

Determining the relationships between structure and function of MPs relies on communication, deposition, and dissemination of structural coordinates. Here we highlight a small selection of discoveries from a plethora that have stemmed from these endeavors. We provide a glimpse into how MP structure determination has been enabled by parallel technological developments, how these structures inform about biological function and mechanism, and how MP structures supply foundations for diverse fields including

protein engineering, the simulation, and further exploration of biological functions and processes associated with membranes, as well as drug discovery and design. The PDB provides an ever-growing treasury of MP structures—an everlasting, powerful, and enriching product of global efforts.

Acknowledgments—Molecular graphics and analyses performed with UCSF *Chimera* and *ChimeraX* (614–616), developed by the Resource for Biocomputing, Visualization, and Informatics at the University of California, San Francisco, with support from National Institutes of Health R01-GM129325 and the Office of Cyber Infrastructure and Computational Biology, National Institute of Allergy and Infectious Diseases. Molecular graphics and analyses performed also used *PyMOL* authored by our dearly loved departed former colleague Warren L. DeLano and maintained under an open-source project licensed by Schrodinger.

Author contributions—F. L., P. F. E., A. J. V., I. A., M. G., J. P., R. B., M. S. D., S. F. -M., B. C. M., and R. M. S. wrote, edited, provided feedback, and generated figures for the manuscript. F. L. and P. F. E. led overall direction and planning and provided final formatting and proofreading. R. M. S. supervised the project.

Funding and additional information—F. L. is supported by National Institutes of Health Grant K99MH119591. P. F. E. is supported by National Institutes of Health Grants R21AI125983 and R01GM120173. A. J. V. is supported by National Institutes of Health Grant R35GM138368. R. M. S., M. G., M. S. D., are supported by NIGMS GM24485 to R. M. S. R. M. S. and J. P. are supported by P50 AI50476 (Krogan). R. B. is supported by American Heart Association Fellowship Award 19POST3437010. B. C. M. is supported by Health Research Council of New Zealand grant 19/397 and S. F. -M. is supported by National Institutes of Health Grant NIH R21AG057951.

Conflict of interest—The authors declare that they have no conflicts of interest with the contents of this article.

Abbreviations—The abbreviations used are: -NPA-, -Asparagine-Proline-Alanine; 2D, Two-Dimensional; 3D, Three-Dimensional; ACE2, Angiotensin Converting Enzyme 2; AmT, Ammonia Transport; AQP, Aquaporin; aR, Aromatic Arginine; BAM, β-Barrel Assembly Machinery; cCpE, C-terminal Domain of CpE; CF, Cystic Fibrosis; CFTR, Cystic Fibrosis Transmembrane-Conductance Regulator; CHIP28, Channel-like Integral membrane Protein of 28 kDa; ChR, Channel Rhodopsin; CLDN, Claudin; COVID-19, Coronavirus Disease 2019; CpE, *Clostridium perfringens* Enterotoxin; cpEGFP, Circularly Permutated Enhanced Green Fluorescent Protein; CPR, NADPH-Cytochrome P450 Reductase; DA, Dopamine; DAT, Dopamine Transporter; dLight, Dopamine Fluorescent Sensor; ECS, Extracellular Segment; EMC, Endoplasmic Reticulum Membrane Complex; ENC, Extracellular Negative Clusters; ER, Endoplasmic Reticulum; GABA R, Gamma-Amino Butyric Acid Receptor; GET, Guided-entry of Tail-Anchored; GFP, Green Fluorescent Protein; GLUT, Glucose Transporter; GPCR, G-Protein-Coupled Receptor; HCS, Hydrophobic Constriction Site; IA, Influenza A; IBD, Inflammatory Bowel Disease; ICH, Intracellular Helix; iGluSnFR, Intensity-Based Glutamate-Sensing Fluorescent Reporter; INC, Intracellular Negative Clusters; KcsA, K^+-Channel of *Streptomyces lividans* A; K_v, Voltage-Gated K^+-channel; LacY, Lactose Permease; LCP, Lipidic Cubic Phase; LeuT, Leucine Transporter; LGIC, Ligand-Gated Ion Channel; MAOIs, Monoamine Oxidase Inhibitors; MBP, Maltose-Binding Protein; MD, Molecular Dynamics; MFS, Major Facilitator Superfamily; MP, Membrane Protein; Na_v, Voltage-Gated Na^+-channel; NavAb, Voltage-Gated Na^+-Channel from *Arcobacter butzleri*; NBD, Nucleotide-Binding Domain; NET, Noradrenaline Transporter; NSS, Neurotransmitter Sodium Symporter; PDB, Protein Data Bank; *Pf*, *Plasmodium falciparum*; PTEX, Plasmodium Translocon of Exported proteins; Rh, Rhesus Factor; RNC, Ribosome-Nascent Chain; SARS-Cov, Severe Acute Respiratory Syndrome Coronavirus; SERT, Serotonin Transporter; SF, Selectivity Filter; SLC, Solute Carrier; SR, SRP receptor; SRP, Signal Recognition Particle; SSRI, Selective Serotonin Reuptake Inhibitors; TA, Tail-Anchored; TC, Targeting Complex; TCA, Tricyclic Antidepressant; TJ, Tight Junction; TM, Trans-Membrane α-helix; TMD, Trans-Membrane Domain; TPC3, Two-Pore channel 3; TRP, Transient Receptor Potential; VGIC, Voltage-Gated Ion Channel; VSD, Voltage-Sensing Domains; VP, Viroporin.

References

1. Dickerson, R. E. (2002) PDB. *Newsletter* **13**, 3
2. White, S. H. (2009) Biophysical dissection of membrane proteins. *Nature* **459**, 344–346
3. Newport, T. D., Sansom, M. S. P., and Stansfeld, P. J. (2019) The MemProtMD database: A resource for membrane-embedded protein structures and their lipid interactions. *Nucleic Acids Res.* **47**, D390–D397
4. Oesterhelt, D., and Stoeckenius, W. (1971) Rhodopsin-like protein from the purple membrane of Halobacterium halobium. *Nat. New Biol.* **233**, 149–152
5. Racker, E., and Stoeckenius, W. (1974) Reconstitution of purple membrane vesicles catalyzing light-driven proton uptake and adenosine triphosphate formation. *J. Biol. Chem.* **249**, 662–663
6. Henderson, R., and Unwin, P. N. (1975) Three-dimensional model of purple membrane obtained by electron microscopy. *Nature* **257**, 28–32
7. Michel, H., and Oesterhelt, D. (1980) Electrochemical proton gradient across the cell membrane of Halobacterium halobium: Comparison of the light-induced increase with the increase of intracellular adenosine triphosphate under steady-state illumination. *Biochemistry* **19**, 4615–4619
8. Michel, H., and Oesterhelt, D. (1980) Three-dimensional crystals of membrane proteins: Bacteriorhodopsin. *Proc. Natl. Acad. Sci. U. S. A.* **77**, 1283–1285
9. Michel, H., Oesterhelt, D., and Henderson, R. (1980) Orthorhombic two-dimensional crystal form of purple membrane. *Proc. Natl. Acad. Sci. U. S. A.* **77**, 338–342
10. Michel, H. (1982) Characterization and crystal packing of three-dimensional bacteriorhodopsin crystals. *EMBO J.* **1**, 1267–1271
11. Blaurock, A. E., and Stoeckenius, W. (1971) Structure of the purple membrane. *Nat. New Biol.* **233**, 152–155
12. Blaurock, A. E. (1975) Bacteriorhodospin: A trans-membrane pump containing alpha-helix. *J. Mol. Biol.* **93**, 139–158
13. Khorana, H. G., Gerber, G. E., Herlihy, W. C., Gray, C. P., Anderegg, R. J., Nihei, K., and Biemann, K. (1979) Amino acid sequence of bacteriorhodopsin. *Proc. Natl. Acad. Sci. U. S. A.* **76**, 5046–5050
14. Ovchinnikov, Y. A., Abdulaev, N. G., Feigina, M. Y., Kiselev, A. V., and Lobanov, N. A. (1977) Recent findings in the structure-functional characteristics of bacteriorhodopsin. *FEBS Lett.* **84**, 1–4
15. Ovchinnikov, Y. A., Abdulaev, N. G., Feigina, M. Y., Kiselev, A. V., and Lobanov, N. A. (1979) The structural basis of the functioning of bacteriorhodopsin: An overview. *FEBS Lett.* **100**, 219–224
16. Agard, D. A., and Stroud, R. M. (1982) Linking regions between helices in bacteriorhodopsin revealed. *Biophys. J.* **37**, 589–602

17. Hayward, S. B., Grano, D. A., Glaeser, R. M., and Fisher, K. A. (1978) Molecular orientation of bacteriorhodopsin within the purple membrane of Halobacterium halobium. *Proc. Natl. Acad. Sci. U. S. A.* **75**, 4320–4324
18. Jap, B. K., Maestre, M. F., Hayward, S. B., and Glaeser, R. M. (1983) Peptide-chain secondary structure of bacteriorhodopsin. *Biophys. J.* **43**, 81–89
19. Hayward, S. B., and Stroud, R. M. (1981) Projected structure of purple membrane determined to 3.7 A resolution by low temperature electron microscopy. *J. Mol. Biol.* **151**, 491–517
20. Grigorieff, N., Beckmann, E., and Zemlin, F. (1995) Lipid location in deoxycholate-treated purple membrane at 2.6 A. *J. Mol. Biol.* **254**, 404–415
21. Grigorieff, N., Ceska, T. A., Downing, K. H., Baldwin, J. M., and Henderson, R. (1996) Electron-crystallographic refinement of the structure of bacteriorhodopsin. *J. Mol. Biol.* **259**, 393–421
22. Pebay-Peyroula, E., Rummel, G., Rosenbusch, J. P., and Landau, E. M. (1997) X-ray structure of bacteriorhodopsin at 2.5 angstroms from microcrystals grown in lipidic cubic phases. *Science* **277**, 1676–1681
23. Gennis, R., and Ferguson-Miller, S. (1995) Structure of cytochrome c oxidase, energy generator of aerobic life. *Science* **269**, 1063–1064
24. Tsukihara, T., Aoyama, H., Yamashita, E., Tomizaki, T., Yamaguchi, H., Shinzawa-Itoh, K., Nakashima, R., Yaono, R., and Yoshikawa, S. (1995) Structures of metal sites of oxidized bovine heart cytochrome c oxidase at 2.8 A. *Science* **269**, 1069–1074
25. Schmidt, J., and Raftery, M. A. (1973) Purification of acetylcholine receptors from Torpedo californica electroplax by affinity chromatography. *Biochemistry* **12**, 852–856
26. Raftery, M. A., Vandlen, R., Michaelson, D., Bode, J., Moody, T., Chao, Y., Reed, K., Deutsch, J., and Duguid, J. (1974) The biochemistry of an acetylcholine receptor. *J. Supramol. Struct.* **2**, 582–592
27. Devillers-Thiery, A., Changeux, J. P., Paroutaud, P., and Strosberg, A. D. (1979) The amino-terminal sequence of the 40,000 molecular weight subunit of the acetylcholine receptor protein from Torpedo marmorata. *FEBS Lett.* **104**, 99–105
28. Raftery, M. A., Hunkapiller, M. W., Strader, C. D., and Hood, L. E. (1980) Acetylcholine receptor: Complex of homologous subunits. *Science* **208**, 1454–1456
29. Devillers-Thiery, A., Giraudat, J., Bentaboulet, M., and Changeux, J. P. (1983) Complete mRNA coding sequence of the acetylcholine binding alpha-subunit of Torpedo marmorata acetylcholine receptor: A model for the transmembrane organization of the polypeptide chain. *Proc. Natl. Acad. Sci. U. S. A.* **80**, 2067–2071
30. Ross, M. J., Klymkowsky, M. W., Agard, D. A., and Stroud, R. M. (1977) Structural studies of a membrane-bound acetylcholine receptor from Torpedo californica. *J. Mol. Biol.* **116**, 635–659
31. Kistler, J., and Stroud, R. M. (1981) Crystalline arrays of membrane-bound acetylcholine receptor. *Proc. Natl. Acad. Sci. U. S. A.* **78**, 3678–3682
32. Kistler, J., Stroud, R. M., Klymkowsky, M. W., Lalancette, R. A., and Fairclough, R. H. (1982) Structure and function of an acetylcholine receptor. *Biophys. J.* **37**, 371–383
33. Brisson, A., and Unwin, P. N. (1984) Tubular crystals of acetylcholine receptor. *J. Cell Biol.* **99**, 1202–1211
34. Brisson, A., and Unwin, P. N. (1985) Quaternary structure of the acetylcholine receptor. *Nature* **315**, 474–477
35. Mitra, A. K., McCarthy, M. P., and Stroud, R. M. (1989) Three-dimensional structure of the nicotinic acetylcholine receptor and location of the major associated 43-kD cytoskeletal protein, determined at 22 A by low dose electron microscopy and x-ray diffraction to 12.5 A. *J. Cell Biol.* **109**, 755–774
36. Hunkapiller, M. W., Strader, C. D., Hood, L., and Raftery, M. A. (1979) Amino terminal amino acid sequence of the major polypeptide subunit of Torpedo californica acetylcholine receptor. *Biochem. Biophys. Res. Commun.* **91**, 164–169
37. Noda, M., Takahashi, H., Tanabe, T., Toyosato, M., Kikyotani, S., Furutani, Y., Hirose, T., Takashima, H., Inayama, S., Miyata, T., and Numa, S. (1983) Structural homology of Torpedo californica acetylcholine receptor subunits. *Nature* **302**, 528–532
38. Pauling, L., Corey, R. B., and Branson, H. R. (1951) The structure of proteins; two hydrogen-bonded helical configurations of the polypeptide chain. *Proc. Natl. Acad. Sci. U. S. A.* **37**, 205–211
39. Finer-Moore, J., and Stroud, R. M. (1984) Amphipathic analysis and possible formation of the ion channel in an acetylcholine receptor. *Proc. Natl. Acad. Sci. U. S. A.* **81**, 155–159
40. Unwin, N. (2013) Nicotinic acetylcholine receptor and the structural basis of neuromuscular transmission: Insights from Torpedo postsynaptic membranes. *Q. Rev. Biophys.* **46**, 283–322
41. Morales-Perez, C. L., Noviello, C. M., and Hibbs, R. E. (2016) X-ray structure of the human alpha4beta2 nicotinic receptor. *Nature* **538**, 411–415
42. Deisenhofer, J., Epp, O., Miki, K., Huber, R., and Michel, H. (1984) X-ray structure analysis of a membrane protein complex. Electron density map at 3 A resolution and a model of the chromophores of the photosynthetic reaction center from Rhodopseudomonas viridis. *J. Mol. Biol.* **180**, 385–398
43. Milder, S. J., Thorgeirsson, T. E., Miercke, L. J., Stroud, R. M., and Kliger, D. S. (1991) Effects of detergent environments on the photocycle of purified monomeric bacteriorhodopsin. *Biochemistry* **30**, 1751–1761
44. Hodgkin, A. L., and Huxley, A. F. (1952) Currents carried by sodium and potassium ions through the membrane of the giant axon of Loligo. *J. Physiol.* **116**, 449–472
45. Hodgkin, A. L., and Huxley, A. F. (1952) Movement of sodium and potassium ions during nervous activity. *Cold Spring Harb. Symp. Quant. Biol.* **17**, 43–52
46. Hodgkin, A. L., Huxley, A. F., and Katz, B. (1952) Measurement of current-voltage relations in the membrane of the giant axon of Loligo. *J. Physiol.* **116**, 424–448
47. Doyle, D. A., Morais Cabral, J., Pfuetzner, R. A., Kuo, A., Gulbis, J. M., Cohen, S. L., Chait, B. T., and MacKinnon, R. (1998) The structure of the potassium channel: Molecular basis of K+ conduction and selectivity. *Science* **280**, 69–77
48. Preston, G. M., Carroll, T. P., Guggino, W. B., and Agre, P. (1992) Appearance of water channels in Xenopus oocytes expressing red cell CHIP28 protein. *Science* **256**, 385–387
49. Benga, G., Popescu, O., Borza, V., Pop, V. I., Muresan, A., Mocsy, I., Brain, A., and Wrigglesworth, J. M. (1986) Water permeability in human erythrocytes: Identification of membrane proteins involved in water transport. *Eur. J. Cell Biol.* **41**, 252–262
50. Benga, G., Popescu, O., Pop, V. I., and Holmes, R. P. (1986) p-(Chloromercuri)benzenesulfonate binding by membrane proteins and the inhibition of water transport in human erythrocytes. *Biochemistry* **25**, 1535–1538
51. Nielsen, S., and Agre, P. (1995) The aquaporin family of water channels in kidney. *Kidney Int.* **48**, 1057–1068
52. Agre, P., Preston, G. M., Smith, B. L., Jung, J. S., Raina, S., Moon, C., Guggino, W. B., and Nielsen, S. (1993) Aquaporin CHIP: The archetypal molecular water channel. *Am. J. Physiol.* **265**, F463–F476
53. Murata, K., Mitsuoka, K., Hirai, T., Walz, T., Agre, P., Heymann, J. B., Engel, A., and Fujiyoshi, Y. (2000) Structural determinants of water permeation through aquaporin-1. *Nature* **407**, 599–605
54. Fu, D. X., Libson, A., Miercke, L. J. W., Weitzman, C., Nollert, P., Krucinski, J., and Stroud, R. M. (2000) Structure of a glycerol-conducting channel and the basis for its selectivity. *Science* **290**, 481–486
55. Ho, J. D., Yeh, R., Sandstrom, A., Chorny, I., Harries, W. E., Robbins, R. A., Miercke, L. J., and Stroud, R. M. (2009) Crystal structure of human aquaporin 4 at 1.8 A and its mechanism of conductance. *Proc. Natl. Acad. Sci. U. S. A.* **106**, 7437–7442
56. Abrahams, J. P., Leslie, A. G., Lutter, R., and Walker, J. E. (1994) Structure at 2.8 A resolution of F1-ATPase from bovine heart mitochondria. *Nature* **370**, 621–628
57. Shaffer, P. L., Goehring, A., Shankaranarayanan, A., and Gouaux, E. (2009) Structure and mechanism of a Na+-independent amino acid transporter. *Science* **325**, 1010–1014

58. Singh, S. K., Piscitelli, C. L., Yamashita, A., and Gouaux, E. (2008) A competitive inhibitor traps LeuT in an open-to-out conformation. *Science* **322**, 1655–1661
59. Singh, S. K., Yamashita, A., and Gouaux, E. (2007) Antidepressant binding site in a bacterial homologue of neurotransmitter transporters. *Nature* **448**, 952–956
60. Yamashita, A., Singh, S. K., Kawate, T., Jin, Y., and Gouaux, E. (2005) Crystal structure of a bacterial homologue of Na+/Cl–dependent neurotransmitter transporters. *Nature* **437**, 215–223
61. Piscitelli, C. L., Krishnamurthy, H., and Gouaux, E. (2010) Neurotransmitter/sodium symporter orthologue LeuT has a single high-affinity substrate site. *Nature* **468**, 1129–1132
62. Wang, X., Sato, R., Brown, M. S., Hua, X., and Goldstein, J. L. (1994) SREBP-1, a membrane-bound transcription factor released by sterol-regulated proteolysis. *Cell* **77**, 53–62
63. Sakai, J., Duncan, E. A., Rawson, R. B., Hua, X., Brown, M. S., and Goldstein, J. L. (1996) Sterol-regulated release of SREBP-2 from cell membranes requires two sequential cleavages, one within a transmembrane segment. *Cell* **85**, 1037–1046
64. Yang, T., Espenshade, P. J., Wright, M. E., Yabe, D., Gong, Y., Aebersold, R., Goldstein, J. L., and Brown, M. S. (2002) Crucial step in cholesterol homeostasis: Sterols promote binding of SCAP to INSIG-1, a membrane protein that facilitates retention of SREBPs in ER. *Cell* **110**, 489–500
65. Wang, Y., Zhang, Y., and Ha, Y. (2006) Crystal structure of a rhomboid family intramembrane protease. *Nature* **444**, 179–180
66. Bai, X. C., Rajendra, E., Yang, G., Shi, Y., and Scheres, S. H. (2015) Sampling the conformational space of the catalytic subunit of human gamma-secretase. *Elife* **4**, e11182
67. Bai, X. C., Yan, C., Yang, G., Lu, P., Ma, D., Sun, L., Zhou, R., Scheres, S. H. W., and Shi, Y. (2015) An atomic structure of human gamma-secretase. *Nature* **525**, 212–217
68. Lu, P., Bai, X. C., Ma, D., Xie, T., Yan, C., Sun, L., Yang, G., Zhao, Y., Zhou, R., Scheres, S. H. W., and Shi, Y. (2014) Three-dimensional structure of human gamma-secretase. *Nature* **512**, 166–170
69. Kaller, M. R., Harried, S. S., Albrecht, B., Amarante, P., Babu-Khan, S., Bartberger, M. D., Brown, J., Brown, R., Chen, K., Cheng, Y., Citron, M., Croghan, M. D., Graceffa, R., Hickman, D., Judd, T., *et al.* (2012) A potent and orally efficacious, hydroxyethylamine-based inhibitor of beta-secretase. *ACS Med. Chem. Lett.* **3**, 886–891
70. Monenschein, H., Horne, D. B., Bartberger, M. D., Hitchcock, S. A., Nguyen, T. T., Patel, V. F., Pennington, L. D., and Zhong, W. (2012) Structure guided P1' modifications of HEA derived beta-secretase inhibitors for the treatment of Alzheimer's disease. *Bioorg. Med. Chem. Lett.* **22**, 3607–3611
71. Zhao, J., Liu, X., Xia, W., Zhang, Y., and Wang, C. (2020) Targeting amyloidogenic processing of APP in Alzheimer's disease. *Front. Mol. Neurosci.* **13**, 137
72. Gao, Y., Cao, E., Julius, D., and Cheng, Y. (2016) TRPV1 structures in nanodiscs reveal mechanisms of ligand and lipid action. *Nature* **534**, 347–351
73. Cheng, Y. (2015) Single-particle cryo-EM at crystallographic resolution. *Cell* **161**, 450–457
74. Cao, E., Liao, M., Cheng, Y., and Julius, D. (2013) TRPV1 structures in distinct conformations reveal activation mechanisms. *Nature* **504**, 113–118
75. Du, J., Lu, W., Wu, S., Cheng, Y., and Gouaux, E. (2015) Glycine receptor mechanism elucidated by electron cryo-microscopy. *Nature* **526**, 224–229
76. Yan, Z., Bai, X., Yan, C., Wu, J., Li, Z., Xie, T., Peng, W., Yin, C., Li, X., Scheres, S. H. W., Shi, Y., and Yan, N. (2015) Structure of the rabbit ryanodine receptor RyR1 at near-atomic resolution. *Nature* **517**, 50–55
77. Hite, R. K., Yuan, P., Li, Z., Hsuing, Y., Walz, T., and MacKinnon, R. (2015) Cryo-electron microscopy structure of the Slo2.2 Na(+)-activated K(+) channel. *Nature* **527**, 198–203
78. Whicher, J. R., and MacKinnon, R. (2016) Structure of the voltage-gated K(+) channel Eag1 reveals an alternative voltage sensing mechanism. *Science* **353**, 664–669
79. Kintzer, A. F., Green, E. M., Dominik, P. K., Bridges, M., Armache, J. P., Deneka, D., Kim, S. S., Hubbell, W., Kossiakoff, A. A., Cheng, Y., and Stroud, R. M. (2018) Structural basis for activation of voltage sensor domains in an ion channel TPC1. *Proc. Natl. Acad. Sci. U. S. A.* **115**, E9095–E9104
80. Li, F., Eriksen, J., Finer-Moore, J., Chang, R., Nguyen, P., Bowen, A., Myasnikov, A., Yu, Z., Bulkley, D., Cheng, Y., Edwards, R. H., and Stroud, R. M. (2020) Ion transport and regulation in a synaptic vesicle glutamate transporter. *Science* **368**, 893–897
81. Goodsell, D. S., Zardecki, C., Berman, H. M., and Burley, S. K. (2020) Insights from 20 years of the molecule of the month. *Biochem. Mol. Biol. Educ.* **48**, 350–355
82. Shinzawa-Itoh, K., Aoyama, H., Muramoto, K., Terada, H., Kurauchi, T., Tadehara, Y., Yamasaki, A., Sugimura, T., Kurono, S., Tsujimoto, K., Mizushima, T., Yamashita, E., Tsukihara, T., and Yoshikawa, S. (2007) Structures and physiological roles of 13 integral lipids of bovine heart cytochrome c oxidase. *EMBO J.* **26**, 1713–1725
83. Tsukihara, T., Aoyama, H., Yamashita, E., Tomizaki, T., Yamaguchi, H., Shinzawa-Itoh, K., Nakashima, R., Yaono, R., and Yoshikawa, S. (1996) The whole structure of the 13-subunit oxidized cytochrome c oxidase at 2.8 A. *Science* **272**, 1136–1144
84. Qin, L., Hiser, C., Mulichak, A., Garavito, R. M., and Ferguson-Miller, S. (2006) Identification of conserved lipid/detergent-binding sites in a high-resolution structure of the membrane protein cytochrome c oxidase. *Proc. Natl. Acad. Sci. U. S. A.* **103**, 16117–16122
85. Varanasi, L., Mills, D., Murphree, A., Gray, J., Purser, C., Baker, R., and Hosler, J. (2006) Altering conserved lipid binding sites in cytochrome c oxidase of Rhodobacter sphaeroides perturbs the interaction between subunits I and III and promotes suicide inactivation of the enzyme. *Biochemistry* **45**, 14896–14907
86. Qin, L., Sharpe, M. A., Garavito, R. M., and Ferguson-Miller, S. (2007) Conserved lipid-binding sites in membrane proteins: A focus on cytochrome c oxidase. *Curr. Opin. Struct. Biol.* **17**, 444–450
87. Qin, L., Mills, D. A., Buhrow, L., Hiser, C., and Ferguson-Miller, S. (2008) A conserved steroid binding site in cytochrome C oxidase. *Biochemistry* **47**, 9931–9933
88. Xia, D., Yu, C. A., Kim, H., Xia, J. Z., Kachurin, A. M., Zhang, L., Yu, L., and Deisenhofer, J. (1997) Crystal structure of the cytochrome bc1 complex from bovine heart mitochondria. *Science* **277**, 60–66
89. Iwata, S., Lee, J. W., Okada, K., Lee, J. K., Iwata, M., Rasmussen, B., Link, T. A., Ramaswamy, S., and Jap, B. K. (1998) Complete structure of the 11-subunit bovine mitochondrial cytochrome bc1 complex. *Science* **281**, 64–71
90. Lange, C., Nett, J. H., Trumpower, B. L., and Hunte, C. (2001) Specific roles of protein-phospholipid interactions in the yeast cytochrome bc1 complex structure. *EMBO J.* **20**, 6591–6600
91. Baniulis, D., Zhang, H., Zakharova, T., Hasan, S. S., and Cramer, W. A. (2011) Purification and crystallization of the cyanobacterial cytochrome b6f complex. *Methods Mol. Biol.* **684**, 65–77
92. Bhaduri, S., Zhang, H., Erramilli, S., and Cramer, W. A. (2019) Structural and functional contributions of lipids to the stability and activity of the photosynthetic cytochrome b 6 f lipoprotein complex. *J. Biol. Chem.* **294**, 17758–17767
93. Newstead, S., Ferrandon, S., and Iwata, S. (2008) Rationalizing alpha-helical membrane protein crystallization. *Protein Sci.* **17**, 466–472
94. Sonoda, Y., Newstead, S., Hu, N. J., Alguel, Y., Nji, E., Beis, K., Yashiro, S., Lee, C., Leung, J., Cameron, A. D., Byrne, B., Iwata, S., and Drew, D. (2011) Benchmarking membrane protein detergent stability for improving throughput of high-resolution X-ray structures. *Structure* **19**, 17–25
95. Rosevear, P., VanAken, T., Baxter, J., and Ferguson-Miller, S. (1980) Alkyl glycoside detergents: A simpler synthesis and their effects on kinetic and physical properties of cytochrome c oxidase. *Biochemistry* **19**, 4108–4115
96. VanAken, T., Foxall-VanAken, S., Castleman, S., and Ferguson-Miller, S. (1986) Alkyl glycoside detergents: Synthesis and applications to the study of membrane proteins. *Methods Enzymol.* **125**, 27–35
97. Chae, P. S., Rasmussen, S. G., Rana, R. R., Gotfryd, K., Chandra, R., Goren, M. A., Kruse, A. C., Nurva, S., Loland, C. J., Pierre, Y., Drew, D.,

Popot, J. L., Picot, D., Fox, B. G., Guan, L., *et al.* (2010) Maltose-neopentyl glycol (MNG) amphiphiles for solubilization, stabilization and crystallization of membrane proteins. *Nat. Methods* **7**, 1003–1008
98. Kaback, H. R., Dunten, R., Frillingos, S., Venkatesan, P., Kwaw, I., Zhang, W., and Ermolova, N. (2007) Site-directed alkylation and the alternating access model for LacY. *Proc. Natl. Acad. Sci. U. S. A.* **104**, 491–494
99. Forrest, L. R., Zhang, Y. W., Jacobs, M. T., Gesmonde, J., Xie, L., Honig, B. H., and Rudnick, G. (2008) Mechanism for alternating access in neurotransmitter transporters. *Proc. Natl. Acad. Sci. U. S. A.* **105**, 10338–10343
100. Svensson-Ek, M., Abramson, J., Larsson, G., Tornroth, S., Brzezinski, P., and Iwata, S. (2002) The X-ray crystal structures of wild-type and EQ(I-286) mutant cytochrome c oxidases from Rhodobacter sphaeroides. *J. Mol. Biol.* **321**, 329–339
101. de Grotthus, C. J. T. (1806) Theory of decomposition of liquids by electric currents. *Ann. Chim.* **58**, 54–73
102. Agmon, N. (1995) The Grotthuss mechanism. *Chem. Phys. Lett.* **244**, 456–462
103. Zhou, A., Rohou, A., Schep, D. G., Bason, J. V., Montgomery, M. G., Walker, J. E., Grigorieff, N., and Rubinstein, J. L. (2015) Structure and conformational states of the bovine mitochondrial ATP synthase by cryo-EM. *Elife* **4**, e10180
104. Srivastava, A. P., Luo, M., Zhou, W., Symersky, J., Bai, D., Chambers, M. G., Faraldo-Gomez, J. D., Liao, M., and Mueller, D. M. (2018) High-resolution cryo-EM analysis of the yeast ATP synthase in a lipid membrane. *Science* **360**, eaas9699
105. Kuhlbrandt, W. (2019) Structure and mechanisms of F-type ATP synthases. *Annu. Rev. Biochem.* **88**, 515–549
106. Landau, E. M., and Rosenbusch, J. P. (1996) Lipidic cubic phases: A novel concept for the crystallization of membrane proteins. *Proc. Natl. Acad. Sci. U. S. A.* **93**, 14532–14535
107. Caffrey, M. (2015) A comprehensive review of the lipid cubic phase or in meso method for crystallizing membrane and soluble proteins and complexes. *Acta Crystallogr. F Struct. Biol. Commun.* **71**, 3–18
108. Gouaux, E. (1998) It's not just a phase: Crystallization and X-ray structure determination of bacteriorhodopsin in lipidic cubic phases. *Structure* **6**, 5–10
109. Li, F., Liu, J., Zheng, Y., Garavito, R. M., and Ferguson-Miller, S. (2015) Protein structure. Crystal structures of translocator protein (TSPO) and mutant mimic of a human polymorphism. *Science* **347**, 555–558
110. Lyons, J. A., Aragão, D., Slattery, O., Pisliakov, A. V., Soulimane, T., and Caffrey, M. (2012) Structural insights into electron transfer in caa3-type cytochrome oxidase. *Nature* **487**, 514–518
111. Rasmussen, S. G., DeVree, B. T., Zou, Y., Kruse, A. C., Chung, K. Y., Kobilka, T. S., Thian, F. S., Chae, P. S., Pardon, E., Calinski, D., Mathiesen, J. M., Shah, S. T., Lyons, J. A., Caffrey, M., Gellman, S. H., *et al.* (2011) Crystal structure of the beta2 adrenergic receptor-Gs protein complex. *Nature* **477**, 549–555
112. Sanders, C. R., 2nd, and Landis, G. C. (1995) Reconstitution of membrane proteins into lipid-rich bilayered mixed micelles for NMR studies. *Biochemistry* **34**, 4030–4040
113. Bayburt, T. H., and Sligar, S. G. (2003) Self-assembly of single integral membrane proteins into soluble nanoscale phospholipid bilayers. *Protein Sci.* **12**, 2476–2481
114. Tribet, C., Audebert, R., and Popot, J. L. (1996) Amphipols: Polymers that keep membrane proteins soluble in aqueous solutions. *Proc. Natl. Acad. Sci. U. S. A.* **93**, 15047–15050
115. Popot, J. L., Althoff, T., Bagnard, D., Baneres, J. L., Bazzacco, P., Billon-Denis, E., Catoire, L. J., Champeil, P., Charvolin, D., Cocco, M. J., Cremel, G., Dahmane, T., de la Maza, L. M., Ebel, C., Gabel, F., *et al.* (2011) Amphipols from A to Z. *Annu. Rev. Biophys.* **40**, 379–408
116. Dorr, J. M., Scheidelaar, S., Koorengevel, M. C., Dominguez, J. J., Schafer, M., van Walree, C. A., and Killian, J. A. (2016) The styrene-maleic acid copolymer: A versatile tool in membrane research. *Eur. Biophys. J.* **45**, 3–21
117. Sun, C., Benlekbir, S., Venkatakrishnan, P., Wang, Y., Hong, S., Hosler, J., Tajkhorshid, E., Rubinstein, J. L., and Gennis, R. B. (2018) Structure of the alternative complex III in a supercomplex with cytochrome oxidase. *Nature* **557**, 123–126
118. Baradaran, R., Berrisford, J. M., Minhas, G. S., and Sazanov, L. A. (2013) Crystal structure of the entire respiratory complex I. *Nature* **494**, 443–448
119. Zickermann, V., Wirth, C., Nasiri, H., Siegmund, K., Schwalbe, H., Hunte, C., and Brandt, U. (2015) Structural biology. Mechanistic insight from the crystal structure of mitochondrial complex I. *Science* **347**, 44–49
120. Zhu, J., Vinothkumar, K. R., and Hirst, J. (2016) Structure of mammalian respiratory complex I. *Nature* **536**, 354–358
121. Schäfer, E., Dencher, N. A., Vonck, J., and Parcej, D. N. (2007) Three-dimensional structure of the respiratory chain supercomplex I1III2IV1 from bovine heart mitochondria. *Biochemistry* **46**, 12579–12585
122. Dudkina, N. V., Kouril, R., Peters, K., Braun, H. P., and Boekema, E. J. (2010) Structure and function of mitochondrial supercomplexes. *Biochim. Biophys. Acta* **1797**, 664–670
123. Letts, J. A., Fiedorczuk, K., and Sazanov, L. A. (2016) The architecture of respiratory supercomplexes. *Nature* **537**, 644–648
124. Althoff, T., Mills, D. J., Popot, J. L., and Kuhlbrandt, W. (2011) Arrangement of electron transport chain components in bovine mitochondrial supercomplex I1III2IV1. *EMBO J.* **30**, 4652–4664
125. Lapuente-Brun, E., Moreno-Loshuertos, R., Acín-Pérez, R., Latorre-Pellicer, A., Colás, C., Balsa, E., Perales-Clemente, E., Quirós, P. M., Calvo, E., Rodríguez-Hernández, M. A., Navas, P., Cruz, R., Carracedo, Á., López-Otín, C., Pérez-Martos, A., *et al.* (2013) Supercomplex assembly determines electron flux in the mitochondrial electron transport chain. *Science* **340**, 1567–1570
126. Milenkovic, D., Blaza, J. N., Larsson, N. G., and Hirst, J. (2017) The enigma of the respiratory chain supercomplex. *Cell Metab.* **25**, 765–776
127. Hirst, J. (2018) Open questions: Respiratory chain supercomplexes-why are they there and what do they do? *BMC Biol.* **16**, 111
128. Guo, R., Zong, S., Wu, M., Gu, J., and Yang, M. (2017) Architecture of human mitochondrial respiratory megacomplex I2III2IV2. *Cell* **170**, 1247–1257.e1212
129. Ferguson-Miller, S., Hochman, J., and Schindler, M. (1986) Aggregation and diffusion in the mitochondrial electron-transfer chain: Role in electron flow and energy transfer. *Biochem. Soc. Trans.* **14**, 822–824
130. Shinzawa-Itoh, K., Sugimura, T., Misaki, T., Tadehara, Y., Yamamoto, S., Hanada, M., Yano, N., Nakagawa, T., Uene, S., Yamada, T., Aoyama, H., Yamashita, E., Tsukihara, T., Yoshikawa, S., and Muramoto, K. (2019) Monomeric structure of an active form of bovine cytochrome c oxidase. *Proc. Natl. Acad. Sci. U. S. A.* **116**, 19945–19951
131. Ramzan, R., Rhiel, A., Weber, P., Kadenbach, B., and Vogt, S. (2019) Reversible dimerization of cytochrome c oxidase regulates mitochondrial respiration. *Mitochondrion* **49**, 149–155
132. Blobel, G., and Sabatini, D. D. (1971) Ribosome-membrane interaction in eukaryotic cells. In: Manson, L. A., ed. *Biomembranes*, Springer, Boston, MA: 193–195
133. Nielsen, H., Tsirigos, K. D., Brunak, S., and von Heijne, G. (2019) A brief history of protein sorting prediction. *Protein J.* **38**, 200–216
134. Cymer, F., von Heijne, G., and White, S. H. (2015) Mechanisms of integral membrane protein insertion and folding. *J. Mol. Biol.* **427**, 999–1022
135. Popot, J. L., and Engelman, D. M. (2016) Membranes do not tell proteins how to fold. *Biochemistry* **55**, 5–18
136. Egea, P. F., Stroud, R. M., and Walter, P. (2005) Targeting proteins to membranes: Structure of the signal recognition particle. *Curr. Opin. Struct. Biol.* **15**, 213–220
137. Ataide, S. F., Schmitz, N., Shen, K., Ke, A., Shan, S. O., Doudna, J. A., and Ban, N. (2011) The crystal structure of the signal recognition particle in complex with its receptor. *Science* **331**, 881–886
138. Janda, C. Y., Li, J., Oubridge, C., Hernandez, H., Robinson, C. V., and Nagai, K. (2010) Recognition of a signal peptide by the signal recognition particle. *Nature* **465**, 507–510
139. Hainzl, T., Huang, S., Merilainen, G., Brannstrom, K., and Sauer-Eriksson, A. E. (2011) Structural basis of signal-sequence recognition by the signal recognition particle. *Nat. Struct. Mol. Biol.* **18**, 389–391

140. Egea, P. F., Shan, S. O., Napetschnig, J., Savage, D. F., Walter, P., and Stroud, R. M. (2004) Substrate twinning activates the signal recognition particle and its receptor. *Nature* **427**, 215–221
141. Focia, P. J., Shepotinovskaya, I. V., Seidler, J. A., and Freymann, D. M. (2004) Heterodimeric GTPase core of the SRP targeting complex. *Science* **303**, 373–377
142. Shen, K., Arslan, S., Akopian, D., Ha, T., and Shan, S. O. (2012) Activated GTPase movement on an RNA scaffold drives co-translational protein targeting. *Nature* **492**, 271–275
143. Jomaa, A., Boehringer, D., Leibundgut, M., and Ban, N. (2016) Structures of the E. coli translating ribosome with SRP and its receptor and with the translocon. *Nat. Commun.* **7**, 10471
144. Van den Berg, B., Clemons, W. M., Jr., Collinson, I., Modis, Y., Hartmann, E., Harrison, S. C., and Rapoport, T. A. (2004) X-ray structure of a protein-conducting channel. *Nature* **427**, 36–44
145. Park, E., and Rapoport, T. A. (2011) Preserving the membrane barrier for small molecules during bacterial protein translocation. *Nature* **473**, 239–242
146. Tsukazaki, T., Mori, H., Fukai, S., Ishitani, R., Mori, T., Dohmae, N., Perederina, A., Sugita, Y., Vassylyev, D. G., Ito, K., and Nureki, O. (2008) Conformational transition of Sec machinery inferred from bacterial SecYE structures. *Nature* **455**, 988–991
147. Egea, P. F., and Stroud, R. M. (2010) Lateral opening of a translocon upon entry of protein suggests the mechanism of insertion into membranes. *Proc. Natl. Acad. Sci. U. S. A.* **107**, 17182–17187
148. Bischoff, L., Wickles, S., Berninghausen, O., van der Sluis, E. O., and Beckmann, R. (2014) Visualization of a polytopic membrane protein during SecY-mediated membrane insertion. *Nat. Commun.* **5**, 4103
149. Park, E., Menetret, J. F., Gumbart, J. C., Ludtke, S. J., Li, W., Whynot, A., Rapoport, T. A., and Akey, C. W. (2014) Structure of the SecY channel during initiation of protein translocation. *Nature* **506**, 102–106
150. Voorhees, R. M., and Hegde, R. S. (2016) Structure of the Sec61 channel opened by a signal sequence. *Science* **351**, 88–91
151. Woolhead, C. A., McCormick, P. J., and Johnson, A. E. (2004) Nascent membrane and secretory proteins differ in FRET-detected folding far inside the ribosome and in their exposure to ribosomal proteins. *Cell* **116**, 725–736
152. Bhushan, S., Gartmann, M., Halic, M., Armache, J. P., Jarasch, A., Mielke, T., Berninghausen, O., Wilson, D. N., and Beckmann, R. (2010) Alpha-helical nascent polypeptide chains visualized within distinct regions of the ribosomal exit tunnel. *Nat. Struct. Mol. Biol.* **17**, 313–317
153. Marino, J., von Heijne, G., and Beckmann, R. (2016) Small protein domains fold inside the ribosome exit tunnel. *FEBS Lett.* **590**, 655–660
154. Sipos, L., and von Heijne, G. (1993) Predicting the topology of eukaryotic membrane proteins. *Eur. J. Biochem.* **213**, 1333–1340
155. Anfinsen, C. B. (1973) Principles that govern the folding of protein chains. *Science* **181**, 223–230
156. Plath, K., Mothes, W., Wilkinson, B. M., Stirling, C. J., and Rapoport, T. A. (1998) Signal sequence recognition in posttranslational protein transport across the yeast ER membrane. *Cell* **94**, 795–807
157. Braunger, K., Pfeffer, S., Shrimal, S., Gilmore, R., Berninghausen, O., Mandon, E. C., Becker, T., Forster, F., and Beckmann, R. (2018) Structural basis for coupling protein transport and N-glycosylation at the mammalian endoplasmic reticulum. *Science* **360**, 215–219
158. Tsukazaki, T., Mori, H., Echizen, Y., Ishitani, R., Fukai, S., Tanaka, T., Perederina, A., Vassylyev, D. G., Kohno, T., Maturana, A. D., Ito, K., and Nureki, O. (2011) Structure and function of a membrane component SecDF that enhances protein export. *Nature* **474**, 235–238
159. Kumazaki, K., Chiba, S., Takemoto, M., Furukawa, A., Nishiyama, K., Sugano, Y., Mori, T., Dohmae, N., Hirata, K., Nakada-Nakura, Y., Maturana, A. D., Tanaka, Y., Mori, H., Sugita, Y., Arisaka, F., *et al.* (2014) Structural basis of Sec-independent membrane protein insertion by YidC. *Nature* **509**, 516–520
160. Gemmer, M., and Forster, F. (2020) A clearer picture of the ER translocon complex. *J. Cell Sci.* **133**, jcs231340
161. Schuldiner, M., Metz, J., Schmid, V., Denic, V., Rakwalska, M., Schmitt, H. D., Schwappach, B., and Weissman, J. S. (2008) The GET complex mediates insertion of tail-anchored proteins into the ER membrane. *Cell* **134**, 634–645
162. Mateja, A., and Keenan, R. J. (2018) A structural perspective on tail-anchored protein biogenesis by the GET pathway. *Curr. Opin. Struct. Biol.* **51**, 195–202
163. Wang, F., Chan, C., Weir, N. R., and Denic, V. (2014) The Get1/2 transmembrane complex is an endoplasmic-reticulum membrane protein insertase. *Nature* **512**, 441–444
164. Zalisko, B. E., Chan, C., Denic, V., Rock, R. S., and Keenan, R. J. (2017) Tail-anchored protein insertion by a single get1/2 heterodimer. *Cell Rep.* **20**, 2287–2293
165. Mateja, A., Paduch, M., Chang, H. Y., Szydlowska, A., Kossiakoff, A. A., Hegde, R. S., and Keenan, R. J. (2015) Protein targeting. Structure of the Get3 targeting factor in complex with its membrane protein cargo. *Science* **347**, 1152–1155
166. Mariappan, M., Mateja, A., Dobosz, M., Bove, E., Hegde, R. S., and Keenan, R. J. (2011) The mechanism of membrane-associated steps in tail-anchored protein insertion. *Nature* **477**, 61–66
167. Anghel, S. A., McGilvray, P. T., Hegde, R. S., and Keenan, R. J. (2017) Identification of Oxa1 homologs operating in the eukaryotic endoplasmic reticulum. *Cell Rep.* **21**, 3708–3716
168. Pleiner, T., Pinton Tomaleri, G., Januszyk, K., Inglis, A. J., Hazu, M., and Voorhees, R. M. (2020) Structural basis for membrane insertion by the human ER membrane protein complex. *Science* **369**, 433–436
169. Bai, L., You, Q., Feng, X., Kovach, A., and Li, H. (2020) Structure of the ER membrane complex, a transmembrane-domain insertase. *Nature* **584**, 475–478
170. O'Donnell, J. P., Phillips, B. P., Yagita, Y., Juszkiewicz, S., Wagner, A., Malinverni, D., Keenan, R. J., Miller, E. A., and Hegde, R. S. (2020) The architecture of EMC reveals a path for membrane protein insertion. *Elife* **9**, e57887
171. Shurtleff, M. J., Itzhak, D. N., Hussmann, J. A., Schirle Oakdale, N. T., Costa, E. A., Jonikas, M., Weibezahn, J., Popova, K. D., Jan, C. H., Sinitcyn, P., Vembar, S. S., Hernandez, H., Cox, J., Burlingame, A. L., Brodsky, J. L., *et al.* (2018) The ER membrane protein complex interacts cotranslationally to enable biogenesis of multipass membrane proteins. *Elife* **7**, e37018
172. McGilvray, P. T., Anghel, S. A., Sundaram, A., Zhong, F., Trnka, M. J., Fuller, J. R., Hu, H., Burlingame, A. L., and Keenan, R. J. (2020) An ER translocon for multi-pass membrane protein biogenesis. *Elife* **9**, e56889
173. Tsukazaki, T. (2019) Structural basis of the Sec translocon and YidC revealed through X-ray crystallography. *Protein J.* **38**, 249–261
174. Chen, Y., Capponi, S., Zhu, L., Gellenbeck, P., Freites, J. A., White, S. H., and Dalbey, R. E. (2017) YidC insertase of Escherichia coli: Water accessibility and membrane shaping. *Structure* **25**, 1403–1414.e1403
175. Miller-Vedam, L. E., Brauning, B., Popova, K. D., Schirle Oakdale, N. T., Bonnar, J. L., Prabu, J. R., Boydston, E. A., Sevillano, N., Shurtleff, M. J., Stroud, R. M., Craik, C. S., Schulman, B. A., Frost, A., and Weissman, J. S. (2020) Structural and mechanistic basis of the EMC-dependent biogenesis of distinct transmembrane clients. *Elife* **9**, e62611
176. Chitwood, P. J., and Hegde, R. S. (2019) The role of EMC during membrane protein biogenesis. *Trends Cell Biol.* **29**, 371–384
177. Cowan, S. W., Schirmer, T., Rummel, G., Steiert, M., Ghosh, R., Pauptit, R. A., Jansonius, J. N., and Rosenbusch, J. P. (1992) Crystal structures explain functional properties of two E. coli porins. *Nature* **358**, 727–733
178. Weiss, M. S., Abele, U., Weckesser, J., Welte, W., Schiltz, E., and Schulz, G. E. (1991) Molecular architecture and electrostatic properties of a bacterial porin. *Science* **254**, 1627–1630
179. Hohr, A. I., Straub, S. P., Warscheid, B., Becker, T., and Wiedemann, N. (2015) Assembly of beta-barrel proteins in the mitochondrial outer membrane. *Biochim. Biophys. Acta* **1853**, 74–88
180. Noinaj, N., Gumbart, J., and Buchanan, S. (2017) The β-barrel assembly machinery in motion. *Nat. Rev. Microbiol.* **15**, 197–204
181. Tomasek, D., Rawson, S., Lee, J., Wzorek, J. S., Harrison, S. C., Li, Z., and Kahne, D. (2020) Structure of a nascent membrane protein as it folds on the BAM complex. *Nature* **583**, 473–478

182. Bakelar, J., Buchanan, S. K., and Noinaj, N. (2016) The structure of the β-barrel assembly machinery complex. *Science* **351**, 180–186
183. Takeda, H., Tsutsumi, A., Nishizawa, T., Lindau, C., Busto, J. V., Wenz, L.-S., Ellenrieder, L., Imai, K., Straub, S. P., Mossmann, W., Qiu, J., Yamamori, Y., Tomii, K., Suzuki, J., Murata, T., *et al.* (2021) Mitochondrial sorting and assembly machinery operates by β-barrel switching. *Nature* **590**, 163–169
184. Diederichs, K. A., Ni, X., Rollauer, S. E., Botos, I., Tan, X., King, M. S., Kunji, E. R. S., Jiang, J., and Buchanan, S. K. (2020) Structural insight into mitochondrial β-barrel outer membrane protein biogenesis. *Nat. Commun.* **11**, 3290
185. Li, L., Park, E., Ling, J., Ingram, J., Ploegh, H., and Rapoport, T. A. (2016) Crystal structure of a substrate-engaged SecY protein-translocation channel. *Nature* **531**, 395–399
186. Matz, J. M., Beck, J. R., and Blackman, M. J. (2020) The parasitophorous vacuole of the blood-stage malaria parasite. *Nat. Rev. Microbiol.* **18**, 379–391
187. Goldberg, D. E., and Zimmerberg, J. (2020) Hardly vacuous: The parasitophorous vacuolar membrane of malaria parasites. *Trends Parasitol.* **36**, 138–146
188. Martin, R. E. (2020) The transportome of the malaria parasite. *Biol. Rev. Camb. Philos. Soc.* **95**, 305–332
189. de Koning-Ward, T. F., Gilson, P. R., Boddey, J. A., Rug, M., Smith, B. J., Papenfuss, A. T., Sanders, P. R., Lundie, R. J., Maier, A. G., Cowman, A. F., and Crabb, B. S. (2009) A newly discovered protein export machine in malaria parasites. *Nature* **459**, 945–949
190. Peng, M., Cascio, D., and Egea, P. F. (2015) Crystal structure and solution characterization of the thioredoxin-2 from Plasmodium falciparum, a constituent of an essential parasitic protein export complex. *Biochem. Biophys. Res. Commun.* **456**, 403–409
191. Egea, P. F. (2020) Crossing the vacuolar rubicon: Structural insights into effector protein trafficking in apicomplexan parasites. *Microorganisms* **8**, 865
192. Ho, C. M., Beck, J. R., Lai, M., Cui, Y., Goldberg, D. E., Egea, P. F., and Zhou, Z. H. (2018) Malaria parasite translocon structure and mechanism of effector export. *Nature* **561**, 70–75
193. Gilson, P. R., Chisholm, S. A., Crabb, B. S., and de Koning-Ward, T. F. (2017) Host cell remodelling in malaria parasites: A new pool of potential drug targets. *Int. J. Parasitol.* **47**, 119–127
194. AhYoung, A. P., Koehl, A., Cascio, D., and Egea, P. F. (2015) Structural mapping of the ClpB ATPases of Plasmodium falciparum: Targeting protein folding and secretion for antimalarial drug design. *Protein Sci.* **24**, 1508–1520
195. Beck, J. R., Muralidharan, V., Oksman, A., and Goldberg, D. E. (2014) PTEX component HSP101 mediates export of diverse malaria effectors into host erythrocytes. *Nature* **511**, 592–595
196. McCafferty, C. L., Verbeke, E. J., Marcotte, E. M., and Taylor, D. W. (2020) Structural biology in the multi-omics era. *J. Chem. Inf. Model.* **60**, 2424–2429
197. Lewis, A. J. O., and Hegde, R. S. (2020) A unified evolutionary origin for SecY and YidC. *bioRxiv*. https://doi.org/10.1101/2020.12.20.422553
198. Carbrey, J. M., and Agre, P. (2009) Discovery of the aquaporins and development of the field. *Handb. Exp. Pharmacol.*, 3–28
199. Solomon, A. K. (1968) Characterization of biological membranes by equivalent pores. *J. Gen. Physiol.* **51**, 335–364
200. van Hoek, A. N., and Verkman, A. S. (1992) Functional reconstitution of the isolated erythrocyte water channel CHIP28. *J. Biol. Chem.* **267**, 18267–18269
201. Agre, P. (2004) Aquaporin water channels (nobel lecture). *Angew. Chem. Int. Ed. Engl.* **43**, 4278–4290
202. Smith, B. L., and Agre, P. (1991) Erythrocyte Mr 28,000 transmembrane protein exists as a multisubunit oligomer similar to channel proteins. *J. Biol. Chem.* **266**, 6407–6415
203. Benga, G., Banner, M., and Wrigglesworth, J. M. (1996) Quantitation of the water channel protein aquaporin (CHIP28) from red blood cell membranes by densitometry of silver stained polyacrylamide gels. *Electrophoresis* **17**, 715–719
204. Preston, G. M., and Agre, P. (1991) Isolation of the cDNA for erythrocyte integral membrane protein of 28 kilodaltons: Member of an ancient channel family. *Proc. Natl. Acad. Sci. U. S. A.* **88**, 11110–11114
205. Li, H., Lee, S., and Jap, B. K. (1997) Molecular design of aquaporin-1 water channel as revealed by electron crystallography. *Nat. Struct. Biol.* **4**, 263–265
206. Jap, B. K., and Li, H. (1995) Structure of the osmo-regulated H2O-channel, AQP-CHIP, in projection at 3.5 A resolution. *J. Mol. Biol.* **251**, 413–420
207. Zeidel, M. L., Ambudkar, S. V., Smith, B. L., and Agre, P. (1992) Reconstitution of functional water channels in liposomes containing purified red cell CHIP28 protein. *Biochemistry* **31**, 7436–7440
208. Zeidel, M. L., Nielsen, S., Smith, B. L., Ambudkar, S. V., Maunsbach, A. B., and Agre, P. (1994) Ultrastructure, pharmacologic inhibition, and transport selectivity of aquaporin channel-forming integral protein in proteoliposomes. *Biochemistry* **33**, 1606–1615
209. Benga, G., and Borza, T. (1995) Diffusional water permeability of mammalian red blood cells. *Comp. Biochem. Physiol. B Biochem. Mol. Biol.* **112**, 653–659
210. Nollert, P., Harries, W. E., Fu, D., Miercke, L. J., and Stroud, R. M. (2001) Atomic structure of a glycerol channel and implications for substrate permeation in aqua(glycero)porins. *FEBS Lett.* **504**, 112–117
211. Ikeda, M., Beitz, E., Kozono, D., Guggino, W. B., Agre, P., and Yasui, M. (2002) Characterization of aquaporin-6 as a nitrate channel in mammalian cells. Requirement of pore-lining residue threonine 63. *J. Biol. Chem.* **277**, 39873–39879
212. Sui, H., Han, B. G., Lee, J. K., Walian, P., and Jap, B. K. (2001) Structural basis of water-specific transport through the AQP1 water channel. *Nature* **414**, 872–878
213. de Groot, B. L., Engel, A., and Grubmuller, H. (2001) A refined structure of human aquaporin-1. *FEBS Lett.* **504**, 206–211
214. Savage, D. F., Egea, P. F., Robles-Colmenares, Y., O'Connell, J. D., 3rd, and Stroud, R. M. (2003) Architecture and selectivity in aquaporins: 2.5 a X-ray structure of aquaporin Z. *PLoS Biol.* **1**, E72
215. Eriksson, U. K., Fischer, G., Friemann, R., Enkavi, G., Tajkhorshid, E., and Neutze, R. (2013) Subangstrom resolution X-ray structure details aquaporin-water interactions. *Science* **340**, 1346–1349
216. Harries, W. E., Akhavan, D., Miercke, L. J., Khademi, S., and Stroud, R. M. (2004) The channel architecture of aquaporin 0 at a 2.2-A resolution. *Proc. Natl. Acad. Sci. U. S. A.* **101**, 14045–14050
217. Gonen, T., Cheng, Y., Sliz, P., Hiroaki, Y., Fujiyoshi, Y., Harrison, S. C., and Walz, T. (2005) Lipid-protein interactions in double-layered two-dimensional AQP0 crystals. *Nature* **438**, 633–638
218. Engel, A., Fujiyoshi, Y., Gonen, T., and Walz, T. (2008) Junction-forming aquaporins. *Curr. Opin. Struct. Biol.* **18**, 229–235
219. Tajkhorshid, E., Nollert, P., Jensen, M. O., Miercke, L. J., O'Connell, J., Stroud, R. M., and Schulten, K. (2002) Control of the selectivity of the aquaporin water channel family by global orientational tuning. *Science* **296**, 525–530
220. de Groot, B. L., and Grubmuller, H. (2001) Water permeation across biological membranes: Mechanism and dynamics of aquaporin-1 and GlpF. *Science* **294**, 2353–2357
221. Stroud, R. M., Nollert, P., and Miercke, L. (2003) The glycerol facilitator GlpF its aquaporin family of channels, and their selectivity. *Adv. Protein Chem.* **63**, 291–316
222. Padhi, S., and Priyakumar, U. D. (2020) Selectivity and transport in aquaporins from molecular simulation studies. *Vitam. Horm.* **112**, 47–70
223. Chan, R., Falato, M., Liang, H., and Chen, L. Y. (2020) In silico simulations of erythrocyte aquaporins with quantitative *in vitro* validation. *RSC Adv.* **10**, 21283–21291
224. Magni, F., Sarto, C., Ticozzi, D., Soldi, M., Bosso, N., Mocarelli, P., and Kienle, M. G. (2006) Proteomic knowledge of human aquaporins. *Proteomics* **6**, 5637–5649
225. Verkman, A. S. (2009) Knock-out models reveal new aquaporin functions. *Handb. Exp. Pharmacol.*, 359–381
226. Chakrabarti, N., Roux, B., and Pomes, R. (2004) Structural determinants of proton blockage in aquaporins. *J. Mol. Biol.* **343**, 493–510

227. Chakrabarti, N., Tajkhorshid, E., Roux, B., and Pomes, R. (2004) Molecular basis of proton blockage in aquaporins. *Structure* **12**, 65–74
228. Hub, J. S., Grubmuller, H., and de Groot, B. L. (2009) Dynamics and energetics of permeation through aquaporins. What do we learn from molecular dynamics simulations? *Handb. Exp. Pharmacol.*, 57–76
229. Li, H., Chen, H., Steinbronn, C., Wu, B., Beitz, E., Zeuthen, T., and Voth, G. A. (2011) Enhancement of proton conductance by mutations of the selectivity filter of aquaporin-1. *J. Mol. Biol.* **407**, 607–620
230. Burykin, A., and Warshel, A. (2003) What really prevents proton transport through aquaporin? Charge self-energy versus proton wire proposals. *Biophys. J.* **85**, 3696–3706
231. Burykin, A., and Warshel, A. (2004) On the origin of the electrostatic barrier for proton transport in aquaporin. *FEBS Lett.* **570**, 41–46
232. Kato, M., Pisliakov, A. V., and Warshel, A. (2006) The barrier for proton transport in aquaporins as a challenge for electrostatic models: The role of protein relaxation in mutational calculations. *Proteins* **64**, 829–844
233. Aqvist, J., and Warshel, A. (1989) Energetics of ion permeation through membrane channels. Solvation of Na+ by gramicidin A. *Biophys. J.* **56**, 171–182
234. Sagnella, D. E., and Voth, G. A. (1996) Structure and dynamics of hydronium in the ion channel gramicidin A. *Biophys. J.* **70**, 2043–2051
235. Braun-Sand, S., Burykin, A., Chu, Z. T., and Warshel, A. (2005) Realistic simulations of proton transport along the gramicidin channel: Demonstrating the importance of solvation effects. *J. Phys. Chem. B* **109**, 583–592
236. Shi, Q., Izvekov, S., and Voth, G. A. (2006) Mixed atomistic and coarse-grained molecular dynamics: Simulation of a membrane-bound ion channel. *J. Phys. Chem. B* **110**, 15045–15048
237. Khademi, S., O'Connell, J., 3rd, Remis, J., Robles-Colmenares, Y., Miercke, L. J., and Stroud, R. M. (2004) Mechanism of ammonia transport by Amt/MEP/Rh: Structure of AmtB at 1.35 A. *Science* **305**, 1587–1594
238. Gruswitz, F., Chaudhary, S., Ho, J. D., Schlessinger, A., Pezeshki, B., Ho, C. M., Sali, A., Westhoff, C. M., and Stroud, R. M. (2010) Function of human Rh based on structure of RhCG at 2.1 A. *Proc. Natl. Acad. Sci. U. S. A.* **107**, 9638–9643
239. Hodgkin, A. L., and Huxley, A. F. (1952) A quantitative description of membrane current and its application to conduction and excitation in nerve. *J. Physiol.* **117**, 500–544
240. Hodgkin, A. L., and Huxley, A. F. (1952) The dual effect of membrane potential on sodium conductance in the giant axon of Loligo. *J. Physiol.* **116**, 497–506
241. Hodgkin, A. L., and Huxley, A. F. (1952) The components of membrane conductance in the giant axon of Loligo. *J. Physiol.* **116**, 473–496
242. Hille, B. (1975) Ionic selectivity of Na and K channels of nerve membranes. *Membranes* **3**, 255–323
243. Hille, B. (1973) Potassium channels in myelinated nerve. Selective permeability to small cations. *J. Gen. Physiol.* **61**, 669–686
244. Hille, B. (1971) The permeability of the sodium channel to organic cations in myelinated nerve. *J. Gen. Physiol.* **58**, 599–619
245. Noda, M., Shimizu, S., Tanabe, T., Takai, T., Kayano, T., Ikeda, T., Takahashi, H., Nakayama, H., Kanaoka, Y., Minamino, N., Kangawat, K., Matsuot, H., Raftery, M., Hirose, T., Inayama, S., *et al.* (1984) Primary structure of electrophorus electricus sodium channel deduced from cDNA sequence. *Nature* **312**, 121–127
246. Kamb, A., Iverson, L. E., and Tanouye, M. A. (1987) Molecular characterization of Shaker, a Drosophila gene that encodes a potassium channel. *Cell* **50**, 405–413
247. Tempel, B. L., Papazian, D. M., Schwarz, T. L., Jan, Y. N., and Jan, L. Y. (1987) Sequence of a probable potassium channel component encoded at Shaker locus of Drosophila. *Science* **237**, 770–775
248. Papazian, D. M., Schwarz, T. L., Tempel, B. L., Jan, Y. N., and Jan, L. Y. (1987) Cloning of genomic and complementary DNA from Shaker, a putative potassium channel gene from Drosophila. *Science* **237**, 749–753
249. Pongs, O., Kecskemethy, N., Muller, R., Krah-Jentgens, I., Baumann, A., Kiltz, H. H., Canal, I., Llamazares, S., and Ferrus, A. (1988) Shaker encodes a family of putative potassium channel proteins in the nervous system of Drosophila. *EMBO J.* **7**, 1087–1096
250. Hartshorne, R. P., and Catterall, W. A. (1981) Purification of the saxitoxin receptor of the sodium channel from rat brain. *Proc. Natl. Acad. Sci. U. S. A.* **78**, 4620–4624
251. Hartshorne, R. P., Messner, D. J., Coppersmith, J. C., and Catterall, W. A. (1982) The saxitoxin receptor of the sodium channel from rat brain. Evidence for two nonidentical beta subunits. *J. Biol. Chem.* **257**, 13888–13891
252. Catterall, W. A., Hartshorne, R. P., and Beneski, D. A. (1982) Molecular properties of neurotoxin receptors sites associated with sodium channels from mammalian brain. *Toxicon* **20**, 27–40
253. Catterall, W. A. (1984) The molecular basis of neuronal excitability. *Science* **223**, 653–661
254. MacKinnon, R., and Miller, C. (1988) Mechanism of charybdotoxin block of the high-conductance, Ca2+-activated K+ channel. *J. Gen. Physiol.* **91**, 335–349
255. MacKinnon, R., Reinhart, P. H., and White, M. M. (1988) Charybdotoxin block of Shaker K+ channels suggests that different types of K+ channels share common structural features. *Neuron* **1**, 997–1001
256. MacKinnon, R., and Miller, C. (1989) Mutant potassium channels with altered binding of charybdotoxin, a pore-blocking peptide inhibitor. *Science* **245**, 1382–1385
257. MacKinnon, R., and Yellen, G. (1990) Mutations affecting TEA blockade and ion permeation in voltage-activated K+ channels. *Science* **250**, 276–279
258. MacKinnon, R. (1991) Determination of the subunit stoichiometry of a voltage-activated potassium channel. *Nature* **350**, 232–235
259. Yellen, G., Jurman, M. E., Abramson, T., and MacKinnon, R. (1991) Mutations affecting internal TEA blockade identify the probable pore-forming region of a K+ channel. *Science* **251**, 939–942
260. Heginbotham, L., Abramson, T., and MacKinnon, R. (1992) A functional connection between the pores of distantly related ion channels as revealed by mutant K+ channels. *Science* **258**, 1152–1155
261. Heginbotham, L., and MacKinnon, R. (1992) The aromatic binding site for tetraethylammonium ion on potassium channels. *Neuron* **8**, 483–491
262. Heginbotham, L., Lu, Z., Abramson, T., and MacKinnon, R. (1994) Mutations in the K+ channel signature sequence. *Biophys. J.* **66**, 1061–1067
263. MacKinnon, R. (1995) Pore loops: An emerging theme in ion channel structure. *Neuron* **14**, 889–892
264. MacKinnon, R. (2004) Potassium channels and the atomic basis of selective ion conduction (nobel lecture). *Angew. Chem. Int. Ed. Engl.* **43**, 4265–4277
265. Zhou, Y., Morais-Cabral, J. H., Kaufman, A., and MacKinnon, R. (2001) Chemistry of ion coordination and hydration revealed by a K+ channel-Fab complex at 2.0 A resolution. *Nature* **414**, 43–48
266. Payandeh, J., Scheuer, T., Zheng, N., and Catterall, W. A. (2011) The crystal structure of a voltage-gated sodium channel. *Nature* **475**, 353–358
267. Kim, D. M., and Nimigean, C. M. (2016) Voltage-gated potassium channels: A structural examination of selectivity and gating. *Cold Spring Harb. Perspect. Biol.* **8**, a029231
268. Clairfeuille, T., Xu, H., Koth, C. M., and Payandeh, J. (2017) Voltage-gated sodium channels viewed through a structural biology lens. *Curr. Opin. Struct. Biol.* **45**, 74–84
269. Hille, B. (2001) *Ion Channels of Excitable Membranes*, 3rd Ed, Sinauer, Sunderland, MA
270. Catterall, W. A., Wisedchaisri, G., and Zheng, N. (2017) The chemical basis for electrical signaling. *Nat. Chem. Biol.* **13**, 455–463
271. Armstrong, C. M., and Bezanilla, F. (1973) Currents related to movement of the gating particles of the sodium channels. *Nature* **242**, 459–461
272. Bezanilla, F. (2018) Gating currents. *J. Gen. Physiol.* **150**, 911–932
273. Bezanilla, F. (2008) How membrane proteins sense voltage. *Nat. Rev. Mol. Cell Biol.* **9**, 323–332
274. Dai, G., Aman, T. K., DiMaio, F., and Zagotta, W. N. (2019) The HCN channel voltage sensor undergoes a large downward motion during hyperpolarization. *Nat. Struct. Mol. Biol.* **26**, 686–694

275. Jiang, Y., Ruta, V., Chen, J., Lee, A., and MacKinnon, R. (2003) The principle of gating charge movement in a voltage-dependent K+ channel. *Nature* **423**, 42–48
276. Zhang, X., Ren, W., DeCaen, P., Yan, C., Tao, X., Tang, L., Wang, J., Hasegawa, K., Kumasaka, T., He, J., Wang, J., Clapham, D. E., and Yan, N. (2012) Crystal structure of an orthologue of the NaChBac voltage-gated sodium channel. *Nature* **486**, 130–134
277. Zhang, X., and Yan, N. (2013) The conformational shifts of the voltage sensing domains between Na(v)Rh and Na(v)Ab. *Cell Res.* **23**, 444–447
278. Dickinson, M. S., Myasnikov, A., Eriksen, J., Poweleit, N., and Stroud, R. M. (2020) Resting state structure of the hyperdepolarization activated two-pore channel 3. *Proc. Natl. Acad. Sci. U. S. A.* **117**, 1988–1993
279. Yu, A. S. L. (2017) Paracellular transport as a strategy for energy conservation by multicellular organisms? *Tissue Barriers* **5**, e1301852
280. Farquhar, M. G., and Palade, G. E. (1963) Junctional complexes in various epithelia. *J. Cell Biol.* **17**, 375–412
281. Furuse, M., Hirase, T., Itoh, M., Nagafuchi, A., Yonemura, S., Tsukita, S., and Tsukita, S. (1993) Occludin: A novel integral membrane protein localizing at tight junctions. *J. Cell Biol.* **123**, 1777–1788
282. Furuse, M., Fujita, K., Hiiragi, T., Fujimoto, K., and Tsukita, S. (1998) Claudin-1 and -2: Novel integral membrane proteins localizing at tight junctions with no sequence similarity to occludin. *J. Cell Biol.* **141**, 1539–1550
283. Furuse, M., Sasaki, H., Fujimoto, K., and Tsukita, S. (1998) A single gene product, claudin-1 or -2, reconstitutes tight junction strands and recruits occludin in fibroblasts. *J. Cell Biol.* **143**, 391–401
284. Furuse, M., Sasaki, H., and Tsukita, S. (1999) Manner of interaction of heterogeneous claudin species within and between tight junction strands. *J. Cell Biol.* **147**, 891–903
285. Chasiotis, H., Kolosov, D., Bui, P., and Kelly, S. P. (2012) Tight junctions, tight junction proteins and paracellular permeability across the gill epithelium of fishes: A review. *Respir. Physiol. Neurobiol.* **184**, 269–281
286. Furuse, M., Hata, M., Furuse, K., Yoshida, Y., Haratake, A., Sugitani, Y., Noda, T., Kubo, A., and Tsukita, S. (2002) Claudin-based tight junctions are crucial for the mammalian epidermal barrier: A lesson from claudin-1-deficient mice. *J. Cell Biol.* **156**, 1099–1111
287. Nitta, T., Hata, M., Gotoh, S., Seo, Y., Sasaki, H., Hashimoto, N., Furuse, M., and Tsukita, S. (2003) Size-selective loosening of the blood-brain barrier in claudin-5-deficient mice. *J. Cell Biol.* **161**, 653–660
288. Martin, T. A., and Jiang, W. G. (2001) Tight junctions and their role in cancer metastasis. *Histol. Histopathol.* **16**, 1183–1195
289. Oliveira, S. S., and Morgado-Diaz, J. A. (2007) Claudins: Multifunctional players in epithelial tight junctions and their role in cancer. *Cell. Mol. Life Sci.* **64**, 17–28
290. Tabaries, S., and Siegel, P. M. (2017) The role of claudins in cancer metastasis. *Oncogene* **36**, 1176–1190
291. Marco, S., and Skaper, S. D. (2006) Amyloid beta-peptide1-42 alters tight junction protein distribution and expression in brain microvessel endothelial cells. *Neurosci. Lett.* **401**, 219–224
292. Keaney, J., Walsh, D. M., O'Malley, T., Hudson, N., Crosbie, D. E., Loftus, T., Sheehan, F., McDaid, J., Humphries, M. M., Callanan, J. J., Brett, F. M., Farrell, M. A., Humphries, P., and Campbell, M. (2015) Autoregulated paracellular clearance of amyloid-beta across the blood-brain barrier. *Sci. Adv.* **1**, e1500472
293. Lee, H., and Pienaar, I. S. (2014) Disruption of the blood-brain barrier in Parkinson's disease: Curse or route to a cure? *Front. Biosci. (Landmark Ed.)* **19**, 272–280
294. Di Pardo, A., Amico, E., Scalabri, F., Pepe, G., Castaldo, S., Elifani, F., Capocci, L., De Sanctis, C., Comerci, L., Pompeo, F., D'Esposito, M., Filosa, S., Crispi, S., and Maglione, V. (2017) Impairment of blood-brain barrier is an early event in R6/2 mouse model of Huntington disease. *Sci. Rep.* **7**, 41316
295. Garbuzova-Davis, S., Hernandez-Ontiveros, D. G., Rodrigues, M. C., Haller, E., Frisina-Deyo, A., Mirtyl, S., Sallot, S., Saporta, S., Borlongan, C. V., and Sanberg, P. R. (2012) Impaired blood-brain/spinal cord barrier in ALS patients. *Brain Res.* **1469**, 114–128
296. Sandoval, K. E., and Witt, K. A. (2008) Blood-brain barrier tight junction permeability and ischemic stroke. *Neurobiol. Dis.* **32**, 200–219
297. Freedman, J. C., Shrestha, A., and McClane, B. A. (2016) Clostridium perfringens enterotoxin: Action, genetics, and translational applications. *Toxins (Basel)* **8**, 73
298. Bucker, R., Schumann, M., Amasheh, S., and Schulzke, J. D. (2010) Claudins in intestinal function and disease. *Curr. Top. Membr.* **65**, 195–227
299. Edelblum, K. L., and Turner, J. R. (2009) The tight junction in inflammatory disease: Communication breakdown. *Curr. Opin. Pharmacol.* **9**, 715–720
300. Evans, M. J., von Hahn, T., Tscherne, D. M., Syder, A. J., Panis, M., Wolk, B., Hatziioannou, T., McKeating, J. A., Bieniasz, P. D., and Rice, C. M. (2007) Claudin-1 is a hepatitis C virus co-receptor required for a late step in entry. *Nature* **446**, 801–805
301. Harris, H. J., Davis, C., Mullins, J. G., Hu, K., Goodall, M., Farquhar, M. J., Mee, C. J., McCaffrey, K., Young, S., Drummer, H., Balfe, P., and McKeating, J. A. (2010) Claudin association with CD81 defines hepatitis C virus entry. *J. Biol. Chem.* **285**, 21092–21102
302. De Beneddnetto, A., Latchney, L. R., McGirt, L. Y., Vidyasagar, S., Cheadle, C., Barnes, K. C., and Beck, L. A. (2008) The tight junction protein, claudin-1 is dysregulated in atopic dermatitis. *J. Allergy Clin. Immunol.* **121**, S32
303. De Benedetto, A., Rafaels, N. M., McGirt, L. Y., Ivanov, A. I., Georas, S. N., Cheadle, C., Berger, A. E., Zhang, K., Vidyasagar, S., Yoshida, T., Boguniewicz, M., Hata, T., Schneider, L. C., Hanifin, J. M., Gallo, R. L., *et al.* (2011) Tight junction defects in patients with atopic dermatitis. *J. Allergy Clin. Immunol.* **127**, 773–786.e1–7
304. Gruber, R., Bornchen, C., Rose, K., Daubmann, A., Volksdorf, T., Madykowski, E., Vidal-y-Sy, S., Peters, E. M., Danso, M., Bouwstra, J. A., Hennies, H. C., Moll, I., Schmuth, M., and Brandner, J. M. (2015) Diverse regulation of claudin-1 and claudin-4 in atopic dermatitis. *Am. J. Pathol.* **185**, 2777–2789
305. Watson, R. E., Poddar, R., Walker, J. M., McGuill, I., Hoare, L. M., Griffiths, C. E., and O'Neill C, A. (2007) Altered claudin expression is a feature of chronic plaque psoriasis. *J. Pathol.* **212**, 450–458
306. Konrad, M., Schaller, A., Seelow, D., Pandey, A. V., Waldegger, S., Lesslauer, A., Vitzthum, H., Suzuki, Y., Luk, J. M., Becker, C., Schlingmann, K. P., Schmid, M., Rodriguez-Soriano, J., Ariceta, G., Cano, F., *et al.* (2006) Mutations in the tight-junction gene claudin 19 (CLDN19) are associated with renal magnesium wasting, renal failure, and severe ocular involvement. *Am. J. Hum. Genet.* **79**, 949–957
307. Li, J., Ananthapanyasut, W., and Yu, A. S. (2011) Claudins in renal physiology and disease. *Pediatr. Nephrol.* **26**, 2133–2142
308. Naeem, M., Hussain, S., and Akhtar, N. (2011) Mutation in the tight-junction gene claudin 19 (CLDN19) and familial hypomagnesemia, hypercalciuria, nephrocalcinosis (FHHNC) and severe ocular disease. *Am. J. Nephrol.* **34**, 241–248
309. Erickson, K. K., Sundstrom, J. M., and Antonetti, D. A. (2007) Vascular permeability in ocular disease and the role of tight junctions. *Angiogenesis* **10**, 103–117
310. Hudson, N., Celkova, L., Hopkins, A., Greene, C., Storti, F., Ozaki, E., Fahey, E., Theodoropoulou, S., Kenna, P. F., Humphries, M. M., Curtis, A. M., Demmons, E., Browne, A., Liddie, S., Lawrence, M. S., *et al.* (2019) Dysregulated claudin-5 cycling in the inner retina causes retinal pigment epithelial cell atrophy. *JCI Insight* **4**, e130273
311. Wilcox, E. R., Burton, Q. L., Naz, S., Riazuddin, S., Smith, T. N., Ploplis, B., Belyantseva, I., Ben-Yosef, T., Liburd, N. A., Morell, R. J., Kachar, B., Wu, D. K., Griffith, A. J., Riazuddin, S., and Friedman, T. B. (2001) Mutations in the gene encoding tight junction claudin-14 cause autosomal recessive deafness DFNB29. *Cell* **104**, 165–172
312. Gow, A., Davies, C., Southwood, C. M., Frolenkov, G., Chrustowski, M., Ng, L., Yamauchi, D., Marcus, D. C., and Kachar, B. (2004) Deafness in claudin 11-null mice reveals the critical contribution of basal cell tight junctions to stria vascularis function. *J. Neurosci.* **24**, 7051–7062
313. Nakano, Y., Kim, S. H., Kim, H. M., Sanneman, J. D., Zhang, Y., Smith, R. J., Marcus, D. C., Wangemann, P., Nessler, R. A., and Banfi, B. (2009) A claudin-9-based ion permeability barrier is essential for hearing. *PLoS Genet.* **5**, e1000610

314. Morita, K., Furuse, M., Fujimoto, K., and Tsukita, S. (1999) Claudin multigene family encoding four-transmembrane domain protein components of tight junction strands. *Proc. Natl. Acad. Sci. U. S. A.* **96**, 511–516
315. Tepass, U. (2003) Claudin complexities at the apical junctional complex. *Nat. Cell Biol.* **5**, 595–597
316. Loh, Y. H., Christoffels, A., Brenner, S., Hunziker, W., and Venkatesh, B. (2004) Extensive expansion of the claudin gene family in the teleost fish, Fugu rubripes. *Genome Res.* **14**, 1248–1257
317. Van Itallie, C. M., and Anderson, J. M. (2013) Claudin interactions in and out of the tight junction. *Tissue Barriers* **1**, e25247
318. Gunzel, D., and Yu, A. S. (2013) Claudins and the modulation of tight junction permeability. *Physiol. Rev.* **93**, 525–569
319. Lal-Nag, M., and Morin, P. J. (2009) The claudins. *Genome Biol.* **10**, 235
320. Suzuki, H., Ito, Y., Yamazaki, Y., Mineta, K., Uji, M., Abe, K., Tani, K., Fujiyoshi, Y., and Tsukita, S. (2013) The four-transmembrane protein IP39 of Euglena forms strands by a trimeric unit repeat. *Nat. Commun.* **4**, 1766
321. Suzuki, H., Nishizawa, T., Tani, K., Yamazaki, Y., Tamura, A., Ishitani, R., Dohmae, N., Tsukita, S., Nureki, O., and Fujiyoshi, Y. (2014) Crystal structure of a claudin provides insight into the architecture of tight junctions. *Science* **344**, 304–307
322. Krause, G., Winkler, L., Mueller, S. L., Haseloff, R. F., Piontek, J., and Blasig, I. E. (2008) Structure and function of claudins. *Biochim. Biophys. Acta* **1778**, 631–645
323. Van Itallie, C. M., Fanning, A. S., and Anderson, J. M. (2003) Reversal of charge selectivity in cation or anion-selective epithelial lines by expression of different claudins. *Am. J. Physiol. Renal Physiol.* **285**, F1078–F1084
324. Caffrey, M. (2000) A lipid's eye view of membrane protein crystallization in mesophases. *Curr. Opin. Struct. Biol.* **10**, 486–497
325. Colegio, O. R., Van Itallie, C. M., McCrea, H. J., Rahner, C., and Anderson, J. M. (2002) Claudins create charge-selective channels in the paracellular pathway between epithelial cells. *Am. J. Physiol. Cell Physiol.* **283**, C142–C147
326. Veshnyakova, A., Protze, J., Rossa, J., Blasig, I. E., Krause, G., and Piontek, J. (2010) On the interaction of Clostridium perfringens enterotoxin with claudins. *Toxins (Basel)* **2**, 1336–1356
327. Veshnyakova, A., Piontek, J., Protze, J., Waziri, N., Heise, I., and Krause, G. (2012) Mechanism of Clostridium perfringens enterotoxin interaction with claudin-3/-4 protein suggests structural modifications of the toxin to target specific claudins. *J. Biol. Chem.* **287**, 1698–1708
328. Winkler, L., Gehring, C., Wenzel, A., Muller, S. L., Piehl, C., Krause, G., Blasig, I. E., and Piontek, J. (2009) Molecular determinants of the interaction between Clostridium perfringens enterotoxin fragments and claudin-3. *J. Biol. Chem.* **284**, 18863–18872
329. Saitoh, Y., Suzuki, H., Tani, K., Nishikawa, K., Irie, K., Ogura, Y., Tamura, A., Tsukita, S., and Fujiyoshi, Y. (2015) Structural insight into tight junction disassembly by Clostridium perfringens enterotoxin. *Science* **347**, 775–778
330. Shinoda, T., Shinya, N., Ito, K., Ohsawa, N., Terada, T., Hirata, K., Kawano, Y., Yamamoto, M., Kimura-Someya, T., Yokoyama, S., and Shirouzu, M. (2016) Structural basis for disruption of claudin assembly in tight junctions by an enterotoxin. *Sci. Rep.* **6**, 33632
331. Nakamura, S., Irie, K., Tanaka, H., Nishikawa, K., Suzuki, H., Saitoh, Y., Tamura, A., Tsukita, S., and Fujiyoshi, Y. (2019) Morphologic determinant of tight junctions revealed by claudin-3 structures. *Nat. Commun.* **10**, 816
332. Vecchio, A. J., and Stroud, R. M. (2019) Claudin-9 structures reveal mechanism for toxin-induced gut barrier breakdown. *Proc. Natl. Acad. Sci. U. S. A.* **116**, 17817–17824
333. Pahle, J., Menzel, L., Niesler, N., Kobelt, D., Aumann, J., Rivera, M., and Walther, W. (2017) Rapid eradication of colon carcinoma by Clostridium perfringens enterotoxin suicidal gene therapy. *BMC Cancer* **17**, 129
334. Maeda, T., Murata, M., Chiba, H., Takasawa, A., Tanaka, S., Kojima, T., Masumori, N., Tsukamoto, T., and Sawada, N. (2012) Claudin-4-targeted therapy using Clostridium perfringens enterotoxin for prostate cancer. *Prostate* **72**, 351–360
335. Hashimoto, Y., Yagi, K., and Kondoh, M. (2017) Roles of the first-generation claudin binder, Clostridium perfringens enterotoxin, in the diagnosis and claudin-targeted treatment of epithelium-derived cancers. *Pflugers Arch.* **469**, 45–53
336. Liao, Z., Yang, Z., Piontek, A., Eichner, M., Krause, G., Li, L., Piontek, J., and Zhang, J. (2016) Specific binding of a mutated fragment of Clostridium perfringens enterotoxin to endothelial claudin-5 and its modulation of cerebral vascular permeability. *Neuroscience* **327**, 53–63
337. Neuhaus, W., Piontek, A., Protze, J., Eichner, M., Mahringer, A., Subileau, E. A., Lee, I. M., Schulzke, J. D., Krause, G., and Piontek, J. (2018) Reversible opening of the blood-brain barrier by claudin-5-binding variants of Clostridium perfringens enterotoxin's claudin-binding domain. *Biomaterials* **161**, 129–143
338. Suzuki, H., Tani, K., Tamura, A., Tsukita, S., and Fujiyoshi, Y. (2015) Model for the architecture of claudin-based paracellular ion channels through tight junctions. *J. Mol. Biol.* **427**, 291–297
339. Alberini, G., Benfenati, F., and Maragliano, L. (2017) A refined model of claudin-15 tight junction paracellular architecture by molecular dynamics simulations. *PLoS One* **12**, e0184190
340. Samanta, P., Wang, Y., Fuladi, S., Zou, J., Li, Y., Shen, L., Weber, C., and Khalili-Araghi, F. (2018) Molecular determination of claudin-15 organization and channel selectivity. *J. Gen. Physiol.* **150**, 949–968
341. Zhao, J., Krystofiak, E. S., Ballesteros, A., Cui, R., Van Itallie, C. M., Anderson, J. M., Fenollar-Ferrer, C., and Kachar, B. (2018) Multiple claudin-claudin cis interfaces are required for tight junction strand formation and inherent flexibility. *Commun. Biol.* **1**, 50
342. Hempel, C., Protze, J., Altun, E., Riebe, B., Piontek, A., Fromm, A., Lee, I. M., Saleh, T., Gunzel, D., Krause, G., and Piontek, J. (2020) Assembly of tight junction strands: Claudin-10b and claudin-3 form homo-tetrameric building blocks that polymerise in a channel-independent manner. *J. Mol. Biol.* **432**, 2405–2427
343. Irudayanathan, F. J., Wang, N., Wang, X., and Nangia, S. (2017) Architecture of the paracellular channels formed by claudins of the blood-brain barrier tight junctions. *Ann. N. Y. Acad. Sci.* **1405**, 131–146
344. Irudayanathan, F. J., Wang, X., Wang, N., Willsey, S. R., Seddon, I. A., and Nangia, S. (2018) Self-assembly simulations of classic claudins-insights into the pore structure, selectivity, and higher order complexes. *J. Phys. Chem. B* **122**, 7463–7474
345. Yamazaki, Y., Okawa, K., Yano, T., Tsukita, S., and Tsukita, S. (2008) Optimized proteomic analysis on gels of cell-cell adhering junctional membrane proteins. *Biochemistry* **47**, 5378–5386
346. Almén, M. S., Nordström, K. J., Fredriksson, R., and Schiöth, H. B. (2009) Mapping the human membrane proteome: A majority of the human membrane proteins can be classified according to function and evolutionary origin. *BMC Biol.* **7**, 50
347. Ellory, J. C., Elford, B. C., and Newbold, C. I. (1988) Transport mechanisms across cell membranes. *Parasitology* **96 Suppl**, S5–S9
348. Shilton, B. H. (2015) Active transporters as enzymes: An energetic framework applied to major facilitator superfamily and ABC importer systems. *Biochem. J.* **467**, 193–199
349. Neverisky, D. L., and Abbott, G. W. (2015) Ion channel-transporter interactions. *Crit. Rev. Biochem. Mol. Biol.* **51**, 257–267
350. Geck, P., and Heinz, E. (1989) Secondary active transport: Introductory remarks. *Kidney Int.* **36**, 334–341
351. Holland, I. B. (2019) Rise and rise of the ABC transporter families. *Res. Microbiol.* **170**, 304–320
352. Yan, N. (2015) Structural biology of the major facilitator superfamily transporters. *Annu. Rev. Biophys.* **44**, 257–283
353. Davidson, A. L., and Chen, J. (2004) ATP-binding cassette transporters in bacteria. *Annu. Rev. Biochem.* **73**, 241–268
354. Borst, P., and Elferink, R. O. (2002) Mammalian ABC transporters in health and disease. *Annu. Rev. Biochem.* **71**, 537–592
355. Stefková, J., Poledne, R., and Hubácek, J. A. (2004) ATP-binding cassette (ABC) transporters in human metabolism and diseases. *Physiol. Res.* **53**, 235–243

356. ter Beek, J., Guskov, A., and Slotboom, D. J. (2014) Structural diversity of ABC transporters. *J. Gen. Physiol.* **143**, 419–435
357. Thomas, C., and Tampé, R. (2020) Structural and mechanistic principles of ABC transporters. *Annu. Rev. Biochem.* **89**, 605–636
358. Rees, D. C., Johnson, E., and Lewinson, O. (2009) ABC transporters: The power to change. *Nat. Rev. Mol. Cell Biol.* **10**, 218–227
359. Locher, K. P. (2009) Review. Structure and mechanism of ATP-binding cassette transporters. *Philos. Trans. R. Soc. Lond. B Biol. Sci.* **364**, 239–245
360. Rice, A. J., Park, A., and Pinkett, H. W. (2014) Diversity in ABC transporters: Type I, II and III importers. *Crit. Rev. Biochem. Mol. Biol.* **49**, 426–437
361. Theodoulou, F. L., and Kerr, I. D. (2015) ABC transporter research: Going strong 40 years on. *Biochem. Soc. Trans.* **43**, 1033–1040
362. Mächtel, R., Narducci, A., Griffith, D. A., Cordes, T., and Orelle, C. (2019) An integrated transport mechanism of the maltose ABC importer. *Res. Microbiol.* **170**, 321–337
363. Ehrmann, M., Ehrle, R., Hofmann, E., Boos, W., and Schlösser, A. (1998) The ABC maltose transporter. *Mol. Microbiol.* **29**, 685–694
364. Boos, W., and Shuman, H. (1998) Maltose/maltodextrin system of Escherichia coli: Transport, metabolism, and regulation. *Microbiol. Mol. Biol. Rev.* **62**, 204–229
365. Chen, J. (2013) Molecular mechanism of the Escherichia coli maltose transporter. *Curr. Opin. Struct. Biol.* **23**, 492–498
366. Khare, D., Oldham, M. L., Orelle, C., Davidson, A. L., and Chen, J. (2009) Alternating access in maltose transporter mediated by rigid-body rotations. *Mol. Cell* **33**, 528–536
367. Oldham, M. L., and Chen, J. (2011) Crystal structure of the maltose transporter in a pretranslocation intermediate state. *Science* **332**, 1202–1205
368. Oldham, M. L., Khare, D., Quiocho, F. A., Davidson, A. L., and Chen, J. (2007) Crystal structure of a catalytic intermediate of the maltose transporter. *Nature* **450**, 515–521
369. Oldham, M. L., Chen, S., and Chen, J. (2013) Structural basis for substrate specificity in the Escherichia coli maltose transport system. *Proc. Natl. Acad. Sci. U. S. A.* **110**, 18132–18137
370. Treptow, N. A., and Shuman, H. A. (1985) Genetic evidence for substrate and periplasmic-binding-protein recognition by the MalF and MalG proteins, cytoplasmic membrane components of the Escherichia coli maltose transport system. *J. Bacteriol.* **163**, 654–660
371. Dean, D. A., Hor, L. I., Shuman, H. A., and Nikaido, H. (1992) Interaction between maltose-binding protein and the membrane-associated maltose transporter complex in Escherichia coli. *Mol. Microbiol.* **6**, 2033–2040
372. Bajaj, R., Park, M. I., Stauffacher, C. V., and Davidson, A. L. (2018) Conformational dynamics in the binding-protein-independent mutant of the Escherichia coli maltose transporter, MalG511, and its interaction with maltose binding protein. *Biochemistry* **57**, 3003–3015
373. Davidson, A. L., Shuman, H. A., and Nikaido, H. (1992) Mechanism of maltose transport in Escherichia coli: Transmembrane signaling by periplasmic binding proteins. *Proc. Natl. Acad. Sci. U. S. A.* **89**, 2360–2364
374. Covitz, K. M., Panagiotidis, C. H., Hor, L. I., Reyes, M., Treptow, N. A., and Shuman, H. A. (1994) Mutations that alter the transmembrane signalling pathway in an ATP binding cassette (ABC) transporter. *EMBO J.* **13**, 1752–1759
375. Nöll, A., Thomas, C., Herbring, V., Zollmann, T., Barth, K., Mehdipour, A. R., Tomasiak, T. M., Brüchert, S., Joseph, B., Abele, R., Oliéric, V., Wang, M., Diederichs, K., Hummer, G., Stroud, R. M., *et al.* (2017) Crystal structure and mechanistic basis of a functional homolog of the antigen transporter TAP. *Proc. Natl. Acad. Sci. U. S. A.* **114**, E438–E447
376. Kim, J., Wu, S., Tomasiak, T. M., Mergel, C., Winter, M. B., Stiller, S. B., Robles-Colmanares, Y., Stroud, R. M., Tampe, R., Craik, C. S., and Cheng, Y. (2015) Subnanometre-resolution electron cryomicroscopy structure of a heterodimeric ABC exporter. *Nature* **517**, 396–400
377. Hofmann, S., Januliene, D., Mehdipour, A. R., Thomas, C., Stefan, E., Brüchert, S., Kuhn, B. T., Geertsma, E. R., Hummer, G., Tampé, R., and Moeller, A. (2019) Conformation space of a heterodimeric ABC exporter under turnover conditions. *Nature* **571**, 580–583
378. Zhang, J., Yu, Y. C., Yeh, J. T., and Hwang, T. C. (2018) Functional characterization reveals that zebrafish CFTR prefers to occupy closed channel conformations. *PLoS One* **13**, e0209862
379. Zhang, Z., and Chen, J. (2016) Atomic structure of the cystic fibrosis transmembrane conductance regulator. *Cell* **167**, 1586–1597.e1589
380. Zhang, Z., Liu, F., and Chen, J. (2017) Conformational changes of CFTR upon phosphorylation and ATP binding. *Cell* **170**, 483–491.e488
381. Liu, F., Zhang, Z., Csanády, L., Gadsby, D. C., and Chen, J. (2017) Molecular structure of the human CFTR ion channel. *Cell* **169**, 85–95.e88
382. Csanády, L., Vergani, P., and Gadsby, D. C. (2019) Structure, gating, and regulation of the CFTR anion channel. *Physiol. Rev.* **99**, 707–738
383. Johnson, Z. L., and Chen, J. (2017) Structural basis of substrate recognition by the multidrug resistance protein MRP1. *Cell* **168**, 1075–1085.e1079
384. Johnson, Z. L., and Chen, J. (2018) ATP binding enables substrate release from multidrug resistance protein 1. *Cell* **172**, 81–89.e10
385. Wang, L., Johnson, Z. L., Wasserman, M. R., Levring, J., Chen, J., and Liu, S. (2020) Characterization of the kinetic cycle of an ABC transporter by single-molecule and cryo-EM analyses. *Elife* **9**, e56451
386. Alam, A., Küng, R., Kowal, J., McLeod, R. A., Tremp, N., Broude, E. V., Roninson, I. B., Stahlberg, H., and Locher, K. P. (2018) Structure of a zosuquidar and UIC2-bound human-mouse chimeric ABCB1. *Proc. Natl. Acad. Sci. U. S. A.* **115**, E1973–E1982
387. Alam, A., Kowal, J., Broude, E., Roninson, I., and Locher, K. P. (2019) Structural insight into substrate and inhibitor discrimination by human P-glycoprotein. *Science* **363**, 753–756
388. Nosol, K., Romane, K., Irobalieva, R. N., Alam, A., Kowal, J., Fujita, N., and Locher, K. P. (2020) Cryo-EM structures reveal distinct mechanisms of inhibition of the human multidrug transporter ABCB1. *Proc. Natl. Acad. Sci. U. S. A.* **117**, 26245–26253
389. Taylor, N. M. I., Manolaridis, I., Jackson, S. M., Kowal, J., Stahlberg, H., and Locher, K. P. (2017) Structure of the human multidrug transporter ABCG2. *Nature* **546**, 504–509
390. Manolaridis, I., Jackson, S. M., Taylor, N. M. I., Kowal, J., Stahlberg, H., and Locher, K. P. (2018) Cryo-EM structures of a human ABCG2 mutant trapped in ATP-bound and substrate-bound states. *Nature* **563**, 426–430
391. Jackson, S. M., Manolaridis, I., Kowal, J., Zechner, M., Taylor, N. M. I., Bause, M., Bauer, S., Bartholomaeus, R., Bernhardt, G., Koenig, B., Buschauer, A., Stahlberg, H., Altmann, K. H., and Locher, K. P. (2018) Structural basis of small-molecule inhibition of human multidrug transporter ABCG2. *Nat. Struct. Mol. Biol.* **25**, 333–340
392. Orlando, B. J., and Liao, M. (2020) ABCG2 transports anticancer drugs via a closed-to-open switch. *Nat. Commun.* **11**, 2264
393. Klare, J. P., and Steinhoff, H. J. (2015) Spin labeling studies of transmembrane signaling and transport: Applications to phototaxis, ABC transporters and symporters. *Methods Enzymol.* **564**, 315–347
394. Claxton, D. P., Kazmier, K., Mishra, S., and Mchaourab, H. S. (2015) Navigating membrane protein structure, dynamics, and energy landscapes using spin labeling and EPR spectroscopy. *Methods Enzymol.* **564**, 349–387
395. Grote, M., Polyhach, Y., Jeschke, G., Steinhoff, H. J., Schneider, E., and Bordignon, E. (2009) Transmembrane signaling in the maltose ABC transporter MalFGK2-E: Periplasmic MalF-P2 loop communicates substrate availability to the ATP-bound MalK dimer. *J. Biol. Chem.* **284**, 17521–17526
396. Grote, M., Bordignon, E., Polyhach, Y., Jeschke, G., Steinhoff, H. J., and Schneider, E. (2008) A comparative electron paramagnetic resonance study of the nucleotide-binding domains' catalytic cycle in the assembled maltose ATP-binding cassette importer. *Biophys. J.* **95**, 2924–2938
397. Orelle, C., Ayvaz, T., Everly, R. M., Klug, C. S., and Davidson, A. L. (2008) Both maltose-binding protein and ATP are required for nucleotide-binding domain closure in the intact maltose ABC transporter. *Proc. Natl. Acad. Sci. U. S. A.* **105**, 12837–12842

398. Ward, A., Reyes, C. L., Yu, J., Roth, C. B., and Chang, G. (2007) Flexibility in the ABC transporter MsbA: Alternating access with a twist. *Proc. Natl. Acad. Sci. U. S. A.* **104**, 19005–19010
399. Yan, N. (2013) Structural advances for the major facilitator superfamily (MFS) transporters. *Trends Biochem. Sci.* **38**, 151–159
400. Drew, D., and Boudker, O. (2016) Shared molecular mechanisms of membrane transporters. *Annu. Rev. Biochem.* **85**, 543–572
401. Quistgaard, E. M., Low, C., Guettou, F., and Nordlund, P. (2016) Understanding transport by the major facilitator superfamily (MFS): Structures pave the way. *Nat. Rev. Mol. Cell Biol.* **17**, 123–132
402. Cura, A. J., and Carruthers, A. (2012) Role of monosaccharide transport proteins in carbohydrate assimilation, distribution, metabolism, and homeostasis. *Compr. Physiol.* **2**, 863–914
403. Deng, D., Xu, C., Sun, P., Wu, J., Yan, C., Hu, M., and Yan, N. (2014) Crystal structure of the human glucose transporter GLUT1. *Nature* **510**, 121–125
404. Ooi, A. T., and Gomperts, B. N. (2015) Molecular pathways: Targeting cellular energy metabolism in cancer via inhibition of SLC2A1 and LDHA. *Clin. Cancer Res.* **21**, 2440–2444
405. Kapoor, K., Finer-Moore, J. S., Pedersen, B. P., Caboni, L., Waight, A., Hillig, R. C., Bringmann, P., Heisler, I., Muller, T., Siebeneicher, H., and Stroud, R. M. (2016) Mechanism of inhibition of human glucose transporter GLUT1 is conserved between cytochalasin B and phenylalanine amides. *Proc. Natl. Acad. Sci. U. S. A.* **113**, 4711–4716
406. Augustin, R. (2010) The protein family of glucose transport facilitators: It's not only about glucose after all. *IUBMB Life* **62**, 315–333
407. Ruiz, A., Gautschi, I., Schild, L., and Bonny, O. (2018) Human mutations in SLC2A9 (Glut9) affect transport capacity for urate. *Front. Physiol.* **9**, 476
408. Smith, D. E., Clemencon, B., and Hediger, M. A. (2013) Proton-coupled oligopeptide transporter family SLC15: Physiological, pharmacological and pathological implications. *Mol. Aspects Med.* **34**, 323–336
409. Roth, M., Obaidat, A., and Hagenbuch, B. (2012) OATPs, OATs and OCTs: The organic anion and cation transporters of the SLCO and SLC22A gene superfamilies. *Br. J. Pharmacol.* **165**, 1260–1287
410. Koepsell, H. (2013) The SLC22 family with transporters of organic cations, anions and zwitterions. *Mol. Aspects Med.* **34**, 413–435
411. Anne, C., and Gasnier, B. (2014) Vesicular neurotransmitter transporters: Mechanistic aspects. *Curr. Top. Membr.* **73**, 149–174
412. Kumar, H., Finer-Moore, J. S., Kaback, H. R., and Stroud, R. M. (2015) Structure of LacY with an α-substituted galactoside: Connecting the binding site to the protonation site. *Proc. Natl. Acad. Sci. U. S. A.* **112**, 9004–9009
413. Hirai, T., Heymann, J. A., Shi, D., Sarker, R., Maloney, P. C., and Subramaniam, S. (2002) Three-dimensional structure of a bacterial oxalate transporter. *Nat. Struct. Biol.* **9**, 597–600
414. Yin, Y., He, X., Szewczyk, P., Nguyen, T., and Chang, G. (2006) Structure of the multidrug transporter EmrD from Escherichia coli. *Science* **312**, 741–744
415. Newstead, S., Drew, D., Cameron, A. D., Postis, V. L., Xia, X., Fowler, P. W., Ingram, J. C., Carpenter, E. P., Sansom, M. S., McPherson, M. J., Baldwin, S. A., and Iwata, S. (2011) Crystal structure of a prokaryotic homologue of the mammalian oligopeptide-proton symporters, PepT1 and PepT2. *EMBO J.* **30**, 417–426
416. Holyoake, J., and Sansom, M. S. (2007) Conformational change in an MFS protein: MD simulations of LacY. *Structure* **15**, 873–884
417. Smirnova, I., Kasho, V., Choe, J. Y., Altenbach, C., Hubbell, W. L., and Kaback, H. R. (2007) Sugar binding induces an outward facing conformation of LacY. *Proc. Natl. Acad. Sci. U. S. A.* **104**, 16504–16509
418. Madej, M. G., Soro, S. N., and Kaback, H. R. (2012) Apo-intermediate in the transport cycle of lactose permease (LacY). *Proc. Natl. Acad. Sci. U. S. A.* **109**, E2970–E2978
419. Kumar, H., Finer-Moore, J. S., Jiang, X., Smirnova, I., Kasho, V., Pardon, E., Steyaert, J., Kaback, H. R., and Stroud, R. M. (2018) Crystal structure of a ligand-bound LacY-nanobody complex. *Proc. Natl. Acad. Sci. U. S. A.* **115**, 8769–8774
420. Kumar, H., Finer-Moore, J., Smirnova, I., Kasho, V., Pardon, E., Steyaert, J., Kaback, H. R., and Stroud, R. M. (2020) Diversity in kinetics correlated with structure in nano body-stabilized LacY. *PLoS One* **15**, e0232846
421. Kaback, H. R., and Guan, L. (2019) It takes two to tango: The dance of the permease. *J. Gen. Physiol.* **151**, 878–886
422. Madej, M. G. (2014) Function, structure, and evolution of the major facilitator superfamily: The LacY manifesto. *Adv. Biol.* **2014**, 1–20
423. Smirnova, I. N., and Kaback, H. R. (2003) A mutation in the lactose permease of Escherichia coli that decreases conformational flexibility and increases protein stability. *Biochemistry* **42**, 3025–3031
424. Abramson, J., Smirnova, I., Kasho, V., Verner, G., Kaback, H. R., and Iwata, S. (2003) Structure and mechanism of the lactose permease of Escherichia coli. *Science* **301**, 610–615
425. Mirza, O., Guan, L., Verner, G., Iwata, S., and Kaback, H. R. (2006) Structural evidence for induced fit and a mechanism for sugar/H+ symport in LacY. *EMBO J.* **25**, 1177–1183
426. Kumar, H., Kasho, V., Smirnova, I., Finer-Moore, J. S., Kaback, H. R., and Stroud, R. M. (2014) Structure of sugar-bound LacY. *Proc. Natl. Acad. Sci. U. S. A.* **111**, 1784–1788
427. Smirnova, I. N., Kasho, V., and Kaback, H. R. (2008) Protonation and sugar binding to LacY. *Proc. Natl. Acad. Sci. U. S. A.* **105**, 8896–8901
428. Grytsyk, N., Santos Seica, A. F., Sugihara, J., Kaback, H. R., and Hellwig, P. (2019) Arg302 governs the pKa of Glu325 in LacY. *Proc. Natl. Acad. Sci. U. S. A.* **116**, 4934–4939
429. Grytsyk, N., Sugihara, J., Kaback, H. R., and Hellwig, P. (2017) pKa of Glu325 in LacY. *Proc. Natl. Acad. Sci. U. S. A.* **114**, 1530–1535
430. Smirnova, I., Kasho, V., Jiang, X., Pardon, E., Steyaert, J., and Kaback, H. R. (2015) Transient conformers of LacY are trapped by nanobodies. *Proc. Natl. Acad. Sci. U. S. A.* **112**, 13839–13844
431. Jiang, X., Andersson, M., Chau, B. T., Wong, L. Y., Villafuerte, M. K., and Kaback, H. R. (2016) Role of conserved Gly-Gly pairs on the periplasmic side of LacY. *Biochemistry* **55**, 4326–4332
432. Jiang, X., Smirnova, I., Kasho, V., Wu, J., Hirata, K., Ke, M., Pardon, E., Steyaert, J., Yan, N., and Kaback, H. R. (2016) Crystal structure of a LacY-nanobody complex in a periplasmic-open conformation. *Proc. Natl. Acad. Sci. U. S. A.* **113**, 12420–12425
433. Jiang, X., Wu, J., Ke, M., Zhang, S., Yuan, Y., Lin, J. Y., and Yan, N. (2019) Engineered XylE as a tool for mechanistic investigation and ligand discovery of the glucose transporters GLUTs. *Cell Discov.* **5**, 14
434. Sun, L., Zeng, X., Yan, C., Sun, X., Gong, X., Rao, Y., and Yan, N. (2012) Crystal structure of a bacterial homologue of glucose transporters GLUT1-4. *Nature* **490**, 361–366
435. Wisedchaisri, G., Park, M. S., Iadanza, M. G., Zheng, H., and Gonen, T. (2014) Proton-coupled sugar transport in the prototypical major facilitator superfamily protein XylE. *Nat. Commun.* **5**, 4521
436. Faham, S., Watanabe, A., Besserer, G. M., Cascio, D., Specht, A., Hirayama, B. A., Wright, E. M., and Abramson, J. (2008) The crystal structure of a sodium galactose transporter reveals mechanistic insights into Na+/sugar symport. *Science* **321**, 810–814
437. Abramson, J., and Wright, E. M. (2009) Structure and function of Na(+)-symporters with inverted repeats. *Curr. Opin. Struct. Biol.* **19**, 425–432
438. Watanabe, A., Choe, S., Chaptal, V., Rosenberg, J. M., Wright, E. M., Grabe, M., and Abramson, J. (2010) The mechanism of sodium and substrate release from the binding pocket of vSGLT. *Nature* **468**, 988–991
439. Ghezzi, C., Loo, D. D. F., and Wright, E. M. (2018) Physiology of renal glucose handling via SGLT1, SGLT2 and GLUT2. *Diabetologia* **61**, 2087–2097
440. Wright, E. M. (2020) SGLT2 and cancer. *Pflugers Arch.* **472**, 1407–1414
441. Bracken, C. J., Lim, S. A., Solomon, P., Rettko, N. J., Nguyen, D. P., Zha, B. S., Schaefer, K., Byrnes, J. R., Zhou, J., Lui, I., Liu, J., Pance, K., Zhou, X. X., Leung, K. K., and Wells, J. A. (2020) Bi-paratopic and multivalent human VH domains neutralize SARS-CoV-2 by targeting distinct epitopes within the ACE2 binding interface of spike. *bioRxiv*. https://doi.org/10.1101/2020.08.08.242511
442. Chen, X., Li, R., Pan, Z., Qian, C., Yang, Y., You, R., Zhao, J., Liu, P., Gao, L., Li, Z., Huang, Q., Xu, L., Tang, J., Tian, Q., Yao, W., *et al.* (2020) Human monoclonal antibodies block the binding of SARS-CoV-2 spike

protein to angiotensin converting enzyme 2 receptor. *Cell. Mol. Immunol.* **17**, 647–649
443. Xiong, X., Qu, K., Ciazynska, K. A., Hosmillo, M., Carter, A. P., Ebrahimi, S., Ke, Z., Scheres, S. H. W., Bergamaschi, L., Grice, G. L., Zhang, Y., Bradley, J., Lyons, P. A., Smith, K. G. C., Toshner, M., *et al.* (2020) A thermostable, closed SARS-CoV-2 spike protein trimer. *Nat. Struct. Mol. Biol.* **27**, 934–941
444. Takeda, M., Pekosz, A., Shuck, K., Pinto, L. H., and Lamb, R. A. (2002) Influenza a virus M2 ion channel activity is essential for efficient replication in tissue culture. *J. Virol.* **76**, 1391–1399
445. Nieva, J. L., Madan, V., and Carrasco, L. (2012) Viroporins: Structure and biological functions. *Nat. Rev. Microbiol.* **10**, 563–574
446. Castaño-Rodriguez, C., Honrubia, J. M., Gutiérrez-Álvarez, J., DeDiego, M. L., Nieto-Torres, J. L., Jimenez-Guardeño, J. M., Regla-Nava, J. A., Fernandez-Delgado, R., Verdia-Báguena, C., Queralt-Martín, M., Kochan, G., Perlman, S., Aguilella, V. M., Sola, I., and Enjuanes, L. (2018) Role of severe acute respiratory syndrome coronavirus viroporins E, 3a, and 8a in replication and pathogenesis. *mBio* **9**, e02325-17
447. González, M. E., and Carrasco, L. (2005) Viral proteins that enhance membrane permeability. In: Fischer, W. B., ed. *Viral Membrane Proteins: Structure, Function, and Drug Design*, Springer US, Boston, MA: 79–90
448. Holsinger, L. J., Nichani, D., Pinto, L. H., and Lamb, R. A. (1994) Influenza A virus M2 ion channel protein: A structure-function analysis. *J. Virol.* **68**, 1551–1563
449. Salom, D., Hill, B. R., Lear, J. D., and DeGrado, W. F. (2000) pH-dependent tetramerization and amantadine binding of the transmembrane helix of M2 from the influenza A virus. *Biochemistry* **39**, 14160–14170
450. Sharma, M., Yi, M., Dong, H., Qin, H., Peterson, E., Busath, D. D., Zhou, H.-X., and Cross, T. A. (2010) Insight into the mechanism of the influenza A proton channel from a structure in a lipid bilayer. *Science* **330**, 509–512
451. Rossman, J. S., Jing, X. H., Leser, G. P., and Lamb, R. A. (2010) Influenza virus M2 protein mediates ESCRT-independent membrane scission. *Cell* **142**, 902–913
452. Cady, S. D., Schmidt-Rohr, K., Wang, J., Soto, C. S., DeGrado, W. F., and Hong, M. (2010) Structure of the amantadine binding site of influenza M2 proton channels in lipid bilayers. *Nature* **463**, 689–693
453. Miao, Y., Fu, R., Zhou, H.-X., and Cross, T. A. (2015) Dynamic short hydrogen bonds in histidine tetrad of full-length M2 proton channel reveal tetrameric structural heterogeneity and functional mechanism. *Structure* **23**, 2300–2308
454. Thomaston, J. L., and DeGrado, W. F. (2016) Crystal structure of the drug-resistant S31N influenza M2 proton channel. *Protein Sci.* **25**, 1551–1554
455. Andreas, L. B., Barnes, A. B., Corzilius, B., Chou, J. J., Miller, E. A., Caporini, M., Rosay, M., and Griffin, R. G. (2013) Dynamic nuclear polarization study of inhibitor binding to the M2 (18–60) proton transporter from influenza A. *Biochemistry* **52**, 2774–2782
456. Mandala, V. S., Loftis, A. R., Shcherbakov, A. A., Pentelute, B. L., and Hong, M. (2020) Atomic structures of closed and open influenza B M2 proton channel reveal the conduction mechanism. *Nat. Struct. Mol. Biol.* **27**, 160–167
457. Lamb, R. A. (2020) The structure, function, and pathobiology of the influenza A and B virus ion channels. *Cold Spring Harb. Perspect. Med.* **10**, a038505
458. Dubé, M., Bego, M. G., Paquay, C., and Cohen, É. A. (2010) Modulation of HIV-1-host interaction: Role of the Vpu accessory protein. *Retrovirology* **7**, 114
459. Hill, M. S., Ruiz, A., Schmitt, K., and Stephens, E. B. (2010) Identification of amino acids within the second alpha helical domain of the human immunodeficiency virus type 1 Vpu that are critical for preventing CD4 cell surface expression. *Virology* **397**, 104–112
460. Lu, J.-X., Sharpe, S., Ghirlando, R., Yau, W.-M., and Tycko, R. (2010) Oligomerization state and supramolecular structure of the HIV-1 Vpu protein transmembrane segment in phospholipid bilayers: Vpu transmembrane oligomer structure. *Protein Sci.* **19**, 1877–1896
461. Magadán, J. G., and Bonifacino, J. S. (2012) Transmembrane domain determinants of CD4 downregulation by HIV-1 Vpu. *J. Virol.* **86**, 757–772
462. Herrero, L., Monroy, N., and González, M. E. (2013) HIV-1 Vpu protein mediates the transport of potassium in Saccharomyces cerevisiae. *Biochemistry* **52**, 171–177
463. Jia, X., Weber, E., Tokarev, A., Lewinski, M., Rizk, M., Suarez, M., Guatelli, J., and Xiong, Y. (2014) Structural basis of HIV-1 Vpu-mediated BST2 antagonism via hijacking of the clathrin adaptor protein complex 1. *Elife* **3**, e02362
464. Faust, T. B., Binning, J. M., Gross, J. D., and Frankel, A. D. (2017) Making sense of multifunctional proteins: Human immunodeficiency virus type 1 accessory and regulatory proteins and connections to transcription. *Annu. Rev. Virol.* **4**, 241–260
465. Seissler, T., Marquet, R., and Paillart, J.-C. (2017) Hijacking of the ubiquitin/proteasome pathway by the HIV auxiliary proteins. *Viruses* **9**, 322
466. Soper, A., Juarez-Fernandez, G., Aso, H., Moriwaki, M., Yamada, E., Nakano, Y., Koyanagi, Y., and Sato, K. (2017) Various plus unique: Viral protein U as a plurifunctional protein for HIV-1 replication. *Exp. Biol. Med. (Maywood)* **242**, 850–858
467. Park, S. H., Mrse, A. A., Nevzorov, A. A., Mesleh, M. F., Oblatt-Montal, M., Montal, M., and Opella, S. J. (2003) Three-dimensional structure of the channel-forming trans-membrane domain of virus protein "u" (Vpu) from HIV-1. *J. Mol. Biol.* **333**, 409–424
468. Verdiá-Báguena, C., Nieto-Torres, J. L., Alcaraz, A., DeDiego, M. L., Torres, J., Aguilella, V. M., and Enjuanes, L. (2012) Coronavirus E protein forms ion channels with functionally and structurally-involved membrane lipids. *Virology* **432**, 485–494
469. Verdiá-Báguena, C., Nieto-Torres, J. L., Alcaraz, A., DeDiego, M. L., Enjuanes, L., and Aguilella, V. M. (2013) Analysis of SARS-CoV E protein ion channel activity by tuning the protein and lipid charge. *Biochim. Biophys. Acta* **1828**, 2026–2031
470. DeDiego, M. L., Nieto-Torres, J. L., Jimenez-Guardeño, J. M., Regla-Nava, J. A., Castaño-Rodriguez, C., Fernandez-Delgado, R., Usera, F., and Enjuanes, L. (2014) Coronavirus virulence genes with main focus on SARS-CoV envelope gene. *Virus Res.* **194**, 124–137
471. Li, Y., Surya, W., Claudine, S., and Torres, J. (2014) Structure of a conserved Golgi complex-targeting signal in coronavirus envelope proteins. *J. Biol. Chem.* **289**, 12535–12549
472. Cook, G. A., Zhang, H., Park, S. H., Wang, Y., and Opella, S. J. (2011) Comparative NMR studies demonstrate profound differences between two viroporins: p7 of HCV and Vpu of HIV-1. *Biochim. Biophys. Acta* **1808**, 554–560
473. Steinmann, E., Penin, F., Kallis, S., Patel, A. H., Bartenschlager, R., and Pietschmann, T. (2007) Hepatitis C virus p7 protein is crucial for assembly and release of infectious virions. *PLoS Pathog.* **3**, e103
474. Steinmann, E., Whitfield, T., Kallis, S., Dwek, R. A., Zitzmann, N., Pietschmann, T., and Bartenschlager, R. (2007) Antiviral effects of amantadine and iminosugar derivatives against hepatitis C virus. *Hepatology* **46**, 330–338
475. Luik, P., Chew, C., Aittoniemi, J., Chang, J., Wentworth, P., Dwek, R. A., Biggin, P. C., Vénien-Bryan, C., and Zitzmann, N. (2009) The 3-dimensional structure of a hepatitis C virus p7 ion channel by electron microscopy. *Proc. Natl. Acad. Sci. U. S. A.* **106**, 12712–12716
476. StGelais, C., Foster, T. L., Verow, M., Atkins, E., Fishwick, C. W., Rowlands, D., Harris, M., and Griffin, S. (2009) Determinants of hepatitis C virus p7 ion channel function and drug sensitivity identified *in vitro*. *J. Virol.* **83**, 7970–7981
477. Sidorenko, Y., and Reichl, U. (2004) Structured model of influenza virus replication in MDCK cells. *Biotechnol. Bioeng.* **88**, 1–14
478. Hu, J., Fu, R., Nishimura, K., Zhang, L., Zhou, H. X., Busath, D. D., Vijayvergiya, V., and Cross, T. A. (2006) Histidines, heart of the hydrogen ion channel from influenza A virus: Toward an understanding of conductance and proton selectivity. *Proc. Natl. Acad. Sci. U. S. A.* **103**, 6865–6870
479. Hu, F., Luo, W., and Hong, M. (2010) Mechanisms of proton conduction and gating in influenza M2 proton channels from solid-state NMR. *Science* **330**, 505–508

480. Polishchuk, A. L., Lear, J. D., Ma, C. L., Lamb, R. A., Pinto, L. H., and DeGrado, W. F. (2010) A pH-dependent conformational ensemble mediates proton transport through the influenza A/M2 protein. *Biochemistry* **49**, 10061–10071
481. Tang, Y., Zaitseva, F., Lamb, R. A., and Pinto, L. H. (2002) The gate of the influenza virus M2 proton channel is formed by a single tryptophan residue. *J. Biol. Chem.* **277**, 39880–39886
482. Hayden, F. G. (2006) Antiviral resistance in influenza viruses — implications for management and pandemic response. *N. Engl. J. Med.* **354**, 785–788
483. Paulino, J., Pang, X., Hung, I., Zhou, H. X., and Cross, T. A. (2019) Influenza A M2 channel clustering at high protein/lipid ratios: Viral budding implications. *Biophys. J.* **116**, 1075–1084
484. Andreas, L. B., Eddy, M. T., Chou, J. J., and Griffin, R. G. (2012) Magic-angle-spinning NMR of the drug resistant S31N M2 proton transporter from influenza A. *J. Am. Chem. Soc.* **134**, 7215–7218
485. Wang, J., Wu, Y. B., Ma, C. L., Fiorin, G., Wang, J. Z., Pinto, L. H., Lamb, R. A., Klein, M. L., and DeGrado, W. F. (2013) Structure and inhibition of the drug-resistant S31N mutant of the M2 ion channel of influenza A virus. *Proc. Natl. Acad. Sci. U. S. A.* **110**, 1315–1320
486. Wang, J., Ma, C., Jo, H., Canturk, B., Fiorin, G., Pinto, L. H., Lamb, R. A., Klein, M. L., and DeGrado, W. F. (2013) Discovery of novel dual inhibitors of the wild-type and the most prevalent drug-resistant mutant, S31N, of the M2 proton channel from influenza A virus. *J. Med. Chem.* **56**, 2804–2812
487. Kolocouris, A., Tzitzoglaki, C., Johnson, F. B., Zell, R., Wright, A. K., Cross, T. A., Tietjen, I., Fedida, D., and Busath, D. D. (2014) Aminoadamantanes with persistent *in vitro* efficacy against H1N1 (2009) influenza A. *J. Med. Chem.* **57**, 4629–4639
488. Wu, Y., Canturk, B., Jo, H., Ma, C., Gianti, E., Klein, M. L., Pinto, L. H., Lamb, R. A., Fiorin, G., Wang, J., and DeGrado, W. F. (2014) Flipping in the pore: Discovery of dual inhibitors that bind in different orientations to the wild-type versus the amantadine-resistant S31N mutant of the influenza A virus M2 proton channel. *J. Am. Chem. Soc.* **136**, 17987–17995
489. Li, F., Ma, C., Hu, Y., Wang, Y., and Wang, J. (2016) Discovery of potent antivirals against amantadine-resistant influenza A viruses by targeting the M2-S31N proton channel. *ACS Infect. Dis.* **2**, 726–733
490. Hu, Y., Hau, R. K., Wang, Y., Tuohy, P., Zhang, Y., Xu, S., Ma, C., and Wang, J. (2018) Structure-property relationship studies of influenza A virus AM2-S31N proton channel blockers. *ACS Med. Chem. Lett.* **9**, 1111–1116
491. Scott, C., Kankanala, J., Foster, T. L., Goldhill, D. H., Bao, P., Simmons, K., Pingen, M., Bentham, M., Atkins, E., Loundras, E., Elderfield, R., Claridge, J. K., Thompson, J., Stilwell, P. R., Tathineni, R., *et al.* (2020) Site-directed M2 proton channel inhibitors enable synergistic combination therapy for rimantadine-resistant pandemic influenza. *PLoS Pathog.* **16**, e1008716
492. Musharrafieh, R., Ma, C., and Wang, J. (2020) Discovery of M2 channel blockers targeting the drug-resistant double mutants M2-S31N/L26I and M2-S31N/V27A from the influenza A viruses. *Eur. J. Pharm. Sci.* **141**, 105124
493. Santos, R., Ursu, O., Gaulton, A., Bento, A. P., Donadi, R. S., Bologa, C. G., Karlsson, A., Al-Lazikani, B., Hersey, A., Oprea, T. I., and Overington, J. P. (2017) A comprehensive map of molecular drug targets. *Nat. Rev. Drug Discov.* **16**, 19–34
494. Lin, L., Yee, S. W., Kim, R. B., and Giacomini, K. M. (2015) SLC transporters as therapeutic targets: Emerging opportunities. *Nat. Rev. Drug Discov.* **14**, 543–560
495. International Transporter Consortium, Giacomini, K. M., Huang, S. M., Tweedie, D. J., Benet, L. Z., Brouwer, K. L., Chu, X., Dahlin, A., Evers, R., Fischer, V., Hillgren, K. M., Hoffmaster, K. A., Ishikawa, T., Keppler, D., Kim, R. B., *et al.* (2010) Membrane transporters in drug development. *Nat. Rev. Drug Discov.* **9**, 215–236
496. Wienkers, L. C., and Heath, T. G. (2005) Predicting *in vivo* drug interactions from *in vitro* drug discovery data. *Nat. Rev. Drug Discov.* **4**, 825–833
497. Kobe, B., Ve, T., and Williams, S. J. (2015) Fusion-protein-assisted protein crystallization. *Acta Crystallogr. F Struct. Biol. Commun.* **71**, 861–869
498. Chun, E., Thompson, A. A., Liu, W., Roth, C. B., Griffith, M. T., Katritch, V., Kunken, J., Xu, F., Cherezov, V., Hanson, M. A., and Stevens, R. C. (2012) Fusion partner toolchest for the stabilization and crystallization of G protein-coupled receptors. *Structure* **20**, 967–976
499. Ortiz de Montellano, P. R. (2015) *Cytochrome P450. Structure, Mechanism and Biochemistry*, 4 Ed, Springer International Publishing, Switzerland
500. Rittle, J., and Green, M. T. (2010) Cytochrome P450 compound I: Capture, characterization, and C-H bond activation kinetics. *Science* **330**, 933–937
501. Williams, P. A., Cosme, J., Vinkovic, D. M., Ward, A., Angove, H. C., Day, P. J., Vonrhein, C., Tickle, I. J., and Jhoti, H. (2004) Crystal structures of human cytochrome P450 3A4 bound to metyrapone and progesterone. *Science* **305**, 683–686
502. Hargrove, T. Y., Friggeri, L., Wawrzak, Z., Sivakumaran, S., Yazlovitskaya, E. M., Hiebert, S. W., Guengerich, F. P., Waterman, M. R., and Lepesheva, G. I. (2016) Human sterol 14alpha-demethylase as a target for anticancer chemotherapy: Towards structure-aided drug design. *J. Lipid Res.* **57**, 1552–1563
503. Monk, B. C., Sagatova, A. A., Hosseini, P., Ruma, Y. N., Wilson, R. K., and Keniya, M. V. (2020) Fungal lanosterol 14alpha-demethylase: A target for next-generation antifungal design. *Biochim. Biophys. Acta Proteins Proteom.* **1868**, 140206
504. Hargrove, T. Y., Wawrzak, Z., Liu, J., Nes, W. D., Waterman, M. R., and Lepesheva, G. I. (2011) Substrate preferences and catalytic parameters determined by structural characteristics of sterol 14alpha-demethylase (CYP51) from Leishmania infantum. *J. Biol. Chem.* **286**, 26838–26848
505. Arnold, F. H. (2019) Innovation by evolution: Bringing new chemistry to life (nobel lecture). *Angew. Chem. Int. Ed. Engl.* **58**, 14420–14426
506. Denisov, I. G., Shih, A. Y., and Sligar, S. G. (2012) Structural differences between soluble and membrane bound cytochrome P450s. *J. Inorg. Biochem.* **108**, 150–158
507. Keniya, M. V., Sabherwal, M., Wilson, R. K., Woods, M. A., Sagatova, A. A., Tyndall, J. D. A., and Monk, B. C. (2018) Crystal structures of full-length lanosterol 14alpha-demethylases of prominent fungal pathogens Candida albicans and Candida glabrata provide tools for antifungal discovery. *Antimicrob. Agents Chemother.* **62**, e01134-18
508. Monk, B. C., Tomasiak, T. M., Keniya, M. V., Huschmann, F. U., Tyndall, J. D., O'Connell, J. D., 3rd, Cannon, R. D., McDonald, J. G., Rodriguez, A., Finer-Moore, J. S., and Stroud, R. M. (2014) Architecture of a single membrane spanning cytochrome P450 suggests constraints that orient the catalytic domain relative to a bilayer. *Proc. Natl. Acad. Sci. U. S. A.* **111**, 3865–3870
509. Monk, B. C., Keniya, M. V., Sabherwal, M., Wilson, R. K., Graham, D. O., Hassan, H. F., Chen, D., and Tyndall, J. D. A. (2019) Azole resistance reduces susceptibility to the tetrazole antifungal VT-1161. *Antimicrob. Agents Chemother.* **63**, e02114-18
510. Sagatova, A. A., Keniya, M. V., Wilson, R. K., Monk, B. C., and Tyndall, J. D. (2015) Structural insights into binding of the antifungal drug fluconazole to Saccharomyces cerevisiae lanosterol 14alpha-demethylase. *Antimicrob. Agents Chemother.* **59**, 4982–4989
511. Tyndall, J. D., Sabherwal, M., Sagatova, A. A., Keniya, M. V., Negroni, J., Wilson, R. K., Woods, M. A., Tietjen, K., and Monk, B. C. (2016) Structural and functional elucidation of yeast lanosterol 14alpha-demethylase in complex with agrochemical antifungals. *PLoS One* **11**, e0167485
512. Caramalho, R., Tyndall, J. D. A., Monk, B. C., Larentis, T., Lass-Florl, C., and Lackner, M. (2017) Intrinsic short-tailed azole resistance in mucormycetes is due to an evolutionary conserved aminoacid substitution of the lanosterol 14alpha-demethylase. *Sci. Rep.* **7**, 15898
513. Sagatova, A. A., Keniya, M. V., Tyndall, J. D. A., and Monk, B. C. (2018) Impact of homologous resistance mutations from pathogenic yeast on Saccharomyces cerevisiae lanosterol 14alpha-demethylase. *Antimicrob. Agents Chemother.* **62**, e02242-17

514. Sagatova, A. A., Keniya, M. V., Wilson, R. K., Sabherwal, M., Tyndall, J. D., and Monk, B. C. (2016) Triazole resistance mediated by mutations of a conserved active site tyrosine in fungal lanosterol 14alpha-demethylase. *Sci. Rep.* **6**, 26213
515. Lepesheva, G. I., and Waterman, M. R. (2011) Structural basis for conservation in the CYP51 family. *Biochim. Biophys. Acta* **1814**, 88–93
516. Hargrove, T. Y., Wawrzak, Z., Fisher, P. M., Child, S. A., Nes, W. D., Guengerich, F. P., Waterman, M. R., and Lepesheva, G. I. (2018) Binding of a physiological substrate causes large-scale conformational reorganization in cytochrome P450 51. *J. Biol. Chem.* **293**, 19344–19353
517. Hargrove, T. Y., Wawrzak, Z., Guengerich, F. P., and Lepesheva, G. I. (2020) A requirement for an active proton delivery network supports a compound I-mediated C-C bond cleavage in CYP51 catalysis. *J. Biol. Chem.* **295**, 9998–10007
518. Mo, C., and Bard, M. (2005) A systematic study of yeast sterol biosynthetic protein-protein interactions using the split-ubiquitin system. *Biochim. Biophys. Acta* **1737**, 152–160
519. Rafeeq, M. M., and Murad, H. A. S. (2017) Cystic fibrosis: Current therapeutic targets and future approaches. *J. Transl. Med.* **15**, 84
520. Ratjen, F., Bell, S. C., Rowe, S. M., Goss, C. H., Quittner, A. L., and Bush, A. (2015) Cystic fibrosis. *Nat. Rev. Dis. Primers* **1**, 15010
521. Collins, F. S. (1992) Cystic fibrosis: Molecular biology and therapeutic implications. *Science* **256**, 774–779
522. MacKenzie, T., Gifford, A. H., Sabadosa, K. A., Quinton, H. B., Knapp, E. A., Goss, C. H., and Marshall, B. C. (2014) Longevity of patients with cystic fibrosis in 2000 to 2010 and beyond: Survival analysis of the cystic fibrosis foundation patient registry. *Ann. Intern. Med.* **161**, 233–241
523. Riordan, J. R., Rommens, J. M., Kerem, B., Alon, N., Rozmahel, R., Grzelczak, Z., Zielenski, J., Lok, S., Plavsic, N., Chou, J. L., Drumm, M. L., Iannuzzi, M. C., Collins, F. S., and Tsui, L. C. (1989) Identification of the cystic fibrosis gene: Cloning and characterization of complementary DNA. *Science* **245**, 1066–1073
524. Kerem, B., Rommens, J. M., Buchanan, J. A., Markiewicz, D., Cox, T. K., Chakravarti, A., Buchwald, M., and Tsui, L. C. (1989) Identification of the cystic fibrosis gene: Genetic analysis. *Science* **245**, 1073–1080
525. Rommens, J. M., Iannuzzi, M. C., Kerem, B., Drumm, M. L., Melmer, G., Dean, M., Rozmahel, R., Cole, J. L., Kennedy, D., Hidaka, N., Zsiga, M., Buchwald, M., Riordan, J. R., Tsui, L. C., and Collins, F. S. (1989) Identification of the cystic fibrosis gene: Chromosome walking and jumping. *Science* **245**, 1059–1065
526. Hyde, S. C., Emsley, P., Hartshorn, M. J., Mimmack, M. M., Gileadi, U., Pearce, S. R., Gallagher, M. P., Gill, D. R., Hubbard, R. E., and Higgins, C. F. (1990) Structural model of ATP-binding proteins associated with cystic fibrosis, multidrug resistance and bacterial transport. *Nature* **346**, 362–365
527. Anderson, M. P., Gregory, R. J., Thompson, S., Souza, D. W., Paul, S., Mulligan, R. C., Smith, A. E., and Welsh, M. J. (1991) Demonstration that CFTR is a chloride channel by alteration of its anion selectivity. *Science* **253**, 202–205
528. Cheng, S. H., Rich, D. P., Marshall, J., Gregory, R. J., Welsh, M. J., and Smith, A. E. (1991) Phosphorylation of the R domain by cAMP-dependent protein kinase regulates the CFTR chloride channel. *Cell* **66**, 1027–1036
529. Gentzsch, M., and Mall, M. A. (2018) Ion channel modulators in cystic fibrosis. *Chest* **154**, 383–393
530. Keating, D., Marigowda, G., Burr, L., Daines, C., Mall, M. A., McKone, E. F., Ramsey, B. W., Rowe, S. M., Sass, L. A., Tullis, E., McKee, C. M., Moskowitz, S. M., Robertson, S., Savage, J., Simard, C., *et al.* (2018) VX-445-tezacaftor-ivacaftor in patients with cystic fibrosis and one or two Phe508del alleles. *N. Engl. J. Med.* **379**, 1612–1620
531. Hadida, S., Van Goor, F., Zhou, J., Arumugam, V., McCartney, J., Hazlewood, A., Decker, C., Negulescu, P., and Grootenhuis, P. D. (2014) Discovery of N-(2,4-di-tert-butyl-5-hydroxyphenyl)-4-oxo-1,4-dihydroquinoline-3-carboxamide (VX-770, ivacaftor), a potent and orally bioavailable CFTR potentiator. *J. Med. Chem.* **57**, 9776–9795
532. Van der Plas, S. E., Kelgtermans, H., De Munck, T., Martina, S. L. X., Dropsit, S., Quinton, E., De Blieck, A., Joannesse, C., Tomaskovic, L., Jans, M., Christophe, T., van der Aar, E., Borgonovi, M., Nelles, L., Gees, M., *et al.* (2018) Discovery of N-(3-Carbamoyl-5,5,7,7-tetramethyl-5,7-dihydro-4H-thieno[2,3-c]pyran-2-yl)-lH-pyr azole-5-carboxamide (GLPG1837), a novel potentiator which can open class III mutant cystic fibrosis transmembrane conductance regulator (CFTR) channels to a high extent. *J. Med. Chem.* **61**, 1425–1435
533. Zhang, Z., Liu, F., and Chen, J. (2018) Molecular structure of the ATP-bound, phosphorylated human CFTR. *Proc. Natl. Acad. Sci. U. S. A.* **115**, 12757–12762
534. Liu, F., Zhang, Z., Levit, A., Levring, J., Touhara, K. K., Shoichet, B. K., and Chen, J. (2019) Structural identification of a hotspot on CFTR for potentiation. *Science* **364**, 1184–1188
535. Martinez-Outschoorn, U. E., Peiris-Pages, M., Pestell, R. G., Sotgia, F., and Lisanti, M. P. (2017) Cancer metabolism: A therapeutic perspective. *Nat. Rev. Clin. Oncol.* **14**, 113
536. Siebeneicher, H., Cleve, A., Rehwinkel, H., Neuhaus, R., Heisler, I., Muller, T., Bauser, M., and Buchmann, B. (2016) Identification and optimization of the first highly selective GLUT1 inhibitor BAY-876. *ChemMedChem* **11**, 2261–2271
537. Watson, R. T., and Pessin, J. E. (2001) Intracellular organization of insulin signaling and GLUT4 translocation. *Recent Prog. Horm. Res.* **56**, 175–193
538. Medina, R. A., and Owen, G. I. (2002) Glucose transporters: Expression, regulation and cancer. *Biol. Res.* **35**, 9–26
539. Santer, R., Schneppenheim, R., Dombrowski, A., Gotze, H., Steinmann, B., and Schaub, J. (1997) Mutations in GLUT2, the gene for the liver-type glucose transporter, in patients with Fanconi-Bickel syndrome. *Nat. Genet.* **17**, 324–326
540. Klepper, J., Fischbarg, J., Vera, J. C., Wang, D., and De Vivo, D. C. (1999) GLUT1-deficiency: Barbiturates potentiate haploinsufficiency *in vitro*. *Pediatr. Res.* **46**, 677–683
541. Hellwig, B., and Joost, H. G. (1991) Differentiation of erythrocyte-(GLUT1), liver-(GLUT2), and adipocyte-type (GLUT4) glucose transporters by binding of the inhibitory ligands cytochalasin B, forskolin, dipyridamole, and isobutylmethylxanthine. *Mol. Pharmacol.* **40**, 383–389
542. George Thompson, A. M., Iancu, C. V., Nguyen, T. T., Kim, D., and Choe, J. Y. (2015) Inhibition of human GLUT1 and GLUT5 by plant carbohydrate products; insights into transport specificity. *Sci. Rep.* **5**, 12804
543. Mishra, R. K., Wei, C., Hresko, R. C., Bajpai, R., Heitmeier, M., Matulis, S. M., Nooka, A. K., Rosen, S. T., Hruz, P. W., Schiltz, G. E., and Shanmugam, M. (2015) In silico modeling-based identification of glucose transporter 4 (GLUT4)-selective inhibitors for cancer therapy. *J. Biol. Chem.* **290**, 14441–14453
544. Ung, P. M., Song, W., Cheng, L., Zhao, X., Hu, H., Chen, L., and Schlessinger, A. (2016) Inhibitor discovery for the human GLUT1 from homology modeling and virtual screening. *ACS Chem. Biol.* **11**, 1908–1916
545. Qureshi, A. A., Suades, A., Matsuoka, R., Brock, J., McComas, S. E., Nji, E., Orellana, L., Claesson, M., Delemotte, L., and Drew, D. (2020) The molecular basis for sugar import in malaria parasites. *Nature* **578**, 321–325
546. Jiang, X., Yuan, Y., Huang, J., Zhang, S., Luo, S., Wang, N., Pu, D., Zhao, N., Tang, Q., Hirata, K., Yang, X., Jiao, Y., Sakata-Kato, T., Wu, J. W., Yan, C., *et al.* (2020) Structural basis for blocking sugar uptake into the malaria parasite Plasmodium falciparum. *Cell* **183**, 258–268.e12
547. Chaudhry, F. A., Reimer, R. J., and Edwards, R. H. (2002) The glutamine commute: Take the N line and transfer to the A. *J. Cell Biol.* **157**, 349–355
548. Edwards, R. H. (2007) The neurotransmitter cycle and quantal size. *Neuron* **55**, 835–858
549. Blakely, R. D., and Edwards, R. H. (2012) Vesicular and plasma membrane transporters for neurotransmitters. *Cold Spring Harb. Perspect. Biol.* **4**, a005595
550. Meriney, S. D., and Fanselow, E. E. (2019) Ionotropic receptors. In *Synaptic Transmission*, Elsevier Academic Press, Cambridge, MA: 215–243

551. Meriney, S. D., and Fanselow, E. E. (2019) Metabotropic G-protein-coupled receptors and their cytoplasmic signaling pathways. In *Synaptic Transmission*, Elsevier Academic Press, Cambridge, MA: 245–273
552. Amara, S. G., and Kuhar, M. J. (1993) Neurotransmitter transporters: Recent progress. *Annu. Rev. Neurosci.* **16**, 73–93
553. Focke, P. J., Wang, X., and Larsson, H. P. (2013) Neurotransmitter transporters: Structure meets function. *Structure* **21**, 694–705
554. Colovic, M. B., Krstic, D. Z., Lazarevic-Pasti, T. D., Bondzic, A. M., and Vasic, V. M. (2013) Acetylcholinesterase inhibitors: Pharmacology and toxicology. *Curr. Neuropharmacol.* **11**, 315–335
555. Overington, J. P., Al-Lazikani, B., and Hopkins, A. L. (2006) How many drug targets are there? *Nat. Rev. Drug Discov.* **5**, 993–996
556. Miller, P. S., and Aricescu, A. R. (2014) Crystal structure of a human GABAA receptor. *Nature* **512**, 270–275
557. Lynagh, T., and Pless, S. A. (2014) Principles of agonist recognition in Cys-loop receptors. *Front. Physiol.* **5**, 160
558. Althoff, T., Hibbs, R. E., Banerjee, S., and Gouaux, E. (2014) X-ray structures of GluCl in apo states reveal a gating mechanism of Cys-loop receptors. *Nature* **512**, 333–337
559. Huang, X., Chen, H., Michelsen, K., Schneider, S., and Shaffer, P. L. (2015) Crystal structure of human glycine receptor-alpha3 bound to antagonist strychnine. *Nature* **526**, 277–280
560. Huang, X., Chen, H., and Shaffer, P. L. (2017) Crystal structures of human GlyRalpha3 bound to Ivermectin. *Structure* **25**, 945–950.e942
561. Huang, X., Shaffer, P. L., Ayube, S., Bregman, H., Chen, H., Lehto, S. G., Luther, J. A., Matson, D. J., McDonough, S. I., Michelsen, K., Plant, M. H., Schneider, S., Simard, J. R., Teffera, Y., Yi, S., *et al.* (2017) Crystal structures of human glycine receptor alpha3 bound to a novel class of analgesic potentiators. *Nat. Struct. Mol. Biol.* **24**, 108–113
562. Bregman, H., Simard, J. R., Andrews, K. L., Ayube, S., Chen, H., Gunaydin, H., Guzman-Perez, A., Hu, J., Huang, L., Huang, X., Krolikowski, P. H., Lehto, S. G., Lewis, R. T., Michelsen, K., Pegman, P., *et al.* (2017) The discovery and hit-to-lead optimization of tricyclic sulfonamides as potent and efficacious potentiators of glycine receptors. *J. Med. Chem.* **60**, 1105–1125
563. Walsh, R. M., Jr., Roh, S. H., Gharpure, A., Morales-Perez, C. L., Teng, J., and Hibbs, R. E. (2018) Structural principles of distinct assemblies of the human alpha4beta2 nicotinic receptor. *Nature* **557**, 261–265
564. Phulera, S., Zhu, H., Yu, J., Claxton, D. P., Yoder, N., Yoshioka, C., and Gouaux, E. (2018) Cryo-EM structure of the benzodiazepine-sensitive alpha1beta1gamma2S tri-heteromeric GABAA receptor in complex with GABA. *Elife* **7**, e39383
565. Gharpure, A., Teng, J., Zhuang, Y., Noviello, C. M., Walsh, R. M., Jr., Cabuco, R., Howard, R. J., Zaveri, N. T., Lindahl, E., and Hibbs, R. E. (2019) Agonist selectivity and ion permeation in the alpha3beta4 ganglionic nicotinic receptor. *Neuron* **104**, 501–511.e506
566. Laverty, D., Desai, R., Uchanski, T., Masiulis, S., Stec, W. J., Malinauskas, T., Zivanov, J., Pardon, E., Steyaert, J., Miller, K. W., and Aricescu, A. R. (2019) Cryo-EM structure of the human alpha1beta3gamma2 GABAA receptor in a lipid bilayer. *Nature* **565**, 516–520
567. Masiulis, S., Desai, R., Uchanski, T., Serna Martin, I., Laverty, D., Karia, D., Malinauskas, T., Zivanov, J., Pardon, E., Kotecha, A., Steyaert, J., Miller, K. W., and Aricescu, A. R. (2019) GABAA receptor signalling mechanisms revealed by structural pharmacology. *Nature* **565**, 454–459
568. Zhu, S., Noviello, C. M., Teng, J., Walsh, R. M., Jr., Kim, J. J., and Hibbs, R. E. (2018) Structure of a human synaptic GABAA receptor. *Nature* **559**, 67–72
569. Rahman, M. M., Teng, J., Worrell, B. T., Noviello, C. M., Lee, M., Karlin, A., Stowell, M. H. B., and Hibbs, R. E. (2020) Structure of the native muscle-type nicotinic receptor and inhibition by snake venom toxins. *Neuron* **106**, 952–962.e955
570. Olsen, R. W., and Sieghart, W. (2009) GABA A receptors: Subtypes provide diversity of function and pharmacology. *Neuropharmacology* **56**, 141–148
571. Olsen, R. W., and Tobin, A. J. (1990) Molecular biology of GABAA receptors. *FASEB J.* **4**, 1469–1480
572. Artigas, F., Nutt, D. J., and Shelton, R. (2002) Mechanism of action of antidepressants. *Psychopharmacol. Bull.* **36 Suppl 2**, 123–132
573. Wang, H., Goehring, A., Wang, K. H., Penmatsa, A., Ressler, R., and Gouaux, E. (2013) Structural basis for action by diverse antidepressants on biogenic amine transporters. *Nature* **503**, 141–145
574. Penmatsa, A., Wang, K. H., and Gouaux, E. (2013) X-ray structure of dopamine transporter elucidates antidepressant mechanism. *Nature* **503**, 85–90
575. Wang, K. H., Penmatsa, A., and Gouaux, E. (2015) Neurotransmitter and psychostimulant recognition by the dopamine transporter. *Nature* **521**, 322–327
576. Coleman, J. A., Green, E. M., and Gouaux, E. (2016) X-ray structures and mechanism of the human serotonin transporter. *Nature* **532**, 334–339
577. Coleman, J. A., and Gouaux, E. (2018) Structural basis for recognition of diverse antidepressants by the human serotonin transporter. *Nat. Struct. Mol. Biol.* **25**, 170–175
578. Coleman, J. A., Yang, D., Zhao, Z., Wen, P. C., Yoshioka, C., Tajkhorshid, E., and Gouaux, E. (2019) Serotonin transporter-ibogaine complexes illuminate mechanisms of inhibition and transport. *Nature* **569**, 141–145
579. Coleman, J. A., Navratna, V., Antermite, D., Yang, D., Bull, J. A., and Gouaux, E. (2020) Chemical and structural investigation of the paroxetine-human serotonin transporter complex. *Elife* **9**, e56427
580. Deisseroth, K., and Hegemann, P. (2017) The form and function of channelrhodopsin. *Science* **357**, eaan5544
581. Deisseroth, K. (2015) Optogenetics: 10 years of microbial opsins in neuroscience. *Nat. Neurosci.* **18**, 1213–1225
582. Boyden, E. S., Zhang, F., Bamberg, E., Nagel, G., and Deisseroth, K. (2005) Millisecond-timescale, genetically targeted optical control of neural activity. *Nat. Neurosci.* **8**, 1263–1268
583. Gunaydin, L. A., Yizhar, O., Berndt, A., Sohal, V. S., Deisseroth, K., and Hegemann, P. (2010) Ultrafast optogenetic control. *Nat. Neurosci.* **13**, 387–392
584. Bamann, C., Gueta, R., Kleinlogel, S., Nagel, G., and Bamberg, E. (2010) Structural guidance of the photocycle of channelrhodopsin-2 by an interhelical hydrogen bond. *Biochemistry* **49**, 267–278
585. Berndt, A., Yizhar, O., Gunaydin, L. A., Hegemann, P., and Deisseroth, K. (2009) Bi-stable neural state switches. *Nat. Neurosci.* **12**, 229–234
586. Yizhar, O., Fenno, L. E., Prigge, M., Schneider, F., Davidson, T. J., O'Shea, D. J., Sohal, V. S., Goshen, I., Finkelstein, J., Paz, J. T., Stehfest, K., Fudim, R., Ramakrishnan, C., Huguenard, J. R., Hegemann, P., *et al.* (2011) Neocortical excitation/inhibition balance in information processing and social dysfunction. *Nature* **477**, 171–178
587. Zhang, F., Prigge, M., Beyriere, F., Tsunoda, S. P., Mattis, J., Yizhar, O., Hegemann, P., and Deisseroth, K. (2008) Red-shifted optogenetic excitation: A tool for fast neural control derived from Volvox carteri. *Nat. Neurosci.* **11**, 631–633
588. Gradinaru, V., Zhang, F., Ramakrishnan, C., Mattis, J., Prakash, R., Diester, I., Goshen, I., Thompson, K. R., and Deisseroth, K. (2010) Molecular and cellular approaches for diversifying and extending optogenetics. *Cell* **141**, 154–165
589. Wang, H., Sugiyama, Y., Hikima, T., Sugano, E., Tomita, H., Takahashi, T., Ishizuka, T., and Yawo, H. (2009) Molecular determinants differentiating photocurrent properties of two channelrhodopsins from chlamydomonas. *J. Biol. Chem.* **284**, 5685–5696
590. Lin, J. Y., Lin, M. Z., Steinbach, P., and Tsien, R. Y. (2009) Characterization of engineered channelrhodopsin variants with improved properties and kinetics. *Biophys. J.* **96**, 1803–1814
591. Kato, H. E., and Nureki, O. (2013) Crystal structure of channelrhodopsin, a light-gated cation channel - all cations lead through the monomer. *Biophysics (Nagoya-shi)* **9**, 57–61
592. Kato, H. E., Zhang, F., Yizhar, O., Ramakrishnan, C., Nishizawa, T., Hirata, K., Ito, J., Aita, Y., Tsukazaki, T., Hayashi, S., Hegemann, P., Maturana, A. D., Ishitani, R., Deisseroth, K., and Nureki, O. (2012) Crystal structure of the channelrhodopsin light-gated cation channel. *Nature* **482**, 369–374
593. Berndt, A., Lee, S. Y., Ramakrishnan, C., and Deisseroth, K. (2014) Structure-guided transformation of channelrhodopsin into a light-activated chloride channel. *Science* **344**, 420–424

594. Wietek, J., Wiegert, J. S., Adeishvili, N., Schneider, F., Watanabe, H., Tsunoda, S. P., Vogt, A., Elstner, M., Oertner, T. G., and Hegemann, P. (2014) Conversion of channelrhodopsin into a light-gated chloride channel. *Science* **344**, 409–412
595. Nakai, J., Ohkura, M., and Imoto, K. (2001) A high signal-to-noise Ca(2+) probe composed of a single green fluorescent protein. *Nat. Biotechnol.* **19**, 137–141
596. Marvin, J. S., Borghuis, B. G., Tian, L., Cichon, J., Harnett, M. T., Akerboom, J., Gordus, A., Renninger, S. L., Chen, T. W., Bargmann, C. I., Orger, M. B., Schreiter, E. R., Demb, J. B., Gan, W. B., Hires, S. A., *et al.* (2013) An optimized fluorescent probe for visualizing glutamate neurotransmission. *Nat. Methods* **10**, 162–170
597. de Lorimier, R. M., Smith, J. J., Dwyer, M. A., Looger, L. L., Sali, K. M., Paavola, C. D., Rizk, S. S., Sadigov, S., Conrad, D. W., Loew, L., and Hellinga, H. W. (2002) Construction of a fluorescent biosensor family. *Protein Sci.* **11**, 2655–2675
598. Fan, L., Tan, L., Chen, Z., Qi, J., Nie, F., Luo, Z., Cheng, J., and Wang, S. (2020) Haloperidol bound D2 dopamine receptor structure inspired the discovery of subtype selective ligands. *Nat. Commun.* **11**, 1074
599. Wang, S., Wacker, D., Levit, A., Che, T., Betz, R. M., McCorvy, J. D., Venkatakrishnan, A. J., Huang, X. P., Dror, R. O., Shoichet, B. K., and Roth, B. L. (2017) D4 dopamine receptor high-resolution structures enable the discovery of selective agonists. *Science* **358**, 381–386
600. Chien, E. Y., Liu, W., Zhao, Q., Katritch, V., Han, G. W., Hanson, M. A., Shi, L., Newman, A. H., Javitch, J. A., Cherezov, V., and Stevens, R. C. (2010) Structure of the human dopamine D3 receptor in complex with a D2/D3 selective antagonist. *Science* **330**, 1091–1095
601. Sun, F., Zeng, J., Jing, M., Zhou, J., Feng, J., Owen, S. F., Luo, Y., Li, F., Wang, H., Yamaguchi, T., Yong, Z., Gao, Y., Peng, W., Wang, L., Zhang, S., *et al.* (2018) A genetically encoded fluorescent sensor enables rapid and specific detection of dopamine in flies, fish, and mice. *Cell* **174**, 481–496.e419
602. Patriarchi, T., Cho, J. R., Merten, K., Howe, M. W., Marley, A., Xiong, W. H., Folk, R. W., Broussard, G. J., Liang, R., Jang, M. J., Zhong, H., Dombeck, D., von Zastrow, M., Nimmerjahn, A., Gradinaru, V., *et al.* (2018) Ultrafast neuronal imaging of dopamine dynamics with designed genetically encoded sensors. *Science* **360**, eaat4422
603. Gordon, D. E., Hiatt, J., Bouhaddou, M., Rezelj, V. V., Ulferts, S., Braberg, H., Jureka, A. S., Obernier, K., Guo, J. Z., Batra, J., Kaake, R. M., Weckstein, A. R., Owens, T. W., Gupta, M., Pourmal, S., *et al.* (2020) Comparative host-coronavirus protein interaction networks reveal pan-viral disease mechanisms. *Science* **370**, eabe9403
604. Gordon, D. E., Jang, G. M., Bouhaddou, M., Xu, J., Obernier, K., White, K. M., O'Meara, M. J., Rezelj, V. V., Guo, J. Z., Swaney, D. L., Tummino, T. A., Huttenhain, R., Kaake, R. M., Richards, A. L., Tutuncuoglu, B., *et al.* (2020) A SARS-CoV-2 protein interaction map reveals targets for drug repurposing. *Nature* **583**, 459–468
605. Schoof, M., Faust, B., Saunders, R. A., Sangwan, S., Rezelj, V., Hoppe, N., Boone, M., Billesbolle, C. B., Puchades, C., Azumaya, C. M., Kratochvil, H. T., Zimanyi, M., Deshpande, I., Liang, J., Dickinson, S., *et al.* (2020) An ultrapotent synthetic nanobody neutralizes SARS-CoV-2 by stabilizing inactive spike. *Science* **370**, 1473–1479
606. Bracken, C. J., Lim, S. A., Solomon, P., Rettko, N. J., Nguyen, D. P., Zha, B. S., Schaefer, K., Byrnes, J. R., Zhou, J., Lui, I., Liu, J., Pance, K., QCRG Structural Biology Consortium, Zhou, X. X., Leung, K. K., *et al.* (2021) Bi-paratopic and multivalent VH domains block ACE2 binding and neutralize SARS-CoV-2. *Nat. Chem. Biol.* **17**, 113–121
607. Glasgow, A., Glasgow, J., Limonta, D., Solomon, P., Lui, I., Zhang, Y., Nix, M. A., Rettko, N. J., Zha, S., Yamin, R., Kao, K., Rosenberg, O. S., Ravetch, J. V., Wiita, A. P., Leung, K. K., *et al.* (2020) Engineered ACE2 receptor traps potently neutralize SARS-CoV-2. *Proc. Natl. Acad. Sci. U. S. A.* **117**, 28046–28055
608. Watson, A., Ferriera, L., Hwang, P., Xu, J., and Stroud, R. M. (2020) Peptide antidotes to SARS-CoV-2 (COVID-19). *bioRxiv*. https://doi.org/10.1101/2020.08.06.238915
609. Callaway, E. (2020) 'It will change everything': DeepMind's AI makes gigantic leap in solving protein structures. *Nature* **588**, 203–204
610. Josts, I., Veith, K., Normant, V., Schalk, I., and Tidow, H. (2021) Structural insights into a novel family of integral membrane siderophore reductases. *bioRxiv*. https://doi.org/10.1101/2021.01.28.428567
611. Chapman, H. N. (2019) X-ray free-electron lasers for the structure and dynamics of macromolecules. *Annu. Rev. Biochem.* **88**, 35–58
612. Liu, S., Li, S., Yang, Y., and Li, W. (2020) Termini restraining of small membrane proteins enables structure determination at near-atomic resolution. *Sci. Adv.* **6**, eabe3717
613. Murphy, K. C., Nelson, S. J., Nambi, S., Papavinasasundaram, K., Baer, C. E., and Sassetti, C. M. (2018) Orbit: A new paradigm for genetic engineering of mycobacterial chromosomes. *mBio* **9**, e01467-18
614. Goddard, T. D., Huang, C. C., Meng, E. C., Pettersen, E. F., Couch, G. S., Morris, J. H., and Ferrin, T. E. (2018) UCSF ChimeraX: Meeting modern challenges in visualization and analysis. *Protein Sci.* **27**, 14–25
615. Pettersen, E. F., Goddard, T. D., Huang, C. C., Meng, E. C., Couch, G. S., Croll, T. I., Morris, J. H., and Ferrin, T. E. (2020) UCSF ChimeraX: Structure visualization for researchers, educators, and developers. *Protein Sci.* **30**, 70–82
616. Pettersen, E. F., Goddard, T. D., Huang, C. C., Couch, G. S., Greenblatt, D. M., Meng, E. C., and Ferrin, T. E. (2004) UCSF Chimera–a visualization system for exploratory research and analysis. *J. Comput. Chem.* **25**, 1605–1612